DEPARTMENT FÜR ANGEWANDTE GEOWISSENSCHAFTEN UND ERDÖLGEOLOGIE
LEHRSTUHL FÜR ANGEWANDTE GEOPHYSIK
Montanuniversität Leoben
Peter-Tunner-Strasse 25
A-8700 Leoben

Master Thesis

Correlations and empirical relations between static and dynamic elastic ground parameters in shallow geotechnical site investigations

submitted at the

Department für Angewandte Geowissenschaften und Geophysik
Lehrstuhl für Angewandte Geophysik
der
Montanuniversität Leoben

From:
Harald Pölzl
0435014

Tutor:
Hon. Prof. Dr. rer. nat. habil. H.J Schön

Leoben, 20.02.2012

EIDESSTATTLICHE ERKLÄRUNG

Ich erkläre an Eides statt, dass ich diese Arbeit selbständig verfasst, andere als die angegebenen Quellen und Hilfsmittel nicht benutzt und mich auch sonst keiner unerlaubten Hilfsmittel bedient habe.

AFFIDAVIT

I declare in lieu of oath, that I wrote this thesis and performed the associated research myself, using only literature cited in this volume.

Leoben, 27.02.2012

....

Ort, Datum Unterschrift

Acknowledgements

I would like to express my appreciation to Mag. Wolfram Felfer from the Fugro Austria GmbH for facilitating this paper and to Hon. Prof. Dr. rer. nat. habil. Jürgen Schön, University of Leoben for his time, his patience and his excellent petrophysical support.

My gratitude also goes to the following companies for providing access to data:

Fugro Geotechnical Division, ASFINAG-Autobahnen- und Schnellstraßen-Finanzierungs-AG, ÖBB-Österreichische Bundesbahnen AG, 3G Gruppe Geotechnik Graz ZT GmbH and ILF-Beratende Ingenieure ZT Gesellschaft mbH.

The most special thanks go to Heidemarie, Andreas and my parents for supporting me during all the years of my study.

Kurzfassung

Die Ermittlung von Parametern wie Young's Modul, Schermodul und Bulk-Modul ist integraler Bestandteil geotechnischer Baugrunderkundungen. Statische Methoden, die zeit- und kostenintensiv sind, liefern auf der einen Seite punktuell Informationen, die einen großen stress-strain-Bereich abdecken. Dynamische Methoden auf der anderen Seite liefern mit geringerem Aufwand seismische Geschwindigkeiten aus größeren Volumina, die über die Dichte einfach mit dynamischen Modulen verknüpft sind, allerdings auf sehr kleine strains begrenzt sind. Um die Vorteile der beiden Zugänge zu kombinieren bzw. die Nachteile zu kompensieren wird eine Methode präsentiert die einfache, empirische Potenzfunktionen benutzt, um statische Moduli aus den dynamischen ab zu schätzen. Der gewählte Ansatz liefert empirische Gleichungen, die gegenüber linearen Ansätzen eine deutlich genauere Abschätzung erlauben. Die verwendeten Datensätze enthalten statische Methoden, wie den einaxialen Kompressionsversuch, den Triaxial-Test, Dilatometertests und dynamische Methoden wie die spektrale Analyse von Oberflächenwellen, Downhole-Seismik, full waveform sonic logging, PS Suspension Logging, Crosshole-Seismik und Ultraschallgeschwindigkeitsmessungen im Labor, angewandt auf karbonatische, siliziklastische, metamorphe und plutonische Gesteine.

Neben der Modulabschätzung wurde auch mit eher geringem Erfolg eine Abschätzung der einaxialen Druckfestigkeit nur aus den seismischen Geschwindigkeiten versucht. Um eine höhere Genauigkeit zu erreichen wurden in einem Beispiel Geschwindigkeit, Porosität und die Rate der Lastaufbringung zu einem Faktor kombiniert mit dem Ergebnis eines sehr guten linearen Zusammenhangs der einaxiale Druckfestigkeit mit dem gebildeten Faktor.

Abstract

Determination of parameters like Young's Modulus, Shear Modulus and Bulk Modulus is integral part of any geotechnical site investigation. On the one hand well established, but mostly cost and time intensive static methods offer point measurements of moduli over a broad stress and strain range. On the other hand dynamic methods provide measurements of acoustic wave velocities in larger volumes at an arguable amount of time and money that can be easily linked to very small strain dynamic moduli via density. Making use of the advantages and trying to overcome the disadvantages of each approach a method for the derivation of power law empirical relations is presented to estimate static moduli from dynamic moduli with an improved accuracy compared to conventional linear approaches. The available data involves static unconfined compression, triaxial and dilatometer tests and dynamic methods like the spectral analysis of surface waves, downhole seismics, full waveform sonic logging, crosshole seismics and ultrasonic velocity measurements in laboratory performed in carbonatic, siliciclastic, metamorphic and plutonic rocks.

Beside the estimation of static moduli a not very successful attempt of estimating UCS from acoustic velocities only is presented. To increase accuracy of UCS estimation velocity, porosity and stress rate are considered additionally, leading to an excellent linear relation between for UCS.

Index

Page

1 Introduction and scope of work

Dynamic geophysical methods become more and more important in geotechnical site investigations. Especially information about elastic ground parameters including Poisson's Ratio, Young's Modulus, Shear Modulus or Bulk Modulus is of central importance for solving many tasks related to subsurface engineering or construction work. These parameters can be obtained by a palette of testing methods which can be classified from different points of view. Static methods are usually well established in geotechnics. They offer reliable values for the different moduli over a broad stress and strain range representing different conditions that are realized during and after design. One problem is, that static methods offer mostly very localized (mainly point) measurements, that are costly and time intensive.

Geophysical methods on the other hand can be used to obtain moduli at very small strains and high frequencies via measurement of seismic velocities and density. Their advantage is that they can cover large volumes at an arguable amount of time and money.

The scope of this work is to find and analyze correlations between static and dynamic methods and moduli to make use of the advantages of both methods. Reliable correlations between static and dynamic moduli could help to extend the static information from a measurement point to a larger volume that was investigated with dynamic methods.

The first part of this report should give a short introduction on the theoretical background about static and dynamic measurements of ground parameters. It should summarize the main principles of stress and strain in rocks and soil and also includes the basics of acoustic wave propagation in the underground and in boreholes. The last part of the theoretical introduction is about empirical correlations between the different parameters.

As a next step it was planned to compare different static and different dynamic methods separately with each other to get a feeling how congruent the results of different methods are. Unfortunately a direct comparison of different static measurements was not possible because there was too low "data intersection" in the given datasets. Different static methods have not been performed on the same location, so a direct comparison of this kind of methods was not possible. For the dynamic methods the direct comparison is presented.

To obtain dynamic moduli from acoustic measurements, beside density compressional and shear wave velocities are necessary. Shear wave velocity determination is often difficult or impossible, especially in shallow geotechnical investigations, whereas compressional wave velocity determination is less critical. Therefore an empirical approach is presented to derive shear wave velocities from measured compressional velocities in site areas where shear wave velocity could not be measured.

The main part is built by the chapter about correlations between static and dynamic moduli. Although generally large datasets were available, the approach of direct correlation (only moduli from the same location/borehole and the same depth were used for correlations) decreased the amount of data drastically. According to literature, direct and linear

correlations have been tried, resulting in mostly moderate to poor correlations and empirical equations. For this reason a new approach over power law equations has been successfully performed to increase quality of correlations.

Due to the fact that in nearly all datasets unconfined compression strength data was available, the correlation of this strength property with acoustic wave velocities is also involved in this report. On the one hand it was tried to relate unconfined compression strength to wave velocities only, and on the other hand it was tried to involve porosity and stress rate beside the wave velocities to increase the accuracy of unconfined compression strength estimation.

2 Theoretical Background

2.1 Elastic Moduli – Static Approach

Description of elastic behaviour follows Hooke's Law. Generalization of Hook's Law as a tensor has the form (SCHÖN, 1996):

$$\sigma_{ik} = C_{iklm}\varepsilon_{lm} \quad \text{or} \quad \varepsilon_{ik} = D_{iklm}\sigma_{lm} \tag{1}$$

σ_{ik} stress tensor

C_{iklm} elastic stiffness tensor or tensor of elasticity

ε_{lm} strain tensor

D_{iklm} tensor of compliances

The elastic potential, the independence of elastic energy from strain history and the symmetry of stress/strain-tensors are responsible for the fact that 21 or less independent tensor components exist (HELBIG, 1992). In case of an isotropic material only 2 independent properties are necessary (HELBIG, 1992).

Besides the Lame parameters λ and μ, any pair of two of the following moduli can be used for a description of the elastic properties of an isotropic material (HELBIG, 1992, SCHÖN, 2011):

- Young's modulus E, defined as ratio of stress to strain in a uniaxial stress state
- Compressional Wave Modulus M, defined as ratio of stress to strain in a uniaxial strain state
- Bulk Compressional Modulus K or k, defined as ratio of hydrostatic stress to volumetric strain
- Shear modulus G or μ, defined as ratio of shear stress to shear strain
- Poisson's ratio ν, defined as the (negative) ratio of lateral strain to axial strain in an uniaxial stress state

Table 1 shows a table of useful conversions and transformations for different cases of known and unknown parameters in an isotropic medium.

	Compr. Wave Modulus M	**Young's Modulus** E	**Shear Modulus** μ	**Lame Constant** λ	**Bulk Modulus** k	**Poisson's Ratio** ν
E,ν	$\frac{E\cdot(1-\nu)}{(1+\nu)\cdot(1-2\nu)}$	-	$\frac{E}{2\cdot(1+\nu)}$	$\frac{E\cdot\nu}{(1+\nu)(1-2\nu)}$	$\frac{E}{3\cdot(1-2\nu)}$	-
E,μ	$\frac{\mu\cdot(4\mu-E)}{3\mu-E}$	-	-	$\mu\cdot\frac{E-2\mu}{3\mu-E}$	$\frac{\mu\cdot E}{3\cdot(3\mu-E)}$	$\frac{E-2\mu}{2\mu}$
E,k	$\frac{3k\cdot(3k+E)}{9k-E}$	-	$\frac{3kE}{9k-E}$	$\frac{3k\cdot(3k-E)}{9k-E}$	-	$\frac{3k-E}{6k}$
k,ν	$\frac{3k\cdot(1-\nu)}{1+\nu}$	$3k\cdot(1-2\nu)$	$\frac{3k(1-2\nu)}{2\cdot(1+\nu)}$	$3\cdot\frac{k\cdot\nu}{1+\nu}$	-	-
k,μ	$k+\frac{4\mu}{3}$	$\frac{9k\cdot\mu}{3k+\mu}$	-	$k-\frac{2\mu}{3}$	-	$\frac{3k-2\mu}{2\cdot(3k+\mu)}$
k,λ	$3k-2\lambda$	$9k\cdot\frac{k-\lambda}{3k-\lambda}$	$\frac{3}{2}\cdot(k-\lambda)$	-	-	$\frac{\lambda}{3k-\lambda}$
μ,λ	$\lambda+2\mu$	$\mu\cdot\frac{3\lambda+2\mu}{\lambda+\mu}$	-	-	$\lambda+\frac{2}{3}\cdot\mu$	$\frac{\lambda}{2\cdot(\lambda+\mu)}$
μ,ν	$2\mu\cdot\frac{1-\nu}{1-2\cdot\nu}$	$2\mu\cdot(1+\nu)$	-	$\mu\cdot\frac{2\nu}{1-2\nu}$	$\frac{2\mu}{3}\cdot\frac{1+\nu}{1-2\nu}$	-
λ,ν	$\lambda\cdot\frac{1-\nu}{\nu}$	$\lambda\frac{(1+\nu)(1-2\nu)}{\nu}$	$\lambda\cdot\frac{1-2\nu}{2\nu}$	-	$\lambda\cdot\frac{1+\nu}{3\nu}$	-

Table1: Table of useful transformations and conversions for different combinations of known and unkown parameters. In the first column the known parameters are listed, in the first row the parameters that should be calculated with the known parameters are listed (SCHÖN, 2011).

The stress-strain behaviour of rocks is nonlinear and not really ideally elastic (SCHÖN, 1996). Only intact rocks may react approximately elastic (BARTON, 2007). Hook´s law can be expanded with time dependant terms, describing for example a visco-elastic material (SCHÖN, 1983).

Static moduli are based on application of static stress (load per area), the resulting deformation (displacement between two measurement points) and the derived strain (deformation divided by the original length) (LAMA, 1978). Axial strain is accompanied by transverse or lateral strain (LAMA, 1978). Under compression lateral strain is positive and under tension it is negative (LAMA, 1978).

2.1.1 Stress and strain

In general the mechanical state of a system is defined by the position of each part of the system, by the forces acting on and between each part and by the displacement of each part of the system (DE VALLEJO & FERRER, 2011). Stress is the result of acting forces on a plane (DE VALLEJO & FERRER, 2011). Forces might be tensile or compressive causing normal stress in a rock or they might be shear forces leading to shear stress (DE VALLEJO & FERRER, 2011). Strain is defined by the variation in the distance between two particles of the rock system (DE VALLEJO & FERRER, 2011). In general stress is a combined effect of a natural stress field and (maybe) of additional, artificial stress (load, excavation,…) (SCHÖN, 2011).

The triaxial stress state for rocks under confining pressure is described best by the maximum principal stress σ_1, the intermediate principal stress σ_2 and the minimum principal stress σ_3 (MOGI, 2007). The maximum principal stress can be described as a function of the other two stresses $\sigma_1=f(\sigma_2 ,\sigma_3)$ leading to a surface for a given material (MOGI, 2007). Failure strength, fracture angle and ductility are the basic mechanical properties defined by the stress state (MOGI, 2007).

The stress-strain curve (Fig.1) shows different characteristics and parts (MOGI, 2007). The linear part of the curve is caused by elastic behaviour (DE VALLEJO & FERRER, 2011). At the yield point linear, elastic behaviour ends and plastic or ductile deformation starts (DE VALLEJO & FERRER, 2011). The peak strength is the maximum stress that a rock can sustain (DE VALLEJO & FERRER, 2011). Residual strength is the lowered strength value in the post peak phase (DE VALLEJO & FERRER, 2011). At Peak Strength brittle or ductile failure should occur (DE VALLEJO & FERRER, 2011). DE VALLEJO & FERRER, 2011 also mention long time effects like creep or relaxation. Creep is a process where strain still

increases although stress is constant. Relaxation means a decrease in strain at constant stress (DE VALLEJO & FERRER, 2011).

Brittle deformation is responsible for a sudden change in the slope of stress-strain curves followed by a complete loss of cohesion or by a drop in differential stress (MOGI, 2007). Ductile deformation shows a curve without any downward slope after the yield point (MOGI, 2007).

Fig.1 shows a typical stress-strain curve of cyclic loading. The stress-strain relation is highly influenced by the deformation history of rocks (MOGI, 2007).

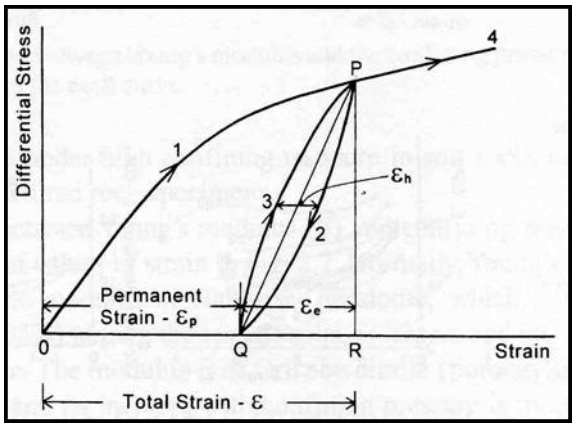

Fig.1: Stress-strain curve and its different components, 0-1-P: loading, P-2-Q: unloading, Q-3-P: reloading. (MOGI, 2007)

The slope of the linear approximation of the loop, created by the different paths of unloading and reloading is the mean Young´s Modulus E (MOGI, 2007). E is a function of strain and confining pressure and shows different characteristics for different lithologies (Fig.3) (MOGI, 2007). Fig.2 shows different approaches to derive moduli from stress –strain curves.

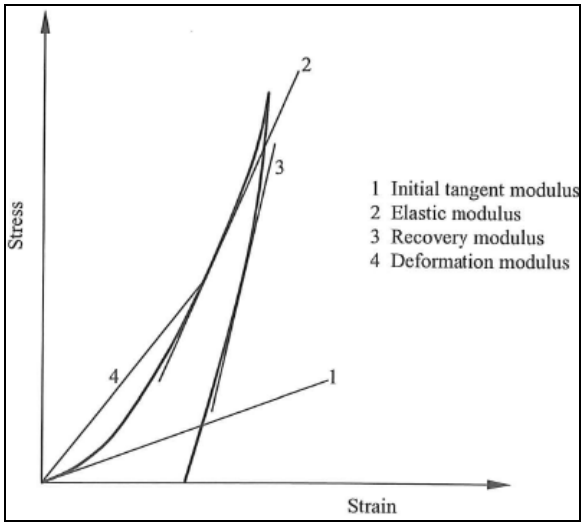

Fig.2: Stress-Strain curve and different approaches to derive deformation moduli. The Initial tangent modulus (1) is determined from a tangent to the initial slope initial slope of the curve. The Elastic modulus (2) is derived from the linear part of the curve. The recovery modulus (3) is a tangent modulus derived from the unloading part of the curve and the defomation modulus (4) or Secant modulus is determined from the slope of a secant between zero and some specified stress level (or between two specified stress levels (after ZHANG, 2005).

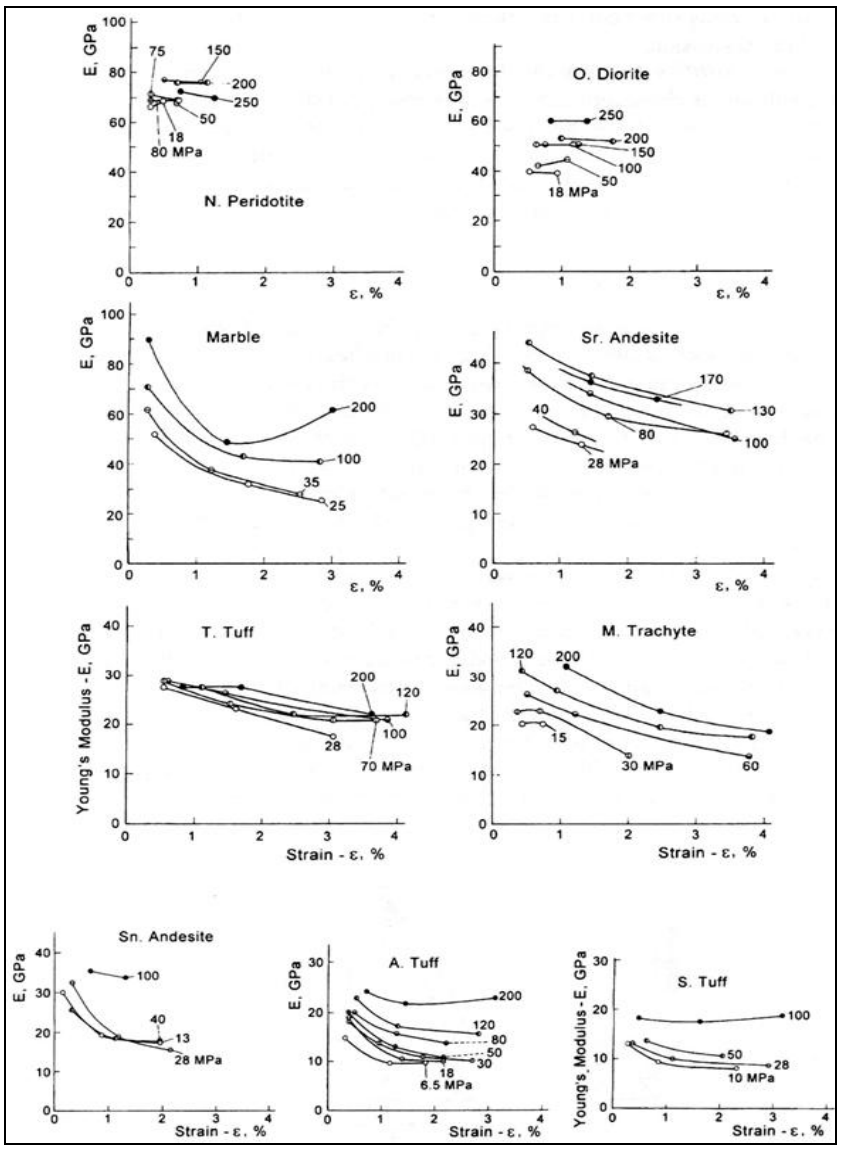

Fig.3: E as a function of strain for different lithologies (MOGI, 2007).

In very compact rocks E is nearly constant (MOGI, 2007): Generally E shows a decrease with increasing strain in porous rocks due to microcracks (MOGI, 2007). Some rocks show an increase of E at large strains because of compaction and closure processes (MOGI, 2007). In siliciclastic rocks porosity is one of the most important factors on mechanical properties, but also the conditions at the grain-grain contact and cementation are important (MOGI, 2007).

Strain can be partly elastic, meaning a full recovery of deformation during a loop and/or partly permanent without full recovery of deformation (MOGI, 2007). Permanent deformation is a result of dislocation processes, viscous flow and microfracturing and expresses non-elastic components (MOGI, 2007).

In porous rocks total stress and the presence of a pore pressure lead to the concept of effective stress (SCHÖN, 2011):

$$\sigma_{eff,ij} = \sigma_{total,ij} - \alpha\sigma_{pore}\delta_{ij} \quad (2)$$

α is the Biot-Willis effective stress parameter and δ is the Kronecker delta function (SCHÖN, 2011).

Young´s Modulus shows also a dependence on previous deformations (MOGI, 2007). Previous compressions for example lead to an increase of the apparent yield stress (MOGI, 2007). The yield stress corresponds to the magnitude of previously applied stress(es) (MOGI, 2007). The history of previous deformation is preserved in the mechanical properties of a rock and elasticity, plasticity, fracture strength and deformation characteristics can help in reconstruction (MOGI, 2007).

The yield stress is the maximum strength value achieved in the brittle state (MOGI, 2007). The ductile failure stress marks the yield stress and shows a knee in the curve at the elastic to plastic transition (MOGI, 2007). At the yield stress the slope of the stress strain-curve becomes approximately constant (Fig.4) (MOGI, 2007).

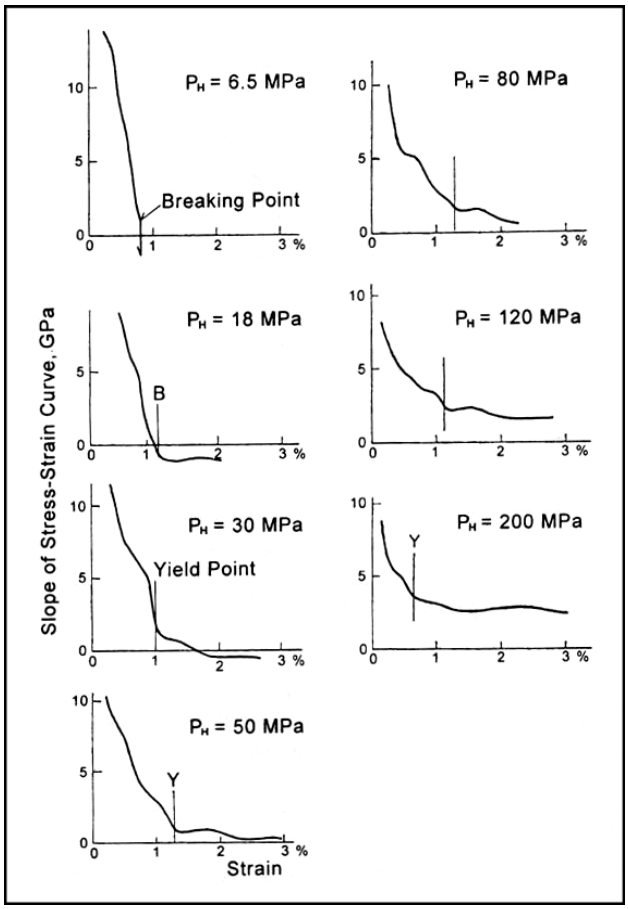

Fig.4: Slope behaviour of the stress-strain curve and yield stress for different stress states (MOGI, 2007).

2.1.2 Strength- and failure criteria – A Short revision

DE VALLEJO & FERRER, 2011 define strength of a rock as function of the principal stresses or strains and a set of parameters representative for the material:

Strength = $f(\sigma_1, \sigma_2, \sigma_3, k_i) = f(\varepsilon_1, \varepsilon_2, \varepsilon_3, k_i)$ (DE VALLEJO & FERRER, 2011)

The strength of rock materials is mainly controlled by type and mechanical quality of particle or solid component bonding (crystal bonding, cementation, cohesion, …), by presence, distribution and orientation of defects (fractures and fissures) and by the internal rock structure (schistosity, lamination, anisotropy) (SCHÖN, 2011).

Different criteria exist and are used to describe the strength and failure behaviour of geomaterials (MOGI, 2007). The linear Mohr-Coulomb-Criterion is widely used but does not fit appropriate for the big variety of rocks. Especially calculation of direction of occurring fractures do not always coincide with lab tests and tensile strength is overestimated (DE VALLEJO & FERRER, 2011). Nonlinear criterions from Drucker-Prager, von Mises or from Tresca show better correlation with real rocks (DE VALLEJO & FERRER, 2011) and include the influence of σ_2 (MOGI, 2007). MOGI, 2007 mentions the following 4 important failure criteria in combination with triaxial compression tests:

- Coulomb Criterion: $\tau = \tau_0 + \mu_i \sigma_n$ or $\sigma_1 = \sigma_c + \mu_i \sigma_3$ (3)
- Mohr criterion: $\tau = f''(\sigma_n)$ or $\sigma_1 = \sigma_c + f'''(\sigma_3)$ (4)
- Griffith criterion: $(\sigma_1 - \sigma_2)^2 = 8\sigma_T(\sigma_1 + \sigma_3)$ (5)
- Modified Griffith criterion: $(\sigma_1 - \sigma_3)\sqrt{(1+\mu)} + \mu(\sigma_1 + \sigma_3) = 4\sigma_T$ (6)

τ is shear stress, σ_n is normal stress, σ_C is uniaxial compressive strength, σ_T is tensile strength and μ is the sliding friction coefficient (MOGI, 2007). The Coulomb criterion is a simple linear solution derived from the Mohr criterion (SCHÖN, 1983). DE VALLEJO & FERRER, 2011 also mention the Hoek-Brown-Criterion:

$$\sigma_1 = \sigma_3 + \sqrt{m_i \sigma_{ci} \sigma_3 + \sigma_{ci}^2} \quad (7)$$

with σ_1 and σ_3 are the major and minor principal stresses, σ_{ci} is the uniaxial compression strength and m is rock mass specific constant.

2.2 Elasticity and elastic moduli – dynamic approach

The dynamic viewpoint is based on time harmonic external stresses and/or strains leading to propagating compressive, tensile and shear stresses (FJAER et al., 1992). Usually rocks show elastic reversible and inelastic irreversible deformation as a function of stress and time (SCHÖN, 1983). Dynamic methods achieve only elastic deformations (SCHÖN, 1983). The discrimination between static and dynamic moduli is necessary for real rocks with non ideal elastic behaviour; for ideal elastic material there is no difference between them (SCHÖN, 1983). For low porosity, massive rocks static and dynamic E is approximately equal (BARTON, 2007).

2.2.1 Waves in and around boreholes I – Body Waves

Compressional waves (p-waves or longitudinal waves (BOYER & MARI, 1997) produce alternating compression and expansion (dilatation) in propagation direction (BARTON, 2007). Shear waves (s-waves or transverse waves (BOYER & MARI, 1997)) are characterised by sinusoidal shear strain perpendicular to propagation direction (BARTON, 2007). Compressional waves produce particle motion in the direction of propagation, whereas shear waves produce particle motion perpendicular to the direction of propagation (Fig.5) (HALDORSEN et al., 2006). If a shear wave is propagating horizontally its transverse motion can be resolved into a horizontal (S_{hh}) and a vertical (S_{hv}) component (ELLIS, 2007). In case of anisotropic material the two components are different (ELLIS, 2007) (→Chapter 2.2.5 shear wave splitting).

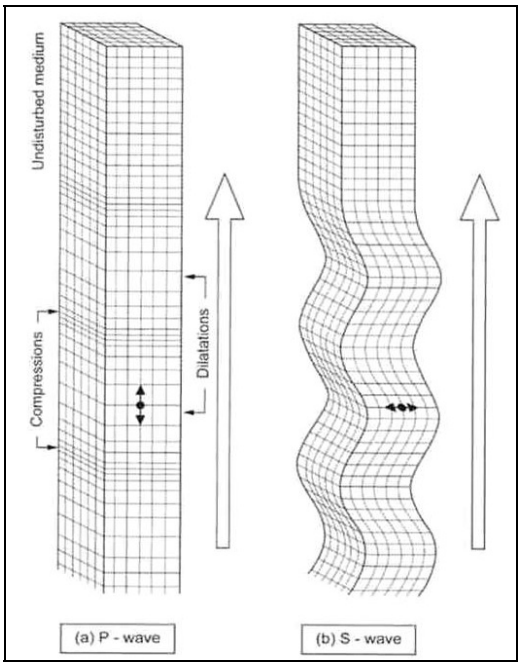

Fig.5: Compressional and shear waves and their propagation characteristics (BARTON, 2007)

The propagation velocity of compressional waves (v_p) can be defined as:

$$v_p = \sqrt{\frac{\lambda + 2\mu}{\rho}} = \sqrt{\frac{E \cdot (1-\nu)}{\rho(1-2\nu)\cdot(1+\nu)}} = \sqrt{\frac{1}{\rho}M} \quad \text{(SCHÖN, 1996)} \tag{8}$$

$$\text{or } v_p = \sqrt{\frac{K + \frac{4}{3}\mu}{\rho}} \quad \text{(BARTON, 2007)} \tag{9}$$

The propagation velocity of shear waves (v_s) can be defined as:

$$v_s = \sqrt{\frac{\mu}{\rho}} = \sqrt{\frac{E}{\rho \cdot 2(1+\nu)}} \quad \text{(SCHÖN, 1996; BARTON, 2007)} \tag{10}$$

Compressional and shear wave velocities can also be linked over the dynamic Poisson Ratio and dynamic Young's modulus can be defined as a function of v_p/v_s -ratio (BARTON, 2007):

$$\frac{v_p}{v_s} = \sqrt{\frac{2\cdot(1-\nu)}{1-2\nu}} \quad \text{(BARTON, 2007)} \tag{11}$$

$$\text{and } \nu = \frac{(\frac{v_p}{v_s})^2 - 2}{2[(\frac{v_p}{v_s}) - 1]} \quad \text{(SCHÖN, 2011)} \tag{12}$$

or

$$E = {v_s}^2 \cdot \rho \cdot \frac{3(\frac{v_p}{v_s})^2 - 4}{(\frac{v_p}{v_s})^2 - 1} \quad \text{(BARTON, 2007)} \tag{13}$$

With estimation of Poisson's Ratio and density moduli can be estimated by only measuring v_p. This estimation is rather inaccurate (BARTON, 2007).

The dynamic shear modulus G or μ is often used in geotechnics as the maximum shear modulus $G_{max=}\rho v_s^2$ (LUNNE et al., 1990). The shear modulus is largest at very low strains and decreases with increasing shear strain (LUNNE et al., 1990). Shear modulus is seen to be constant for shear strains $<10^{-3}$% (LUNNE et al., 1990).

Acoustic wave velocities recorded by sonic log depend on the energy source, wave path and properties of the formation and the borehole (HALDORSEN et al., 2006). Monopole and Dipole sources are mainly used. Monopole transmitters emit energy equally in every direction; dipole transmitters emit energy in two opposite directions. Under the assumption of a homogenous and isotropic formation the propagation direction of waves is always perpendicular to the wave front (HALDORSEN et al., 2006).

In boreholes the 3D problem can be reduced to a 2D problem, leading to a reduction of the wave front to circles (Fig.6). The wave front hits the borehole wall and generates three new wave fronts. The reflected wave returns to the borehole at speed v_m (mud velocity), the compressional wave and the shear wave are refracted and transmitted and propagate along the interface and into the formation at speed v_p and v_s. For fast formations the relation $v_p > v_s > v_m$ is valid (HALDORSEN et al., 2006). The ratio v_p/v_s is a function of the Poisson Ratio and lies mostly between 1.5 and 4 (BOYER & MARI, 1997).

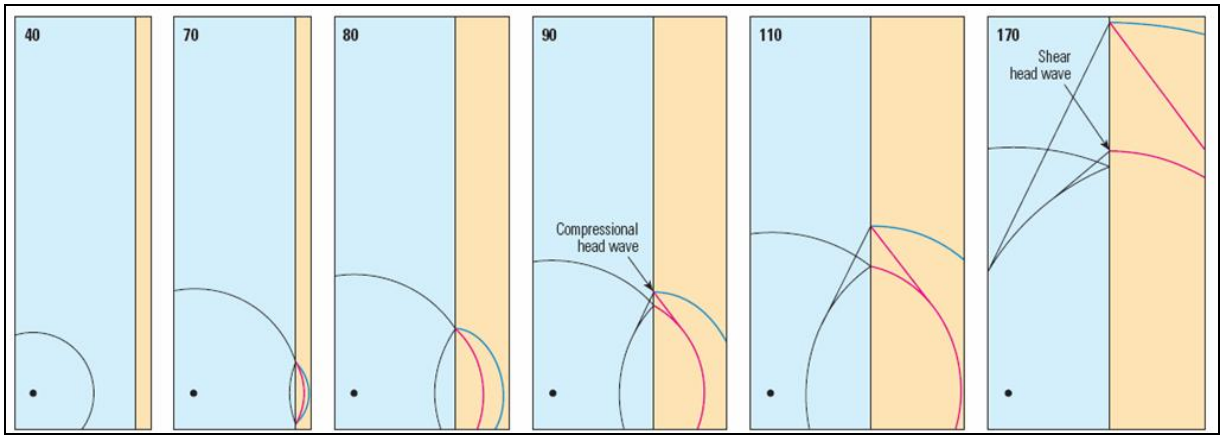

Fig.6: Creation and propagation of compressional and shear head waves in boreholes, assuming point source geometry (HALDORSEN et al., 2006).

The refracted p-wave propagates along the borehole-formation-interface and according to Huygen´s principle every point on the interface acts as a secondary wave source emitting p-waves into the borehole and emitting p- and s-waves into the formation. These secondary waves are responsible for the creation of the linear wave front in the borehole called compressional headwave, which is recorded as the p-wave arrival with sonic tools. The p-wave that propagates into the formation is called body wave (HALDORSEN et al., 2006). Once the body wave hits a reflector in the formation it propagates back towards the borehole as a reflected p-wave. Special applications of sonic logging use this waves (HALDORSEN et al., 2006).

The s-wave propagation is similar. An s-body wave propagates into the formation and in case of a fast formation ($v_s > v_m$) a refracted s-wave propagates along the borehole-formation-

interface and generates another head wave, whose arrival is recorded as the s-wave arrival by full waveform sonic tools (HALDORSEN et al., 2006). In slow formations ($v_s<v_m$) the shear wave front in the formation never forms a right angle with the borehole, so that no shear head wave can develop (HALDORSEN et al., 2006).

In cases where wavelength is much smaller than the borehole diameter the wave fronts can be approximated by planes rather than circles, so that the direction of travel can be imaged as a line perpendicular to the wave front ("ray"). Ray tracing can be useful for basic modelling (e.g. transmitter-receiver spacing of tools in different formations) and for some inversion techniques (e.g. tomographic reconstruction) (HALDORSEN et al., 2006). Using ray tracing the interaction of travelling waves at interfaces can be easily explained (Fig.7)

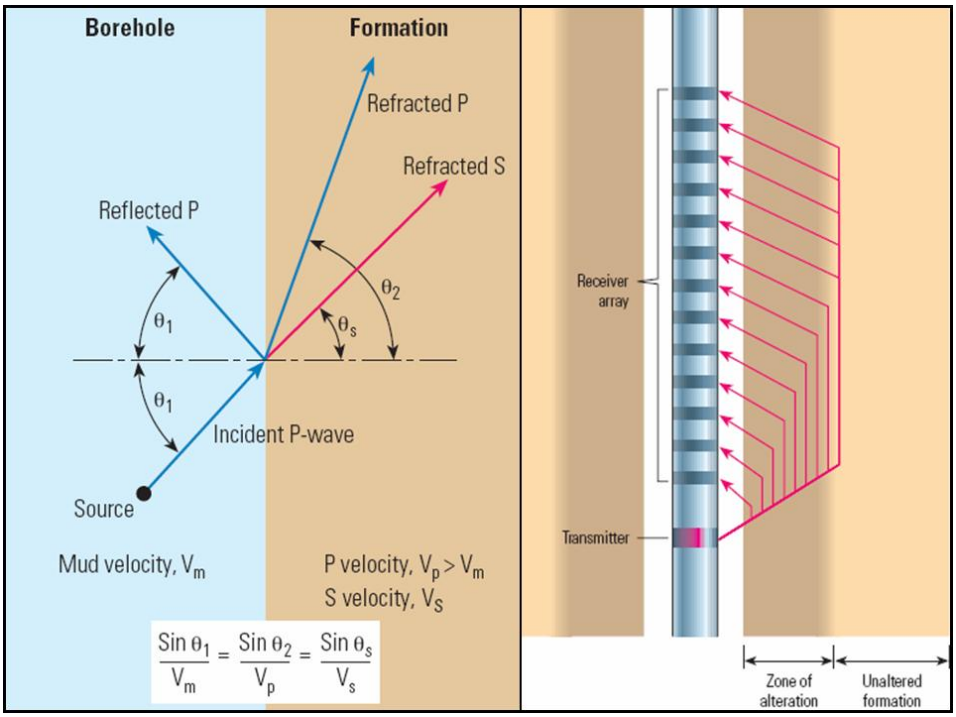

Fig.7: LEFT: Snellius' law applied on waves hitting the borehole-formation-interface. RIGHT: Ray tracing to explain the travel paths of waves in the altered and unaltered zone of a borehole form the transmitter to the receivers. (HALDORSEN et al., 2006)

2.2.2 Waves in and around boreholes II - Direct and reflected mud waves, trapped modes, interface waves

Mud waves arrive at the receiver after p- and s-waves (in case of monopole sources) in fast formations. They are followed by trapped modes and interface waves, which are a result of the cylindrical borehole geometry (HALDORSEN et al., 2006).

Trapped modes are the result of multiple internal reflections inside the borehole (HALDORSEN et al., 2006). An angle of incidence higher than the critical angle enables reflection of wave energy towards the borehole (BOYER & MARI, 1997).

Constructive interference of particular wavelengths of waves bouncing between the borehole walls produces a series of resonances (normal modes). In case of slow formations, parts of the energy of trapped modes propagate into the formation at speeds between v_p and v_s (dispersive leaky modes) (HALDORSEN et al., 2006). These “channelled” modes are normally undetectable because of rapid attenuation. Only in formations where the Poisson Ratio tends to 0.5 the energy of channelled modes is no more attenuated (BOYER & MARI, 1997).

2.2.3 Waves in and around boreholes III - Surface waves

The last arrivals from a monopole source are surface or interface waves. These are waves that propagate along a surface or an interface. Rayleigh Waves (Fig.8) travel along the Earth’s surface and involve a combination of transverse and longitudinal motions with definite phase relation to each other resulting in retrograde elliptical particle motion during the passage of the wave (TELFORD et al., 2004). Their amplitude shows a wavelength dependant (dispersive; different frequencies propagate at different speeds) and exponential decrease with depth (TELFORD et al., 2004). Rayleigh waves are dependant on elastic constants and show always velocities that are lower than shear wave velocity (TELFORD et al., 2004).

Love waves (Fig.8) occur in surface layers overlying a halfspace, leading to transverse particle motion parallel to the surface (TELFORD et al., 2004). The dispersive Love waves show velocities between the shear wave velocities of the surface layers and the shear wave velocities of deeper layers (TELFORD et al., 2004).

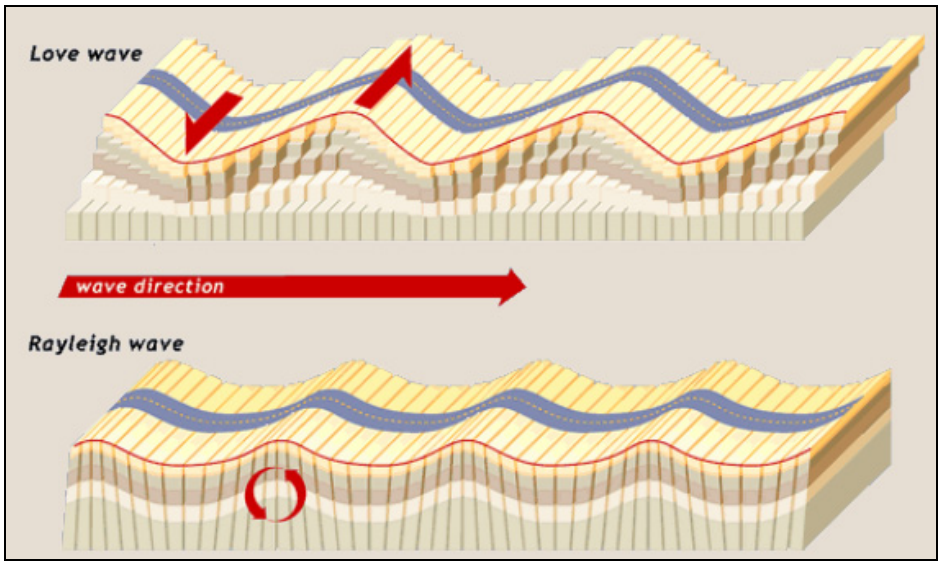

Fig.8: Propagation of Surface Waves. Transverse surface parallel particle motion of Love Waves and retrograde elliptical particle motion of Rayleigh Waves caused by surficial horizontal stress propagation. (http://www.exploratorium.edu/faultline/activezone/slides/rlwaves-slide.html, downloaded 18.12.2011).

In case of logging the waves propagate along the fluid-formation interface and are called Stoneley-, Scholte- or Stoneley-Scholte waves (HALDORSEN et al., 2006). These waves propagate at speeds lower than v_s and v_m. They are slightly dispersive and they show a frequency dependent amplitude decrease with increasing distance from the surface. High frequencies show rapid amplitude decay with distance from the borehole wall, whereas low frequencies (wave lengths comparable to the borehole diameter) show low amplitude decay with distance from the borehole wall. At sufficiently low frequencies the amplitude can remain +/- constant creating a tube wave (HALDORSEN et al., 2006; BOYER&MARI, 1997). Stoneley wave analysis can be used to estimate permeabilities and to detect open fractures (HALDORSEN et al., 2006). More detailed studies on this are published by:

Tang, X.M., Patterson, D., 2004, Estimating formation permeability and anisotropy from borehole Stoneley waves, SPWLA 45th Annual Logging Symposium, 2004, Joyce, R., Patterson D., and Thomas J., 1998, Advanced Interpretation of Fractured Carbonate Reservoirs Using Four-Component Cross-dipole Analysis, 39th Annual Mtg SPWLA, Keystone,CO (June 1998)

Pseudorayleigh waves are reflected, conical waves. They are dispersive. Low frequencies (<5kHz) show a velocity near to v_s; the velocity of high frequencies (>25kHz) show an asymptotic behaviour towards v_p (BOYER & MARI, 1997).

2.2.4 Velocity Anisotropy

In anisotropic media velocity is a function of propagation direction (SCHÖN, 1996). In geology 3 cases of anisotropy are realised (Fig.9) beside the linear elastic, isotropic case which can be defined with two constants (Young and Poisson or Lamé) (BARTON, 2007):

- The transversely isotropic case needs 5 constants for definition (BARTON, 2007). It is realised with a horizontal axis of symmetry (f.ex. vertical jointing) or with a vertical axis of symmetry (f.ex. layering) (BARTON, 2007). According to the axis of symmetry the abbreviations TIH (horizontal axis) and TIV (vertical axis) are used (SCHÖN, 2011).
- The orthorhombic anisotropy (with a vertical or a horizontal axis of symmetry) case needs 9 constants and is realized for example in a combination of horizontal bedding and vertical jointing (BARTON, 2007).

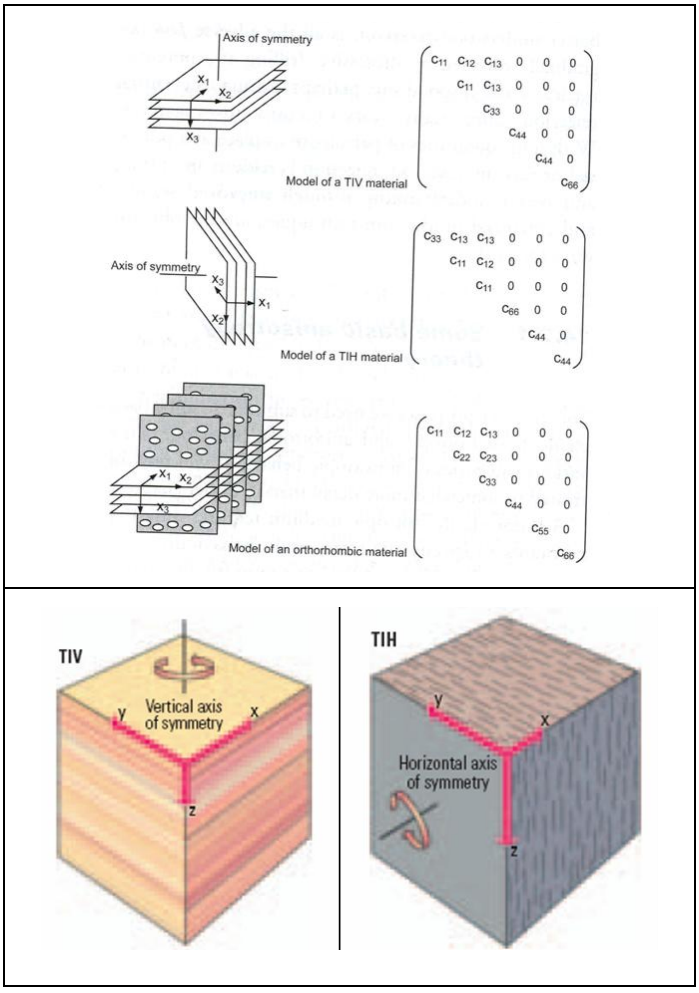

Fig.9: TOP Anisotropy in rock material and its tensor elements (: BARTON, 2007); BOTTOM:The TIH and TIV case of anisotropy in layered or fractured material HALDORSEN et al., 2006)

All anisotropy cases lead to direction dependant velocities and moduli (BARTON, 2007). Applied stress can change an isotropic media to an anisotropic one (BARTON, 2007).

SCHÖN.1996 and BARTON, 2007 summarize the source for “seismic anisotropy (SCHÖN, 1996)”:

- aligned crystals (SCHÖN, 1996)
- direct stress induced anisotropy (SCHÖN, 1996)
- lithological anisotropy (aligned grains) (SCHÖN, 1996), fabric induced anisotropy (slates, schistosis, foliation) (BARTON, 2007)
- structural anisotropy (layering) (SCHÖN, 1996), anisotropy by interbedding (BARTON, 2007)
- stress-aligned crack induced anisotropy (SCHÖN, 1996)
- microcrack and joint induced anisotropy (BARTON, 2007)
- rock joint induced anisotropy (BARTON, 2007)
- large scale fault induced anisotropy (BARTON, 2007)

SCHÖN, 2011 mentions separately clay minerals and their special features, which have influence on elastic properties and anisotropy:

- Clay distribution (structural, laminated, disperse)
- High diversity of clay minerals
- Intrinsic anisotropic properties of clay minerals
- Chemical and physical interactions between clay and fluids
- Compaction effects

SCHÖN, 1996 defines a general anisotropy coefficient: $A_v = \frac{v_{\max} - v_{\min}}{v_{\min}}$ (14)

and an anisotropy ratio $A_v^{\bullet} = \frac{v_{\max}}{v_{\min}} = A_v + 1$ (15)

to characterise anisotropic behaviour of rocks. THOMSEN, 1986 defines three parameters based on the tensor elements to describe the transverse anisotropic case:

$\varepsilon = \frac{c_{11} - c_{33}}{2c_{33}}$, $\gamma = \frac{c_{66} - c_{44}}{2c_{44}}$ and $\delta = \frac{(c_{13} + c_{44})^2 - (c_{33} + c_{44})^2}{2c_{33}(c_{33} - c_{44})}$ (16, 17, 18)

The crack induced anisotropy is pressure dependant (SCHÖN, 1996). Cracks are sensitive to stress changes (BARTON, 1996). Moderate pressures might close fractures in one direction whereas the other direction(s) remain(s) open (SCHÖN, 1996). A preferred closure of cracks aligned perpendicular to the stress direction leads to the largest velocity change in

the direction of the applied stress (BARTON, 2007). Under high pressures all fractures close and the anisotropy that is measured is the intrinsic anisotropy of the rock without fractures (SCHÖN, 1996). Increasing axial stress leads to an anisotropy decrease. The effect of anisotropy is larger for dry rocks than for saturated rocks (BARTON, 2007). Rock joints can cause 20-25% v_p-differences in dependence of measurement direction (BARTON, 2007). Randomly distributed cracks can reduce v_p isotropically compared to the unjointed rock (BARTON, 2007). The fast velocity directions are approximately parallel to the joint direction (BARTON, 2007). Random orientation occurs mainly under hydrostatic state of stress leading to isotropic elasticity (KING et al., 1997). A change in the stress state can lead to alignment and to anisotropic alignment, due to preferred closure of cracks with normals in the direction of the new major stress (KING et al., 1997). Anisotropy in this case is a function of stress change magnitude and pore shape and connectivity (KING et al., 1997). In shallow depths of the crust discontinuities are often aligned by tectonic stresses in a direction normal to the principal stress (KING et al., 1997).

2.2.5 Shear Wave splitting

Shear wave splitting is the division of a s-wave into two separate polarized s-waves travelling at different speeds when encountering an anisotropic medium (WIDARSONO et al., 1998).

Fig.10 shows the splitting of a shear wave in a fast and a slow wave caused by subvertical joints (BARTON, 2007). The difference in travel time is a function of fracture density and fracture compliance (BARTON, 2007). Normally (particle motion of) the faster wave is parallel to the direction of the maximum horizontal stress (BARTON, 2007). Any case of anisotropic behaviour can imply shear wave splitting (BARTON, 2007).

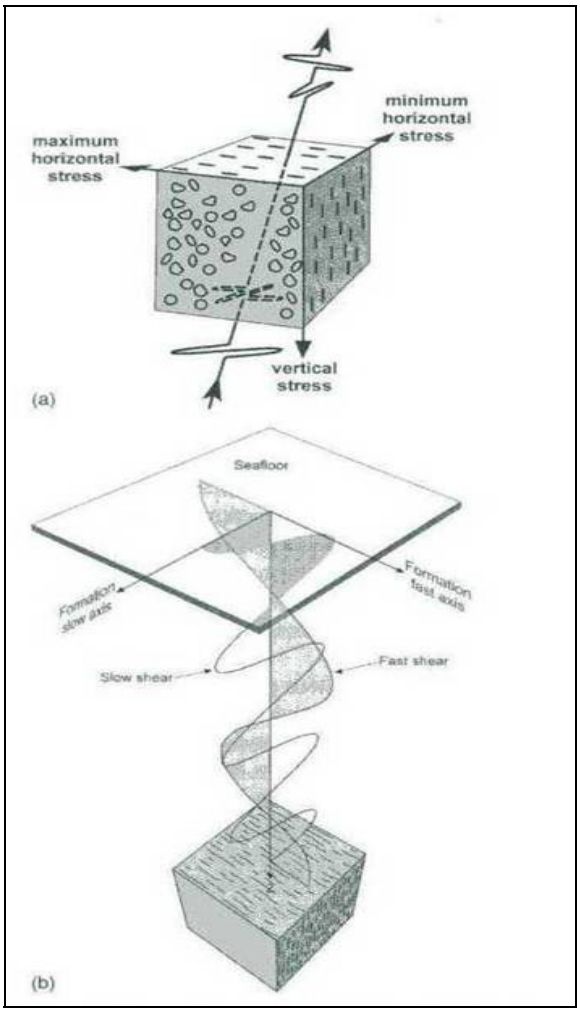

Fig.10: Shear wave splitting. Aligned cracks leading to separation of shear waves in a fast and a slow velocity component (from BARTON, 2007).

2.2.6 Physical Influences on wave velocities

Velocities in rocks are highly influenced by the high variability of geological materials (BARTON, 2007).

This chapter gives a very brief introduction to the main influences that are important in shallow geotechnical applications.

2.2.6.1 Lithology, Mineralogy

Fig.11 shows typical ranges for the compressional and shear wave velocities of different rock types and soils (SCHÖN, 2011).

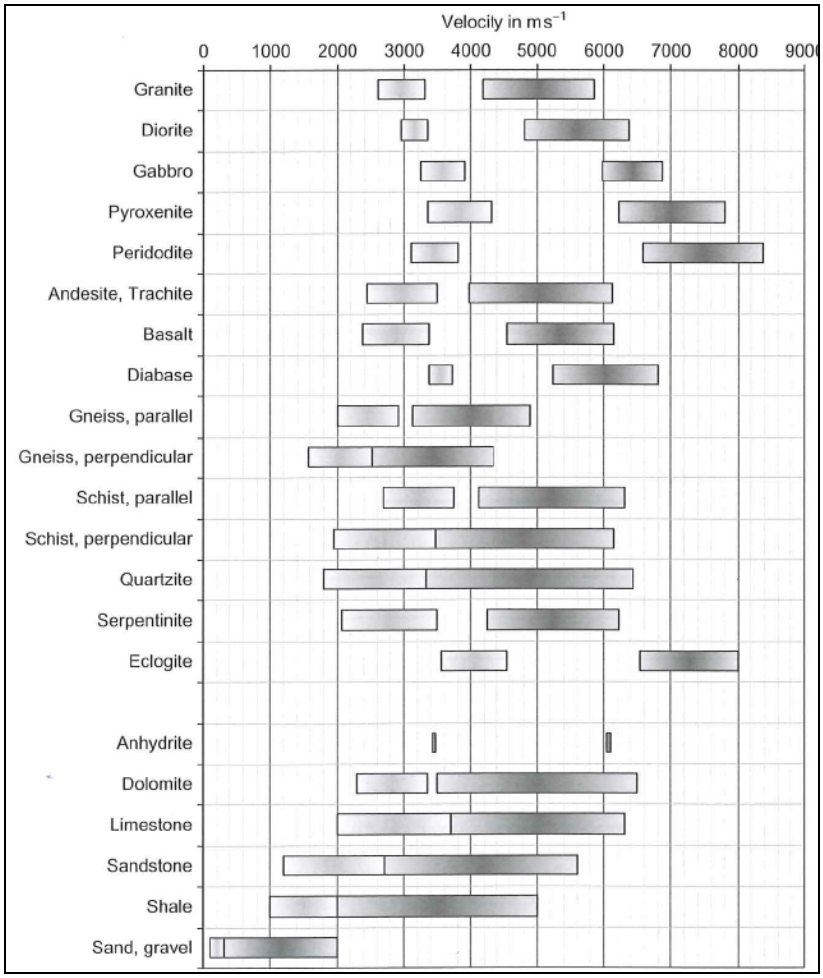

Fig.11: Different lithologies and their acoustic wave velocity. Compressional waves (higher velocities and shear waves (lower velocities) (SCHÖN, 2011)

SCHÖN, 2011 derives the following general trends for the different lithologies:

- Igneous rocks show increasing velocities from acidic to mafic members
- The range for an individual rock type is the result of variations of composition and fracturing
- Metamorphic gneiss and schist can show significant velocity anisotropy with higher velocities parallel to lamination
- The broad velocity range of sedimentary rocks is mainly based on the wide range of porosity
- The lowest velocities occur in dry, unconsolidated sediments as a result of specific grain-grain contacts and high porosity.

2.2.6.2 Density

Density of rocks generally shows stabilization below the weathered zone (BARTON, 2007). Several authors found linear relationships between density and v_p (BARTON, 2007). Density variations are mainly result of high stresses, porosity and mineralogy (BARTON, 2007).

2.2.6.3 Porosity

Porosity shows an approximately inverse proportionality to v_p (BARTON, 2007). Joints and pores are lowering velocities (SCHÖN, 1996). The reasons are changes in bonding between rock constituents and that different velocity of the pore filling (SCHÖN, 1996). SCHÖN, 1996 refers to the influence of structural-textural properties on velocity. Coarser grained granites show lower velocities than finer grained granites at same porosity for example (SCHÖN, 1996). High pressures and clays lead to nonlinearities in porosity distribution. Especially clay reduces v_p with porosity (BARTON, 2007, HAN et al., 1986). In the near surface region weathering is often responsible for the increase of porosity (BARTON, 2007). In high porosity rocks v_p is much stronger dependent on saturation than in low porosity rocks (BARTON, 2007).

2.2.6.4 Weathering, Moisture content and Fluid Saturation

Pore fluids are characterised by their modulus of compression k_f (SCHÖN, 1996). Fluids do not support shear wave propagation; their shear modulus G=0 (SCHÖN, 1996). The influence of pore fluids on the shear wave velocity is limited to density variations between different fluids (SCHÖN, 2011).

In gases wave propagation is an adiabatic process (SCHÖN, 1996) so that the modulus of compression is replaced by the adiabatic compressional modulus (SCHÖN, 1996). The wave velocity and compressibility of fluids depend on chemical composition, pressure and temperature (BATZLE and WANG, 1992). Pore fluids have an influence on the pore space properties and the can influence the particle contact conditions (SCHÖN, 2011). Fluid mixtures can create stress components from interfacial tension and capillary forces (SCHÖN, 2011).

The difference between velocities in a dry and a saturated rock increases with increasing porosity. In partial saturated rocks the elastic behaviour of the rock depends on elastic properties and densities of the pore fillings, the volume fraction of the components, the distribution of components in the pore space and the effect of boundary forces (SCHÖN, 1996). A heterogeneous distribution of saturation (patchy saturation) can lead to the fact that low frequencies can induce drainage of the pores and v_p is lowered (BARTON, 2007).

In the case of high frequencies the fluid relaxation time is large towards the seismic wave period and no drainage will occur leading to a relative higher v_p (BARTON, 2007).

Weathering is often responsible for a heterogenic increase of porosity (BARTON, 2007).

2.2.6.5 Pressure

Acoustic velocity (especially in porous rocks) is a strong function of differential or effective stress (ELLIS, 2007). Generally increasing pressures lead to increasing velocities (SCHÖN, 1996). This effect is smaller for dense rocks (SCHÖN, 1996). Velocity increase is also decreasing with increasing pressures (SCHÖN, 2011). Velocity increase is caused by porosity loss, improvements of grain contacts and (micro)crack closure with increasing pressure (SCHÖN, 2011).

The main factors for stress redistribution in geotechnical approaches are loading (structures) and unloading (excavations) (BARTON, 2007). Excavations often reduce v_p because of radial stress release, building of new joints and drying out (BARTON, 2007). v_p as a function of pressure gives “knee shaped curves” (BARTON, 2007). At very high pressures the velocity curve for the dry state and for the saturated state are converging (Fig.12) (BARTON, 2007). The saturated case shows the highest velocities because of the best coupling for the fractured case (BARTON, 2007).

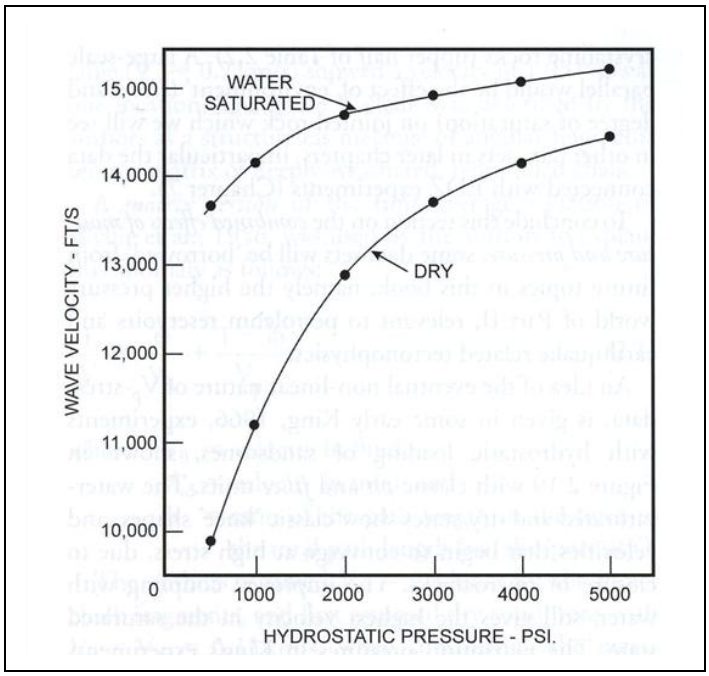

Fig.12: v_p as a function of saturation and hydrostatic pressure for sandstone (Barton, 2007).

Most rocks show sort of a velocity hysteresis. V_p increases with increasing pressure. The pressure effect is caused by closure of cracks (SCHÖN, 1996). The decrease of pressure results in a decrease of v_p, but not to the initial values. This might be interpreted as a fact for the non-reversability of crack opening (BARTON, 2007).

Overpressured zones (which are of interest in petroleum industry, tunnelling and deep mining) normally show high dynamic Poisson ratios (BARTON, 2007). This can be understood when looking at the relationship: $\nu = \frac{1}{2}(1 - \frac{1}{\frac{1}{3} + \frac{K}{G}})$ (BARTON, 2007) (19)

Increasing effective stress will close cracks and lead to a much higher increase of bulk modulus K than increase of shear modulus G (BARTON, 2007). Overall the Poisson ratio will increase (BARTON, 2007). This effect is larger in dry rocks than in saturated rocks (BARTON, 2007). Velocities as “overpressure indicator” are discussed for example by:

Fabricius, I.L., Høier,Chr., Japsen, P., Korsbech, U., 2007, Modelling elastic properties of impure chalk from South Arne Field, North Sea, Geophysical Prospecting, 2007, 55, 487–506

2.2.6.6 Temperature

Especially low temperatures are of interest in geotechnical problems. Ice formation leads to a 20-50% velocity increase for saturated rocks compared to room temperature (BARTON, 2007). The effect is negligible for dry rocks (BARTON, 2007). An interesting fact is that the smallest pores freeze latest because for their less favourable area/volume ratios (BARTON, 2007).

2.3 Correlations

This chapter should give a brief introduction and an overview on research according the correlation between different parameters obtained in situ and/or laboratory measurements. In a first step empirical relations for shear wave velocities from measured compressional wave velocities are introduced. They can provide a tool for shear wave velocity estimation in areas where no shear wave velocity could be obtained.

In a second step relations between static and dynamic moduli and between seismic velocities and the often used unconfined compression strength are summarized. The big advantage of geophysical in situ velocity measurements is that they offer continuous measurement profiles and in case of good correlations to the static point measurements, empirical relations can help in estimation of static parameters throughout larger rock or soil volumes.

2.3.1 Velocity correlation

Many authors tried to correlate seismic wave velocities as a key to determination of lithology from seismic or sonic logs or for seismic identification of pore fluids (MAVKO et al., 1998). Relations are also used to predict shear wave velocity (MAVKO et al., 1998). Table 2 lists some empirical relations out of literature.

Lithology	Regression	References
Sandstone	$v_{s,Sandstone} = 0.8042 v_p - 0.8559$ [km/s]	**CASTAGNA, 1985, THOMSEN, 1986, CASTAGNA et al., 1993**
Shale	$v_{s,Shale} = 0.7700 v_p - 0.8674$ [km/s]	**CASTAGNA, 1985, THOMSEN, 1986, CASTAGNA et al., 1993**
Dolomite	$v_{s,Dolomite} = 0.583 v_p - 0.078$ [km/s]	**CASTAGNA et al., 1993**
Dolomite	$v_s = \frac{v_p}{1.8}$ [km/s]	**Taken from MAVKO et al., 1998 (after PICKETT, 1963*)**
Limestone	$v_s = \frac{v_p}{1.9}$ [km/s]	**Taken from MAVKO et al, 1998 (after PICKETT, 1963*)**
Limestone	$v_{s,Limestone} = -0.055 v_p^2 + 1.017 v_p - 1.031$ km/s]	**CASTAGNA, 1985, THOMSEN, 1986, CASTAGNA et al., 1993**

Table 2: Empirical equations for shear wave velocity from literature.

) PICKETT., G.R., 1963. Acoustic character logs and their applications in formation evaluation: J. Can. Petr. Tech. , Vol.15, p. 659-667.

2.3.2 Static and dynamic Moduli

Moduli for the static (or very low frequency (WHITE, 1983)) case and the dynamic case show significant differences (BARTON, 2007). The dynamic moduli are higher than the static ones (DE VALLEJO & FERRER, 2011), reaching values of 5 to 10 times of the static ones (FJAER et al., 1992). The difference is largest for weak rocks and decreases with increasing pressure (FJAER et al., 1992). The biggest difference occurs for unconsolidated sediments due to grain dislocations and consolidation processes during static load (SCHÖN, 1983). The ratio especially rises in the near surface area (BARTON, 2007).

The differences are caused by the difference in time of stress application ($t_{stat} >> t_{dyn}$) and the difference in particle displacements (strain) (static>>dynamic) (SCHÖN, 1983). The very large difference of stress magnitudes between seismic or ultrasonic wave propagation and static testing techniques is also responsible for discrepancies between static and dynamic moduli (SCHÖN, 2011). During static deformation non-elastic components occur, whereas

ultrasonic and seismic measurements are mainly affected by the elastic response (SCHÖN, 2011). A part of the discrepancies is caused by fluid effects (FJAER et al., 1992).

Fig.13 shows the dependence of shear modulus on strain magnitude and some in situ method examples with the typical strain levels they can achieve (LOOK, 2007).

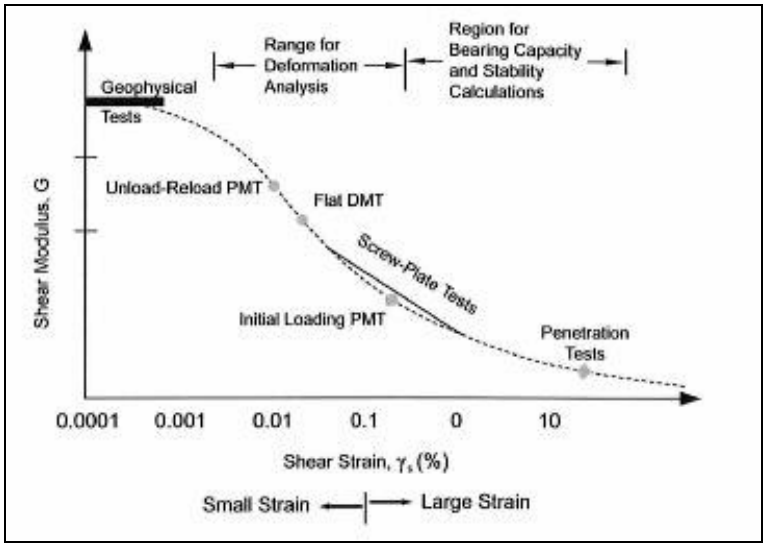

Fig.13: Example of dependence of shear modulus of the strain level that can be achieved with different methods. Dynamic geophysical methods offer the lowest strain levels and therefore the highest moduli (LOOK, 2007).

Dynamic moduli also show frequency dependence, mainly influenced by the frequency dependant mobility of fluids in the pores (CHANG et al., 2006). Generally dynamic (compressional) moduli increase with saturation (CHANG et al., 2006). This effect is higher at higher porosities and differs with fluid type (CHANG et al., 2006). Static Young's Modulus varies depending on loading/unloading path (CHANG et al, 2006). Only in dense rocks the static moduli approach the dynamic ones (SCHÖN, 1983). With increasing porosity and fracturing the difference between static and dynamic moduli increases (SCHÖN, 1983).

In Fig.14 and 15 the observed tendencies for relations between static and dynamic moduli of rocks and unconsolidated materials are presented. SCHÖN, 2011 remarks that due to the magnitude of data scatter especially for unconsolidated materials derived relations are only a raw approximation. They must be derived in each case and for the individual rock type (SCHÖN, 2011). SCHÖN, 2011 also mentions that the use of shear wave velocity should result in better correlations, because shear wave velocities are controlled by the skeleton properties of the rock and these skeleton properties predominantly control static mechanical properties (SCHÖN, 2011).

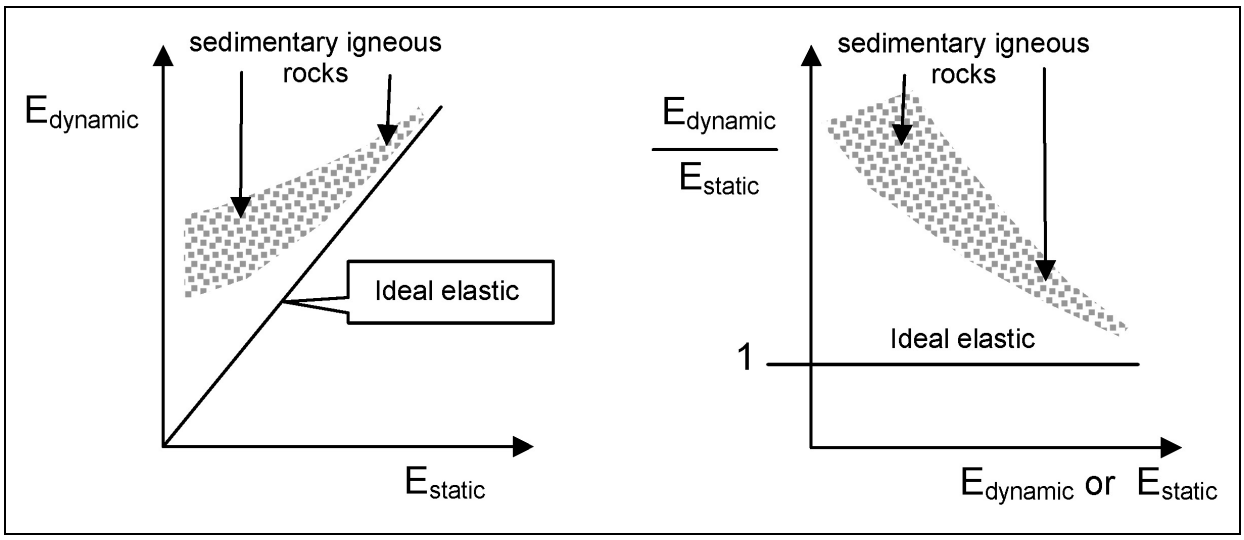

Fig.14: Relation between static and dynamic moduli and the ratio of the moduli versus static or dynamic modulus of rocks. The difference between static and dynamic parameters decreases from rocks with low moduli (or velocities) to rocks with high moduli (or velocities) and from unconsolidated sediments to compact, unfractured rocks (SCHÖN, 2011)

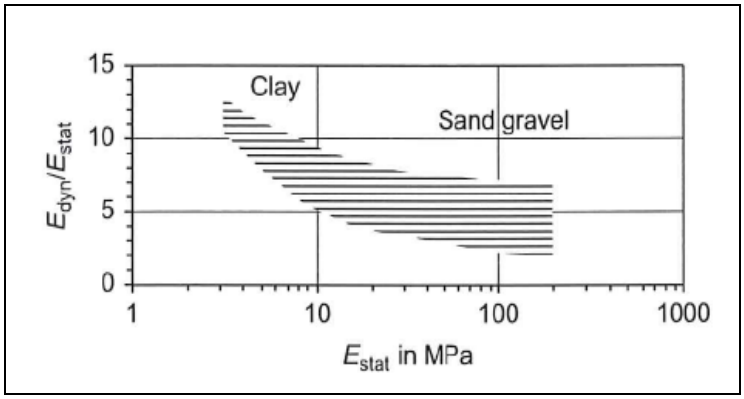

Fig.15: Relation between the static/dynamic ratio and the static modulus in unconsolidated materials (after SCHÖN, 2011).

Fig.16 shows an example for a well working correlation on a granitic rock (taken from SCHÖN, 2011)

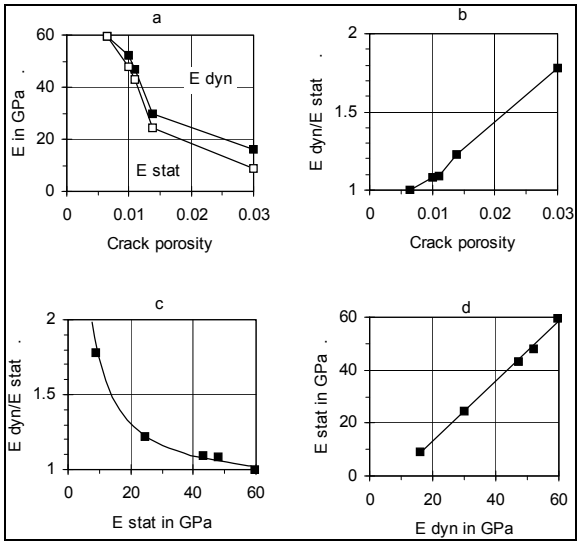

Fig.16: Static and dynamic determined Young's modulus for microcline-granite (figures taken from SCHÖN, 2011; after BELIKOV et al., 1970*))

a) E_{stat} **and** E_{dyn} **as function of the crack porosity** ϕ_c **;**

b) ratio E_{dyn}/E_{stat} **as function of the crack porosity** ϕ_c **;**

c) ratio E_{dyn}/E_{stat} **as function of the static modulus** E_{stat} **;**

d) Correlation between E_{dyn} **and** E_{stat} **.**

) BELIKOV, B.P., ALEXANDROV, K.S., RYSOVA, T.W., 1970. Uprugie Svoistva Porodo-Obrasujscich Mineralvi Gornich Porod. Izdat. Nauka, Moskva.

The Bulk Modulus shows decreasing difference between the static and the dynamic approach with increasing pressure due to compaction and closure of fractures (SCHÖN, 2011).

Table 3 gives a summary on empirical relations between dynamic and static moduli:

Equation	Material	Methods involved	Reference	Unit
$E_{stat} = 0.675E_{dyn} - 3.84$ $k_{stat} = 0.992k_{dyn} - 8.82$ $\mu_{stat} = 0.621\mu_{dyn} - 0.,95$	Brazilian limestone	Triaxial cell and 500kHz sonic measurement	SCHÖN, 2011 after BASTOS et al., 1998*)	[GPa]
$E_{stat} = 0.69E_{dyn} + 6.40$	Jurassic sediments and granites (GB)	FWS-Log and laboratory measurements	MCCANN & ENTWISLE, 1992	[GPa]
$E_{stat} = 0.48E_{dyn} - 3.26$	Swedish igneous and metamorphic rocks	Laboratory measurements	SCHÖN, 2011 after STARZEC, 1999**)	[GPa]
$E_{stat} = 0.076(\frac{304.8}{\Delta t_p})^{3.23}$ $\mu_{stat} = 0.03(\frac{304.8}{\Delta t_p})^{3.30}$	North Sea shales	Travel time in µs/ft Modulus in GPa	HORSRUD, 2001	[GPa] [km/s]
$E_{stat} = 0.085E_{dyn} + 3.0$	Unconsolidated sediments, sand	Shallow seismic measurements an soil mechanic tests	SCHÖN, 2011 after GORJAINOV&LJACHOWICKIJ, 1979***)	[MPa]
$E_{stat} = 0.033E_{dyn} + 6.5$	Unconsolidated sediments, Clay	seismic measurement, soil mechanic tests	SCHÖN, 2011 after GORJAINOV& JACHOWICKIJ, 1979***)	[MPa]

Table 3: Empirical Relations between static and dynamic moduli after literature

)BASTOS, A.C., DILLON, L.D., VASQUEZ, G.F., SOARES, J.A., 1998. Core derived acoustic, porosity and permeability correlations for computation pseudo logs. IN: HARVEY, P.K., LOVELL, M.A. (eds.), Core-Log-Integration, 136. Geological Society, London, pp. 141-146, Special Publication.

)STARZEC, P., 1999. Characterization of the physical properties of rocks. Department of Geology, Chalmers University of Techology, Sweden, Publ. A 90.

****)GORJANINOV, N.N., LJACHOVICKIJ, F.M., 197. Seismiceskie Metody v Insenernoi Geologii. Izdat Nedra, Moskva.***

2.3.3 Unconfined compression Strength (UCS) and internal angle of friction

CHANG et al, 2006 mention UCS and internal angle of friction as key parameters for geomechanical problems. The internal angle of friction is a measure of dependence of rock strength on confining pressure (CHANG et al., 2006). Internal angle of friction and UCS can be used to construct failure criteria (CHANG et al., 2006). Empirical relations can especially be used for estimation of lower boundary of rock strength (CHANG et al., 2006). The correlation between strength properties and seismic velocities is based on the dominant influence of fracturing, porosity and cementation on both parameters (SCHÖN, 2011). Increasing fracturing and/or porosity leads to a decrease of strength and seismic velocities whereas an increase in cementation leads to an increase of both properties (SCHÖN, 2011).

Empirical relations can be used to correlate rock strength with parameters that are measurable with geophysical well logs, especially in areas where no core material is available (CHANG et al., 2006). Compressional wave velocity or interval transit time (slowness), Young's Modulus and porosity are the main geophysical log parameters used for empirical relations (CHANG et al, 2006). Rock strength decreases with transit time and porosity and increases with Young's Modulus (CHANG et al., 2006). All relations need local calibration (CHANG et al., 2006).

Fig.17 to 20 show different empirical equations for UCS of sandstones, shales and limestones from different index parameters (velocities, transit time, porosity, density,…) compiled after CHANG et al., 2006. For sandstones most of the equations underpredict the strength at high transit times (low velocities) (CHANG et al., 2006). Porosity is not a good strength indicator for low porosity sandstones, but a good strength indicator for shales with high porosities (CHANG et al., 2006). In general the angle of internal friction shows an increasing trend with v_p and a decreasing trend with increasing porosity (CHANG et al., 2006).

Eq. no.	UCS (MPa)	Region where developed	General comments	Reference
(1)	$0.035V_p - 31.5$	Thuringia, Germany	–	Freyburg (1972)
(2)	$1200\exp(-0.036\Delta t)$	Bowen Basin, Australia	Fine grained, both consolidated and unconsolidated sandstones with all porosity range	McNally (1987)
(3)	$1.4138 \times 10^7 \Delta t^{-3}$	Gulf Coast	Weak and unconsolidated sandstones	
(4)	$3.3 \times 10^{-20} \rho^2 V_p^4 [(1+\nu)/(1-\nu)]^2(1-2\nu)[1+0.78V_{clay}]$	Gulf Coast	Applicable to sandstones with UCS > 30 MPa	Fjaer et al. (1992)
(5)	$1.745 \times 10^{-9} \rho V_p^2 - 21$	Cook Inlet, Alaska	Coarse grained sandstones and conglomerates	Moos et al. (1999)
(6)	$42.1\exp(1.9 \times 10^{-11} \rho V_p^2)$	Australia	Consolidated sandstones with $0.05 < \phi < 0.12$ and UCS > 80 MPa	
(7)	$3.87\exp(1.14 \times 10^{-10} \rho V_p^2)$	Gulf of Mexico	–	
(8)	$46.2\exp(0.027E)$	–	–	
(9)	$2.28 + 4.1089E$	Worldwide	–	Bradford et al. (1998)
(10)	$254\,(1-2.7\phi)^2$	Sedimentary basins worldwide	Very clean, well-consolidated sandstones with $\phi < 0.3$	Vernik et al. (1993)
(11)	$277\exp(-10\phi)$	–	Sandstones with $2 < UCS < 360$MPa and $0.002 < \phi < 0.33$	

Fig.17: Empirical Equations for UCS-estimation of sandstones (taken from CHANG et al., 2006, unreferenced equations have been unpublished, references below).

FREYBURG, E., 1972. der Untere und mittlere BuntsandsteinSW-Thüringen in seinen gesteinsmechanischen Eigenschaften. Ber. Dtsch. Ges. Geol. Wiss., A; Berlin 176, 911-919.

McNally, G.H., 1987. Estimation of coal measures rock strength using sonic and neutron logs. Geoexploration 24, 381-395. FJAER, E., HOLT, R.M., HORSUD, P., RAAEN, A.M., RISNES, R., 1992. Petroleum Related Rock Mechanics. Elsevier, Amsterdam.

MOOS, D., ZOBACK, M.D., BAILEY, L., 1999. Feasability study of the stability of openhole multilaterals, Cook Inlet, Alaska. 1999 SPE Mid-Continent Operations Symposium held in Oklahoma City, Oklahoma, 28-31 March 1999, SPE 52186

BRADFORD, I.D.R., FULLER, J., THOMPSON, P.J., WALSGROVE, T.R., 1998. Benefits of assessing the solids production risk in a North Sea reservoir using elastoplastic modelling. SPE/ISRM Eurock '98 held in Trondheim, Norway, 8-10 July, 1998, pp. 261-269.

VERNIK, L., BRUNO, M., BOVBERG, C., 1993. Empirical relations between compressive strength and porosity of siliciclastic rocks. Int. J. Rock. Mech. Min. Sci., Geomech. Abstr, 30, 677-680.

Eq. no.	UCS (MPa)	Region where developed	General comments	Reference
(12)	$0.77\,(304.8/\Delta t)^{2.93}$	North Sea	Mostly high porosity Tertiary shales	Horsrud (2001)
(13)	$0.43\,(304.8/\Delta t)^{3.2}$	Gulf of Mexico	Pliocene and younger	
(14)	$1.35\,(304.8/\Delta t)^{2.6}$	Globally	–	
(15)	$0.5\,(304.8/\Delta t)^3$	Gulf of Mexico	–	
(16)	$10\,(304.8/\Delta t - 1)$	North Sea	Mostly high porosity Tertiary shales	Lal (1999)
(17)	$7.97E^{0.91}$	North Sea	Mostly high porosity Tertiary shales	Horsrud (2001)
(18)	$7.22E^{0.712}$	–	Strong and compacted shales	
(19)	$1.001\phi^{-1.143}$	–	Low porosity ($\phi < 0.1$) high strength (~79 MPa) shales	Lashkaripour and Dusseault (1993)
(20)	$2.922\phi^{-0.96}$	North Sea	Mostly high porosity Tertiary shales	Horsrud (2001)
(21)	$0.286\phi^{-1.762}$	–	High porosity ($\phi > 0.27$) shales	

Fig.18: Empirical Equations for UCS estimation of shales (taken from CHANG et al., 2006, unreferenced equations have been unpublished, references after CHANG et al., 2006 below)

HORSRUD, P., 2001. Estimating mechanical properties of shale from empirical correlations. SPE drill. Complet. 16, 68-73.

LAL, M., 1999. Shale stability: drilling fluid interaction and shale strength. SPE Latin American and Caribbean Petroleum Engineering Conference held in Caracas, Venezuela.

LASHKARIPOUR, G.R., DUSSEAULT, M.B., 1993. A statistical study on shale properties, relationship among principal shale properties. Proc. Conference on Probablistic Methods in Geotechnical Engineering, Canberra, Australia, 195-200.

Eq. no.	UCS (MPa)	Region where developed	General comments	Reference
(22)	$(7682/\Delta t)^{1.82}/145$	–	–	Militzer and Stoll (1973)
(23)	$1(^{(2.44+109.14/\Delta t)}/145$	–	–	Golubev and Rabinovich (1976)
(24)	$13.8E^{0.51}$	–	Limestone with 10<UCS<300 MPa	
(25)	$25.1E^{0.34}$	–	Dolomite with 60<UCS<100 MPa	
(26)	$276\,(1-3\phi)^2$	Korobcheyev deposit, Russia	–	Rzhevsky and Novick (1971)
(27)	$143.8\exp(-6.95\phi)$	Middle East	Representing low to moderate porosity ($0.05<\phi<0.2$) and high UCS (30<UCS<150 MPa)	
(28)	$135.9\exp(-4.8\phi)$	–	Representing low to moderate porosity ($0<\phi<0.2$) and high UCS (10<UCS<300 MPa)	

Fig.19 Empirical Equations for UCS estimation of limestones and dolomites (taken from CHANG et al., 2006, unreferenced equations have been unpublished, references after CHANG et al., 2006 below).

MILLITZER, H., STOLL, R., 1973. Einige Beiträge der geophysics zur primadatenerfassung im Bergbau, neue Bergbautechnik, Lipzig 3, 21-25.
GOLUBEV, A.A., RABINOVICH, G.Y., 1976. Resultaty primeneia apparatury akusticeskogo karotasa dlja predeleina proconstych svoistv gornych porod na mestorosdeniaach tverdych isjopaemych. Prikl. Geofiz. Moskva 73, 109-116.
RZHEVSKY, V., NOVICK, G., 1971. The Physics of Rocks. MIR Publ..320pp.

Eq. no.	Φ (degree)	General comments	Reference
(30)	$\sin^{-1}((V_p-1000)/(V_p+1000))$	Shale	Lal (1999)
(31)	$57.8-105\phi$	Sandstone	Weingarten and Perkins (1995)
(32)	$\tan^{-1}\left(\frac{(GR-GR_{sand})\mu_{shale}+(GR_{shale}-GR)\mu_{sand}}{GR_{shale}-GR_{sand}}\right)$	Shaley sedimentary rocks	

Fig.20: Empirical Equations for UCS estimation of siliciclastic rocks from internal angle of friction (taken from CHANG et al., 2006, unreferenced equations have been unpublished, references after CHANG et al., 2006 below).

LAL, M., 1999. Shale stability: drilling fluid interaction and shale strength. SPE Latin American and Caribbean Petroleum Engineering Conference held in Caracas, Venezuela.
WEINGARTEN, J.S., PERKINS, T.K., 1995. Prediction of sand production in gas wells: methods and Gulf of Mexico case studies. J. Petrol. Tech. 596-600.

3 Available methods and data

The following table (Table 4) gives an overview on the data material that was available for this report and the methods that were used to obtain data. Descriptions of the involved methods can be found in the appendix. Details to the sites and projects cannot be published, due to the fact that “sensitive” projects (nuclear power plants for example) are involved and due to the fact that some projects are still in progress.

Country	Project	Dominant lithology	Stat. lab	Stat. in situ	Dyn. lab	Dyn. in situ
USA	NPP	Shaly limestones Sandstones Shale Unconsoloditated sediments	3-AX 1-AX	-	USP shear wave only	SASW/MASW PSSL DH
Austria	Express Highway	Granites (Grano)Diorites Aplites Pegmatites	3-AX 1-AX	DIL	-	FWS+GGD
Austria	Tunnel	Metamorphic rocks (mainly gneisses)	3-AX 1-AX	-	-	FWS+GGD
Hong Kong	Seismic Microzonation	Metasediments Vulcanoclastics Unconsolidated sediments	-	-	-	PSSL CH DH
UK	NPP	Metasediments Microgabbro	3-AX 1-AX	DIL	USP compressional and shear wave	PSSL
Dubai	Infrastructure	Sedimentary rocks Sands	1-AX	-	-	CH
Quatar	Infrastructure	Sedimentary Rocks	1-ax	-	-	PSSL

Table 4: Overview on sites, dominant lithologies and methods that were available fort his report.

Abbreviations:

NPP	Nuclear Power Plant
3-AX	3-axial tests
1-AX	Unconfined Compression Tests
DIL	Dilatometer tests
SASW/MASW	(Multichannel) Analysis of surface waves
PSSL	PS Suspension Logging
FWS+GGD	Full waveform sonic logging with Gamma-Gamma density logging
DH	Downhole seismics
CH	Crosshole seismics
USP	Ultrasonic pulse velocity measurements

4 Comparison of different dynamic methods

Before analysing relationships between static and dynamic methods, a closer look on the dynamic methods for velocity measurements is performed. In this chapter velocities from different available methods are directly compared. A similar comparison for the static methods was unfortunately not possible, because of lacking “data intersection”.

Directly means that it was tried to compare only velocity values that were measured in the same borehole and the same depth (except the velocities obtained with Multichannel Analysis of Surface Waves - MASW). MASW velocities have been compared with velocity values measured with other methods in boreholes as close as possible to the MASW profiles (several meters to several tens of meters away from the MASW profiles).

Fig.21 shows a direct comparison of shear wave velocity measurements with MASW, PS Suspension Logger (PSSL) and downhole seismic measurements in a succession of (shaly) limestones, shales and (shaly) sandstones in the US. Downhole seismics and PSSL have been measured in the same boreholes (BH-1 in Fig.21 left and BH-2 Fig.21 right). MASW measurements were performed very close to the boreholes. The log shows that MASW and PSSL are correlating rather well for both boreholes. The differences between these two methods are mainly caused by the higher vertical resolution of PSSL, which allows displaying smaller scale velocity variations that are not resolved by MASW. A point that must also be taken into account is the difference in measurement frequencies. MASW uses frequencies in the range of a few to a few tens of Hz, whereas PSSL uses frequencies in the range of 0.5 to 5 kHz.

Compared to these two methods, the downhole measurements offer rather ambivalent results. In some areas the downhole velocities correlate very well with the velocities measured with the two other methods, but there are more sections were downhole velocities are far away from the velocities measured with the other two methods. Reason for that might be that the increasing source receiver offset of the downhole measurement leads to increasing attenuation of (especially) higher frequencies in the increasing investigated rock or soil volume. This loss of the higher frequencies increases difficulties in first arrival picking, especially for the shear wave.

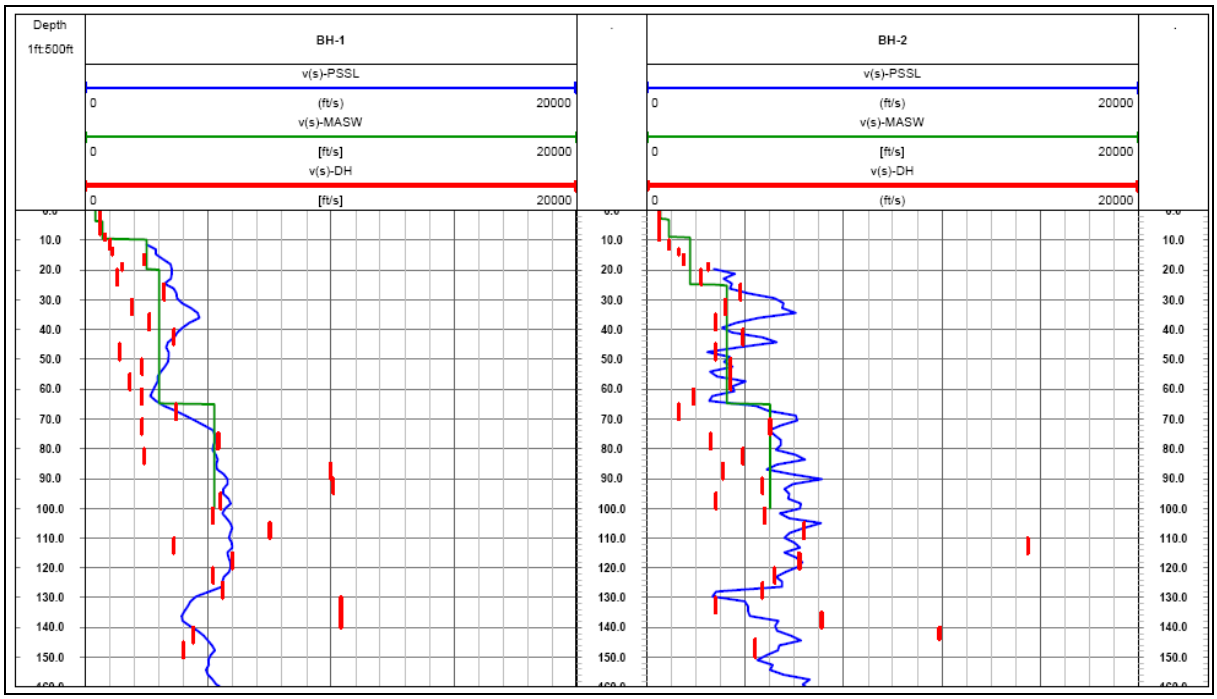

Fig.21: Direct comparison of shear wave velocity measurements with PSSL, MASW and downhole seismics. MASW and PSSL velocities show good correlation. Differences are mainly based on different vertical resolutions (PSSL>MASW) and different measurement frequencies (PSSL>MASW). Downhole velocities show good correlation in some sections and rather bad or no correlation in other sections.

Fig.22 shows a similar plot for direct comparison of v_p from downhole seismic and PSSL and v_s from crosshole seismic, PSSL and downhole measurements in a metamudstone formation in Hong Kong overlain by a few meters of unconsolidated silty sediments. Crosshole measurements have been performed with “splitted” shear waves, meaning that a source has been used, that is capable of activating horizontal propagating, vertical polarized ($v_{s,hv}$) and horizontal propagating, horizontal polarized ($v_{s,hh}$) shear waves. The comparison of v_p (left log) shows a large difference between PSSL and downhole measurements (up to 500 m/s). This might be caused by a combination of a frequency effect, (larger scale) fracturing of the formation and alteration of the borehole wall. Of course the already mentioned effect of high frequency energy loss might play a role too. Shear wave velocity comparison shows that the three methods correlate well up to a depth of about 17.0 m. Beyond this depth PSSL (where available) and crosshole follow a similar shear wave velocity trend, whereas downhole velocities show an increasing difference to the other two methods. The shear wave profile derived from downhole measurements shows rather constant v_s, which seems to be unreliable for the deeper regions of the borehole.

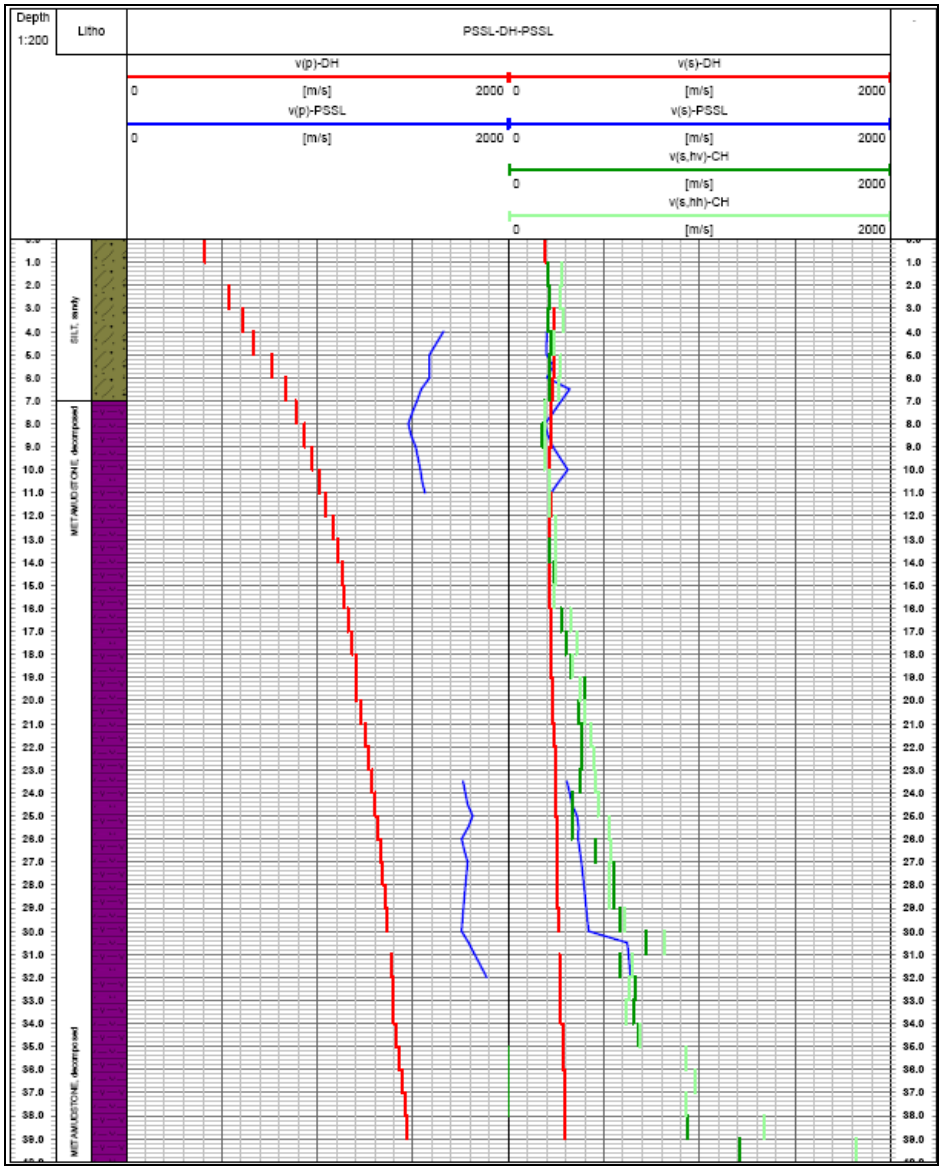

Fig.22: Direct comparison of v_p from downhole and PSSL-measurements (LEFT) and v_s from downhole, PSSL and splitted shear wave crosshole measurements.

In Fig.23 the shear wave velocities from the same data set as in Fig.22 measured with crosshole and PSSL are compared in a velocity crossplot. Generally the velocities show very good correlation and seem to fit to a linear trend. A small population of PSSL velocities shows slightly lower velocity values than the crosshole velocities. This might be interpreted as result of borehole sections with significant wall alteration, which does not really affect crosshole velocities, but has a significant influence on PSSL measurements. Another explanation might be that the difference between the horizontal propagating waves used for crosshole measurements and the vertical propagating waves of PSSL are caused by anisotropic behaviour of the material.

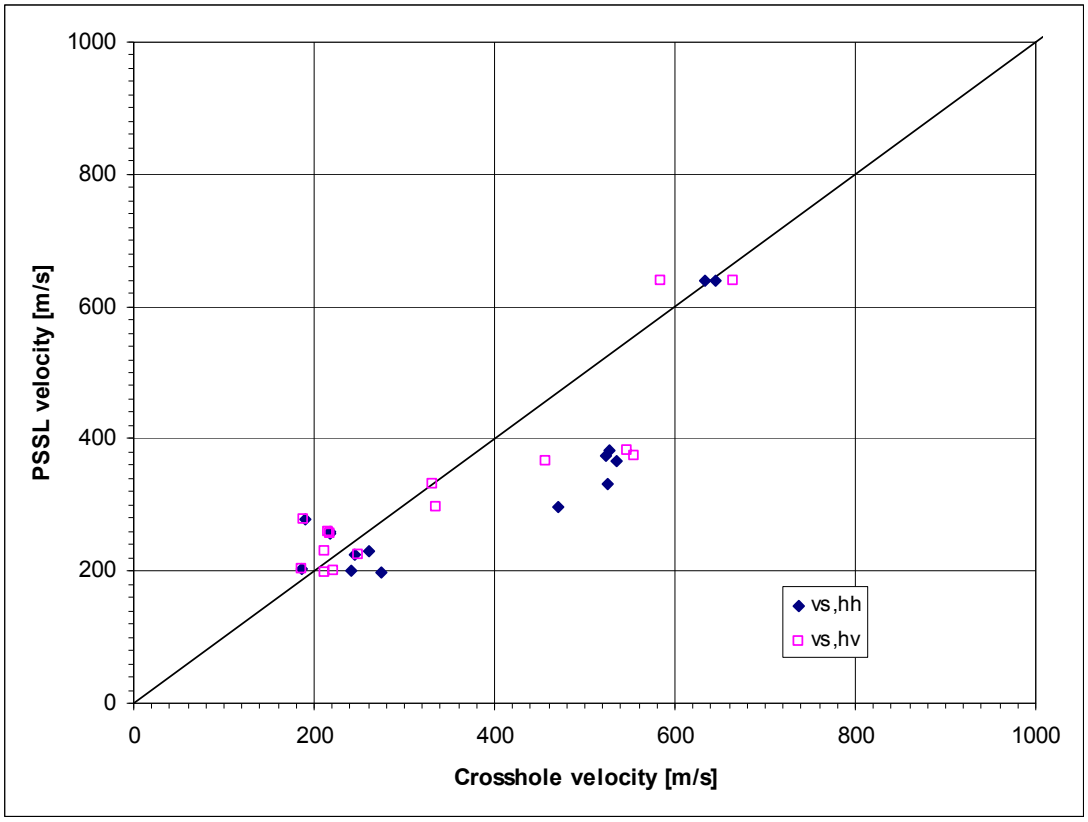

Fig.23: Velocity crossplot to compare shear wave velocities measured with PSSL and crosshole measurements (dual measurements with horizontal and vertical polarized and horizontal propagating shear waves). Generally a good correlation can be observed. A small population of PSSL velocities shows slight deviation from the line of direct proportionality, maybe caused by a higher borehole wall alteration or anisotropy.

The dual crosshole measurements using horizontal propagating shear waves with vertical ($v_{s,hv}$) and horizontal ($v_{s,hh}$) polarization (shear wave splitting) can also be used to estimate velocity anisotropy of the formation(Fig.24), as already indicated by the comparison of crosshole and PSSL measurements. The crossplot of the two shear wave velocities (Fig.24 TOP) already suggests slight anisotropy. A calculated trend line leads to increasing anisotropy with increasing shear wave velocity. Plotting the velocity ratio against the shear wave velocity shows the anisotropic behaviour of the encountered formations a bit better. The velocity ratio reaches values up to 1.6.

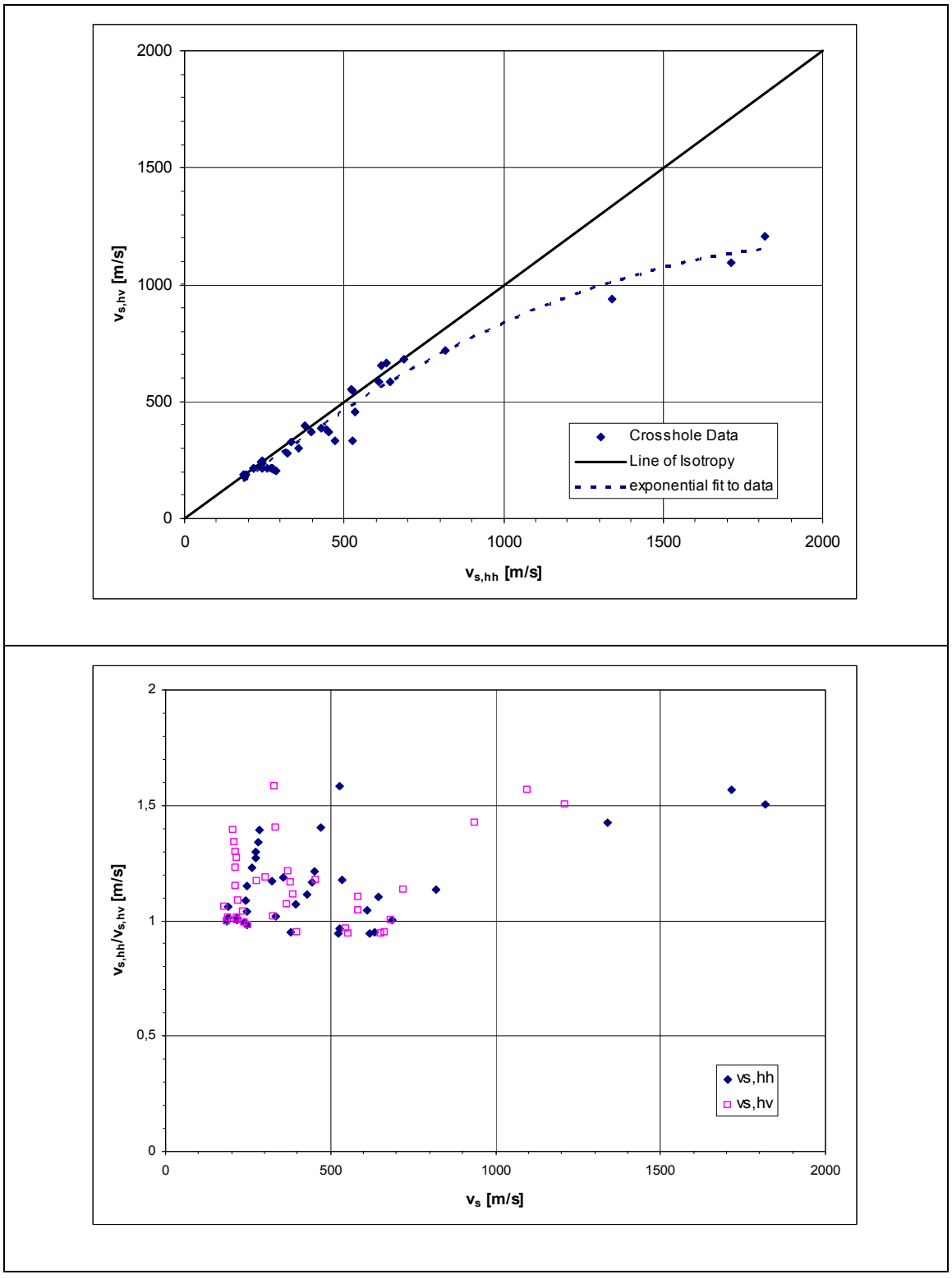

Fig.24: TOP: Velocity of a horizontal propagating, vertical polarized shear wave ($v_{s,hv}$) as a function of the velocity of a horizontal propagating and horizontal polarized shear wave ($v_{s,hh}$) derived from crosshole seismic data. The exponential fit to the data suggests an increasing anisotropy with increasing velocity.

BOTTOM: Crossplot of shear wave velocity ($v_{s,hh}$ and $v_{s,hv}$ versus $v_{s,hh}$/ $v_{s,hv}$-ratio indicating a significant effect of shear wave splitting, which can be interpreted as sign of formation velocity anisotropy.

In Fig.25 downhole measurements and PSSL measurements in two formations are compared. The downhole measurements show very low wave velocities of doubtful reliability. The PSSL measurements offer more scattering data, but the velocities are higher and are therefore seen to be more reliable than the downhole velocities. A small amount of the difference might be caused by a frequency effect. The main problem here might be that first arrival picking on downhole data in highly attenuating formations is very difficult and can lead to mispicks. The PSSL method (or also FWS) with a low and constant source receiver offset should be preferred (if possible).

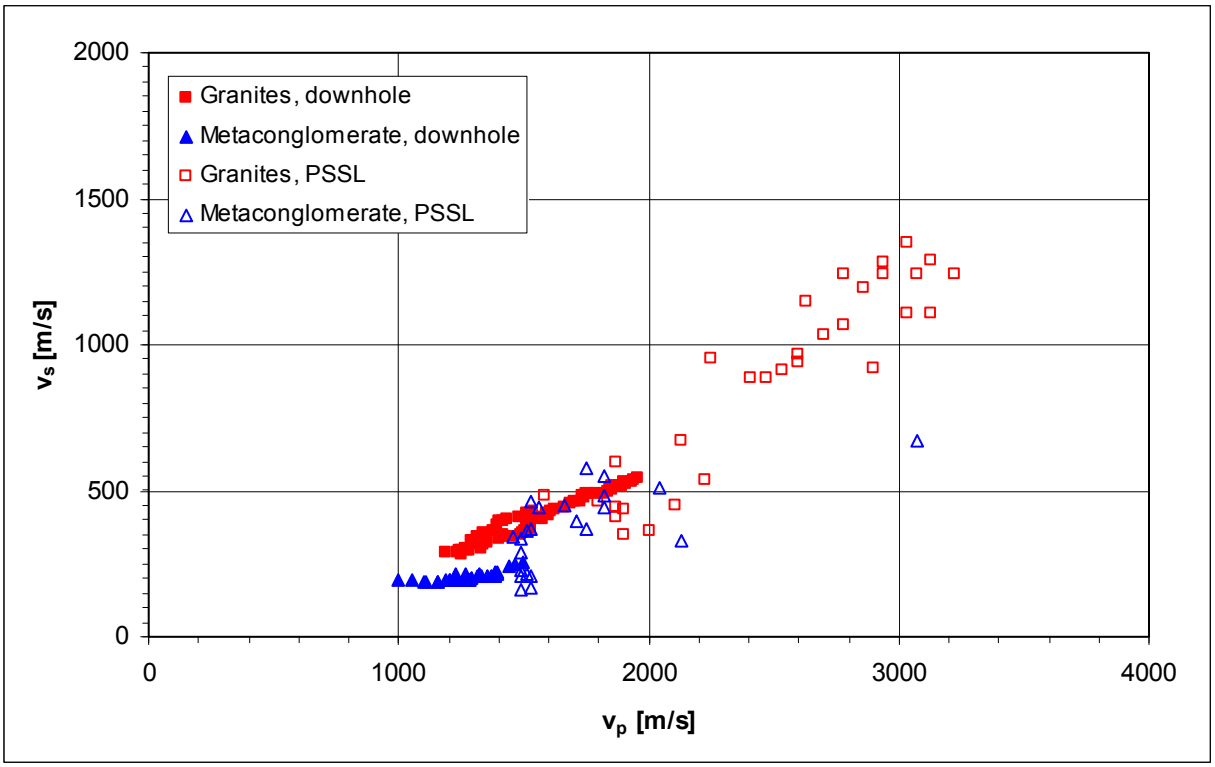

Fig.25: v_p-$v_s$crossplot for downhole and PSSL velocities, measured in the same depths in the same metaconglomerate and granite formation, but not in the same borehole. Downhole velocities for both lithologies show a good linear trend but compared to the PSSL velocities they are significantly lower.

Fig.26 shows direct comparison between PSSL and downhole velocity measurements in a succession of (shaly) limestones, shales and (shaly) sandstones. Except a population of data points with deviating high downhole velocities, which cannot be reasoned for sure; the two methods offer moderate to good correlating compressional and shear wave velocities.

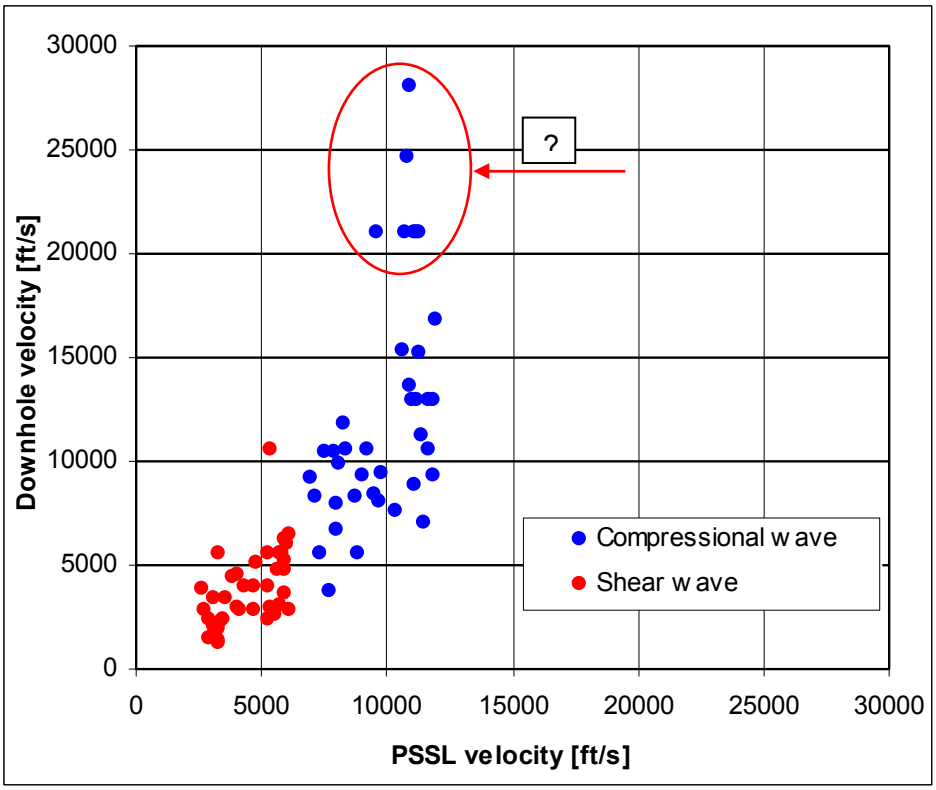

Fig.26: Direct comparison of downhole and PSSL measurements in a succession of (shaly) limestones, shales and (shaly (sandstones). Except the marked data point population the correlation is good to moderate.

A comparison of velocities from laboratory and PSSL measurements is shown in Fig.27 and Fig.28. The two methods show generally good correlation for compressional and shear wave velocity. Laboratory velocities seem to be slightly higher, what might be mainly a result of the higher measurement frequencies in laboratory and the use of compact samples without fractures in case of laboratory specimens. In Fig.27 two outliers can be observed in the high laboratory velocity region >12500 ft/s. This might be caused by measurements on a very clean and rather unaltered limestone sample or the compressional wave velocities of the samples have been measured.

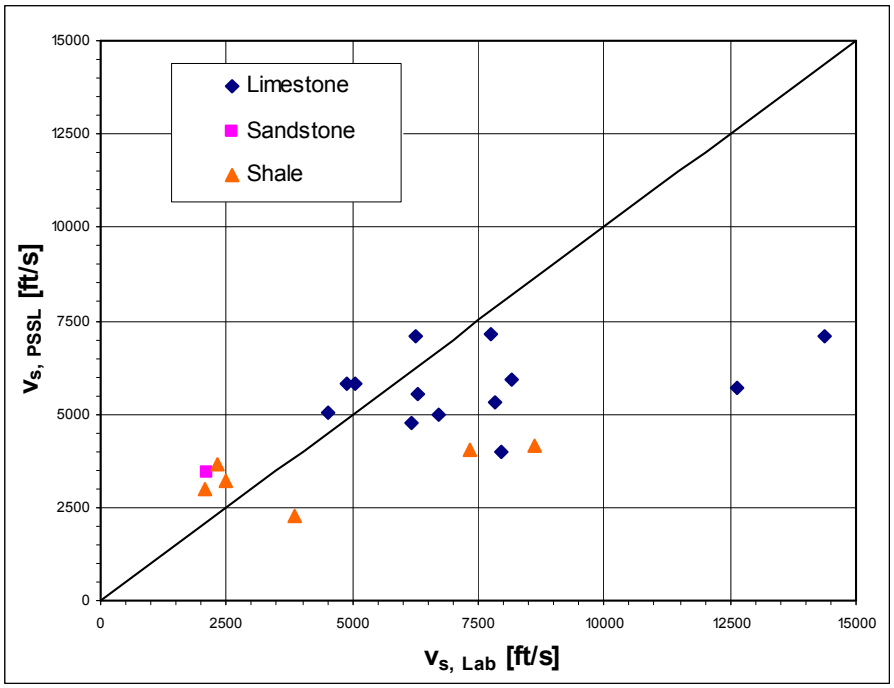

Fig.27: Comparison of shear wave velocity from laboratory transmission measurements and PSSL, showing good to moderate correlation. The extreme outliers on the right plot side might be a result of shear wave velocity measurements in very clean and unaltered limestone samples of the site or instead of shear wave velocity compressional wave velocity was measured.

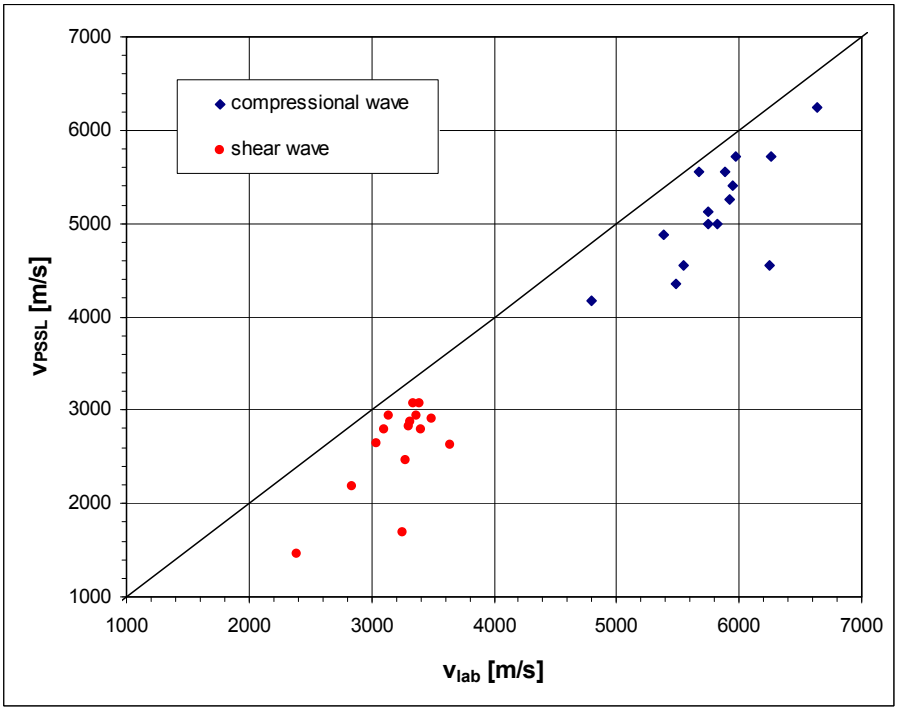

Fig.28: Comparison of shear wave velocities measured with PSSL and data from laboratory in a metasediment dominated lithology providing a moderate to good correlation. Velocities from lab are higher than the PSSL velocities. The difference is seen to be caused mainly by the higher frequencies used in the laboratory measurements.

4.1 Conclusions

Under the assumption of "correct" measurement procedure and data interpretation (especially no widespread first arrival mispicking and no significant depth differences between the compared measurements)) the different dynamic methods for acoustic velocity determination of rocks and soils should offer well to moderately correlating velocity values. Differences between methods are mainly caused by frequency and scale effects. Especially

for the comparison of laboratory velocities to in situ velocities it has to be taken into account that laboratory measurements use relative high frequencies on very small and usually intact samples, whereas in situ measurements use at least slightly lower frequencies and are affected by discontinuities like fractures or faults and use lower frequencies than the laboratory techniques.

Differences in the vertical resolution of the compared methods can also cause local differences between velocities (for example between MASW and PSSL). Although the general velocity trend is the same in the different measurements, the higher resolving method shows locally small scale velocity changes, which are averaged by the method with the lower resolution.

Compared to the other methods the downhole method seems to be the most "problematic". Results can be ambiguous, meaning that the downhole method offers good correlating velocity values in some sections and not correlating values in other sections of a borehole. The biggest problem in the author's opinion is that the source receiver offset is increasing during measurements. The source usually remains at the surface, whereas the receiver is lowered in the borehole. The increasing rock and/or soil volume during measurement leads to increasing attenuation, especially of higher frequencies, what can lead to difficulties in correct first arrival determination. Therefore the downhole method should only be performed where other methods (with constant source and receiver offset like full waveform sonic log for example) cannot be applied (dry holes or unstable holes that require PVC casing for example).

5 Relations between v_p and v_s

The v_p/v_s-ratio is an important property for seismic applications. In order to estimate shear-wave velocities when only compressional wave velocities are available, CASTAGNA et al.,1985 derived an empirical equation commonly referred to as the "mudrock-line" (mudrock: *"clastic silicate rock composed primarily of clay or silt sized particles"*):

$$V_s = 0.8621 \cdot V_p - 1.1724 \qquad \text{[km/s]} \qquad (20)$$

Numerous researchers have published variants of the mudrock equation (SCHÖN, 2011)

According to the principle of the mudrock equation relations between compressional wave velocities (v_p) and shear wave velocities (v_s) for different lithologies and different methods are

analysed in this chapter. Target is to derive reliable empirical relations for v_s from measured v_p. In geotechnical applications this could help in estimation of v_s in areas where it was possible to measure v_p, but not v_s. The relations in this chapter are mainly linear regressions, calculated with MS Excel. The statistical error parameter is the R^2 value, which is automatically calculated by MS Excel.

In a first step a global analysis was tried. Fig.29 shows a v_p-v_s cross plot for the average velocities (including standard deviation bars) from the different available datasets differentiating different lithologies and methods. The standard deviation lies usually beyond or around 5%. An exception with standard deviations exceeding 20% are downhole velocities measured in a layered shale and shaly limestone succession in the intermediate velocity range. The average velocities follow a surprisingly good linear trend (R^2=0.92).

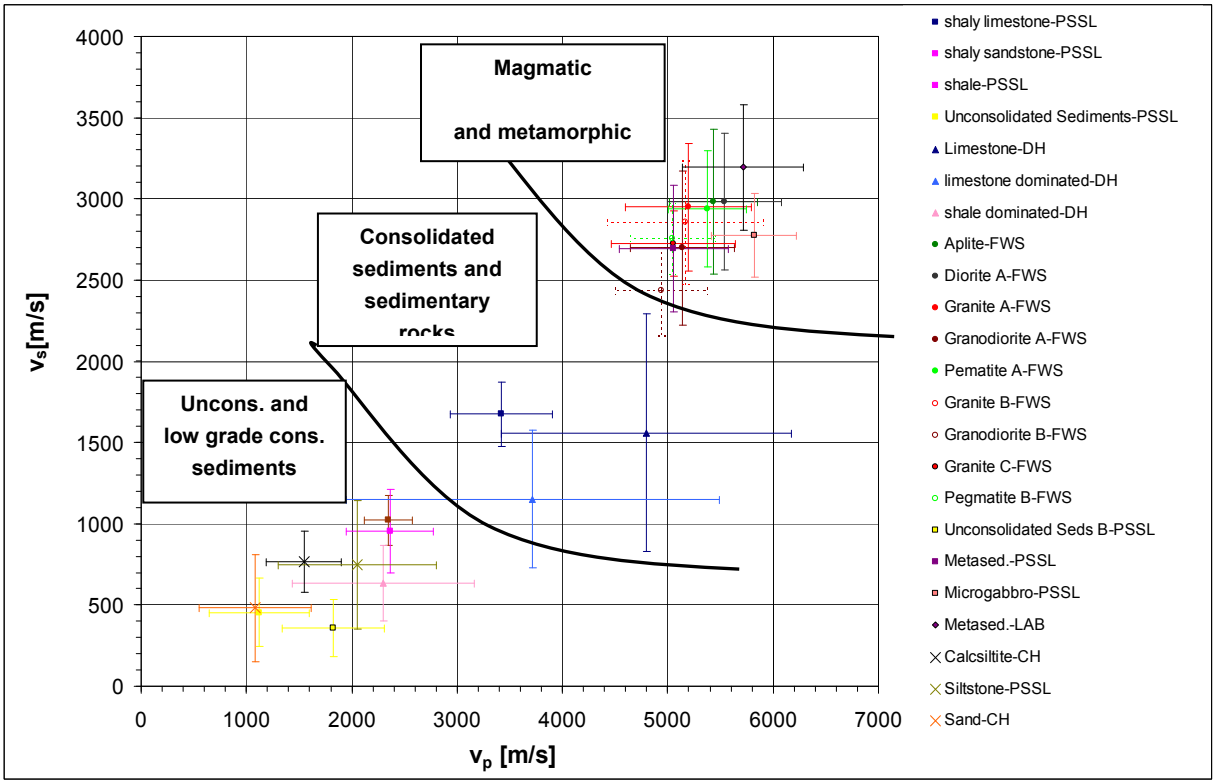

Fig.29: v_p-v_s crossplot for the different methods and lithologies encountered in the data for his report. A rough differentiation of the different lithologies is possible as pointed out in the plot. The intermediate velocity range is only covered by a layered shale limestone succession measured with downhole seismics, showing rather large standard deviations (up to 20%). For the other datasets standard deviations lie around 5%. The resulting velocity distribution can be approximated with a linear regression of rather good fit: $v_s = 0.5901 v_p - 394.17$ with R^2=0.92. Rather high standard deviations occur, because all measurements are performed in the first 100 m below the surface (lithological inhomogeneities, influence of weathering, different saturation degrees, …).

In a next step the v_p-v_s-relations for the different sites and methods were analyzed separately to derive and evaluate empirical relations for each site. Table 5 shows a summary of the found relations sorted by their R^2 value (from highest to lowest).

Relation	R^2	Lithology	Location	Method	Comment	Unit
$v_s = 0.5216v_p - 0.0439$	0.98	Siltstones/Calcsiltites	Dubai	CH	No differentiation of lithologies	[km/s]
$v_s = 0.0977e^{12539v_p}$	0.90	Sands*)	Dubai	CH	Variable degree of cementation	[km/s]
$v_s = 0.4677v_p + 437.95$	0.84	Granites	Austria	FWS	Very shallow, z_{max}=30 m	[m/s]
$v_s = 0.5511v_p - 0.1151$	0.80	Sands*)	Dubai	CH	Variable degree of cementation	[km/s]
$v_s = 0.6173v_p - 1435.1$	0.77	Limestones	US	PSSL	Significant shale content	[ft/s]
$v_s = 0.5124v_p + 134.18$	0.74	Granites	Austria	FWS	z_{max}=110 m	[m/s]
$v_s = 0.3822v_p + 111.05$	0.72	Unconsolidated Sediments	US	PSSL	No "acoustic" differentiaton of different lithologies according to their velocity.	[ft/s]
$v_s = 0.6031v_p - 354.36$	0.64	Metasediments	UK	PSSL	-	[m/s]
$v_s = 0.527v_p - 695.52$	0.61	Sandstones	US	PSSL	Shaly	[ft/s]
$v_s = 0.4843v_p + 42.298$	0.60	Granodiorites	Austria	FWS	Very shallow, z_{max}=30 m	[m/s]
$v_s = 0.474v_p - 540.31$	0.57	Shale	US	PSSL	-	[ft/s]
$v_s = 0.3458v_p + 762.03$	0.29	Microgabbro	UK	PSSL	Low number of data values	[m/s]
$v_s = 0.363v_p + 980.65$	0.23	Plutonic rocks	Austria	FWS	No "acoustic" differentiation between granites, granodiorites and diorites, z_{max}=80 m	[m/s]
$v_s = 0.1261v_p - 2274.9$	0.15	Shaly limestones, sandstones and shale	US	DH	-	[ft/s]
$v_s = 0.2735v_p - 178.24$	0.09	Unconsolidated Sediments	Hong Kong	PSSL	No seismic differentiation between clay, silt and sand	[m/s]

Table 5: Empirical relations for different sites and lithologies sorted after their R^2 value.

*) *Same sands but different regression type. The exponential approach offered slightly better fit to the data than the linear approach.*

In the following section the different relations are discussed separately for consolidated materials and rocks and unconsolidated materials.

5.1.1 v_p-v_s relations in rocks and consolidated materials

This chapter has closer look on empirical velocity relations for rocks and well consolidated materials. Where available, different methods are compared and where possible, different relations were calculated for different rock types.

Fig.30 and 31 show the empirical velocity relations of a US site, where PS Suspension Logging (PSSL) measurements and downhole seismic measurements have been performed in a succession of shaly limestones, shale and shaly sandstones.

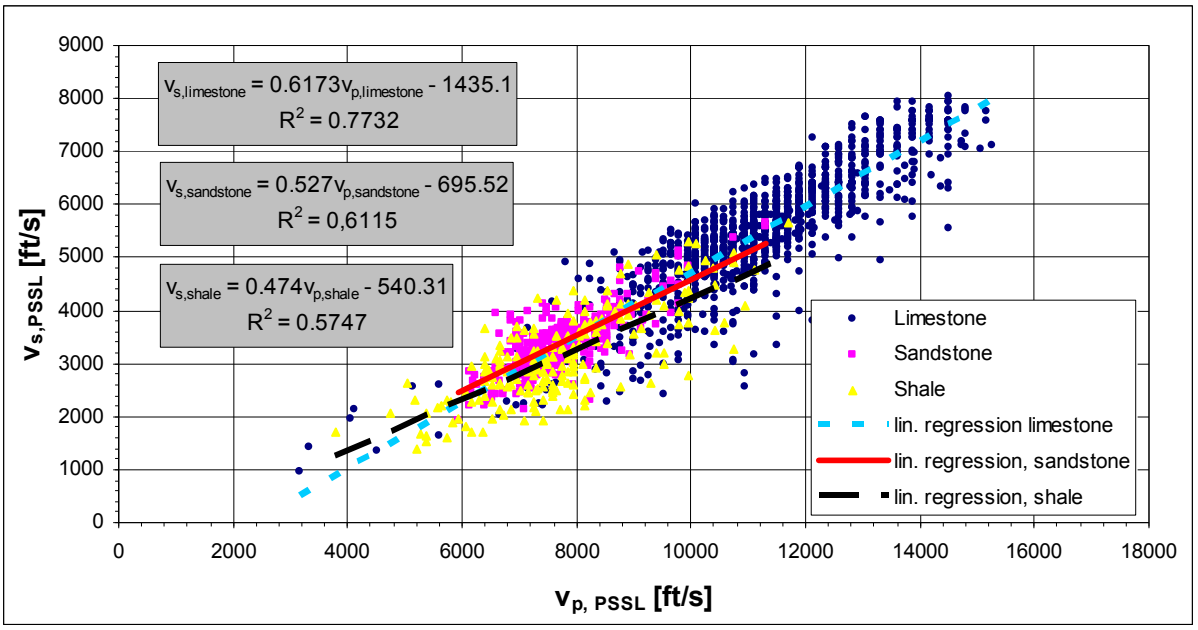

Fig.30: Empirical relations for a layered succession of shale, shaly limestone and shaly sandstone in the US measured with PSSL. The regressions for all three lithologies offer moderate to poor fit (R^2 around 60% for shale and sandstone and 0.77 for limestones). One problem might be the significant shale content in all lithologies. Another problem might be the definition of shale and the differentiation of shale from shaly sandstones on core materials performed by different geologists.

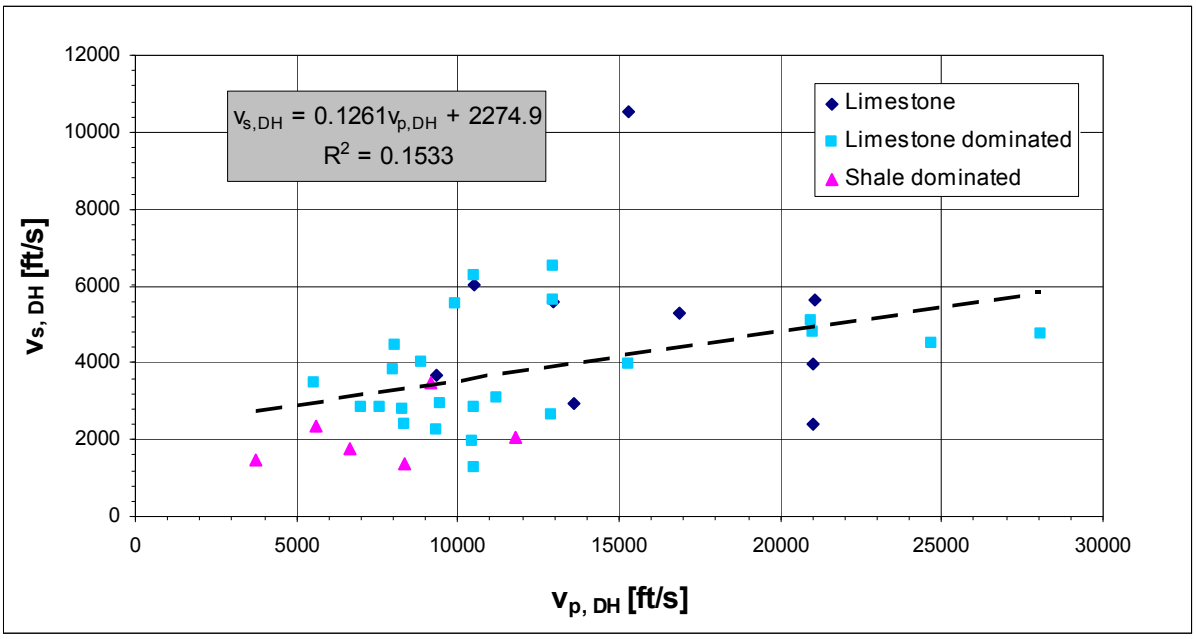

Fig.31: Empirical relation for the same lithological succession derived from velocity measurements with downholeseismics. The derived equation is of no use, because of very low correlation (R^2=0.15). The interval velocities from downhole measurements seem to be inappropriate for derivation of empirical veloctity relations for this dataset.

The PSSL method offers velocity values which result in moderate to poor fitting linear regressions with a maximum R^2 of 0.77 for the shaly limestones. Linear regressions for shale and sandstones offer lower R^2 (around 0.6). The derived linear equations would result in very rough shear wave velocity estimations.

The downhole interval velocities show no useful correlation with a linear regression (R^2=0.15). Problems in this case arise from the “difficult” lithology (significant shale content in all formations). On this site the problems seemed to be caused because of difficulties to transfer source energy from a surficial source through a succession of unconsolidated sediments in the rock sections (attenuation and filtering especially of higher frequencies).

Fig.32 shows the empirical relation for plutonic rocks (granites, (grano)diorites) in Austria measured with a full waveform sonic tool (FWS) to a maximum depth of about 80 m. The different litho types cannot be differentiated according to their v_p-v_s-relation. Therefore only one regression for the plutonic rocks of this site was calculated, resulting in a poor correlation (R^2=0.23). The calculation of separate regressions for each rock type does not increase the correlation significantly (not presented in the plot; for granites R^2=0.30, for the diorites R^2=0.23 and for the granodiorites R^2=0.13). The large scattering in the data is mainly caused by high variance in the weathering grade and grade of fracturing of the rocks.

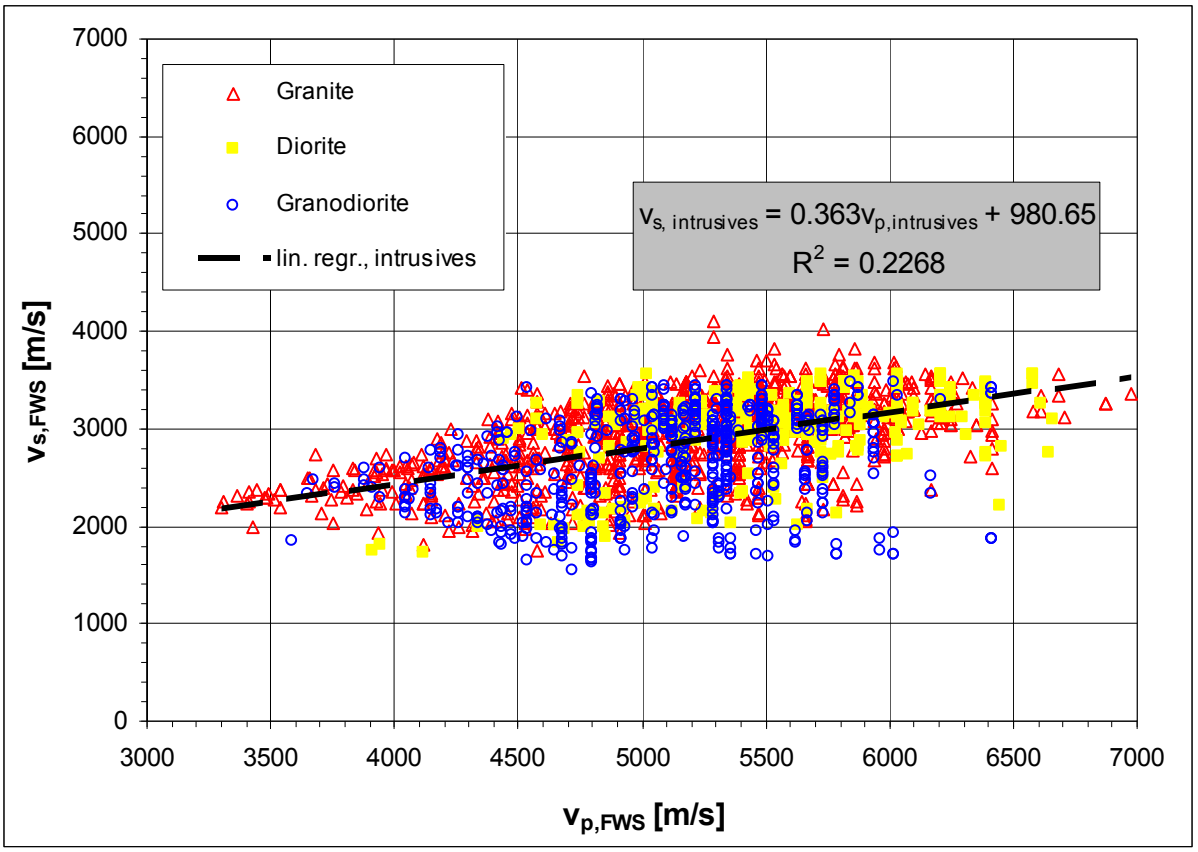

Fig.32: Empirical relation for v_s of plutonic rocks measured with FWS (max. depth of 80 m). The granites and (grano)diorites cannot be differentiated by their v_p-v_s relation. Therefore only one regression was performed resulting in poor correlation to the data (R^2=0.23). A separate calculation of the trendlines does not lead to a quality increase.

Fig.33 presents v_p-v_s crossplots from two different drilling campaigns in different locations in Austria, also dominated by granitic rocks measured with FWS in shallow investigation boreholes (Fig.33, TOP, z_{max}=30 m) and in investigation boreholes of intermediate (on a geotechnical scale) depth (Fig.33, BOTTOM, z_{max}=110 m).

In the data of the shallower boreholes (Fig.33, TOP) a slight differentiation between the granite velocities and the velocities of the granodiorites can be observed. The granite velocities show moderate to good fit to a linear regression (R^2=0.84). For the granodiorites an extremely lower number of data values is available. The velocity data of the granodiorites offers poor fit (R^2=0.60) to the linear regression.

The data of the deeper investigation boreholes is affected by massive scattering. The granite velocities offer moderate fit to a linear regression (R^2=0.74).

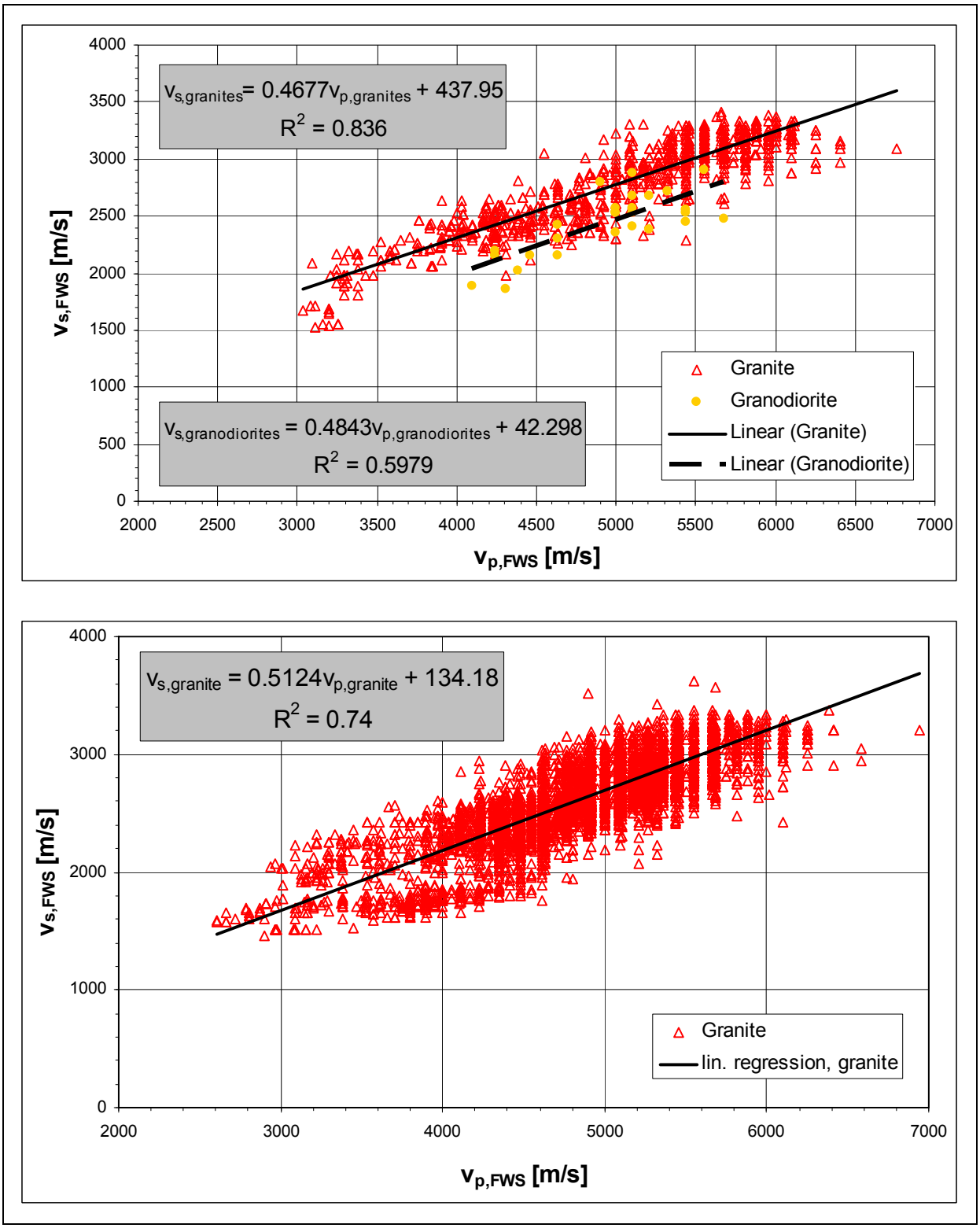

Fig.33: Velocity crossplot for FWS measurements in shallow investigation boreholes with z_{max} around 30 m (TOP) and investigation boreholes of intermediate depth (z_{max} around 110 m) in a mainly granitic environment offering moderate fitting linear trends for granites and poor fitting linear trend for granodiorites.

In Fig.34 the results of crosshole velocity measurements in a calcsiltite-siltstone succession in the Dubai are shown in a velocity crossplot. The different lithologies cannot be clearly differentiated from each other according to their velocities. A high velocity region (>2.250 km/s) for siltstones can be defined. No further differentiation is possible. For this

reason only 1 regression was calculated resulting in a very good fit (R^2=0.98) to the data. The derived equation seems to be reliable and appropriate enough to be used for shear wave velocity estimations on this site.

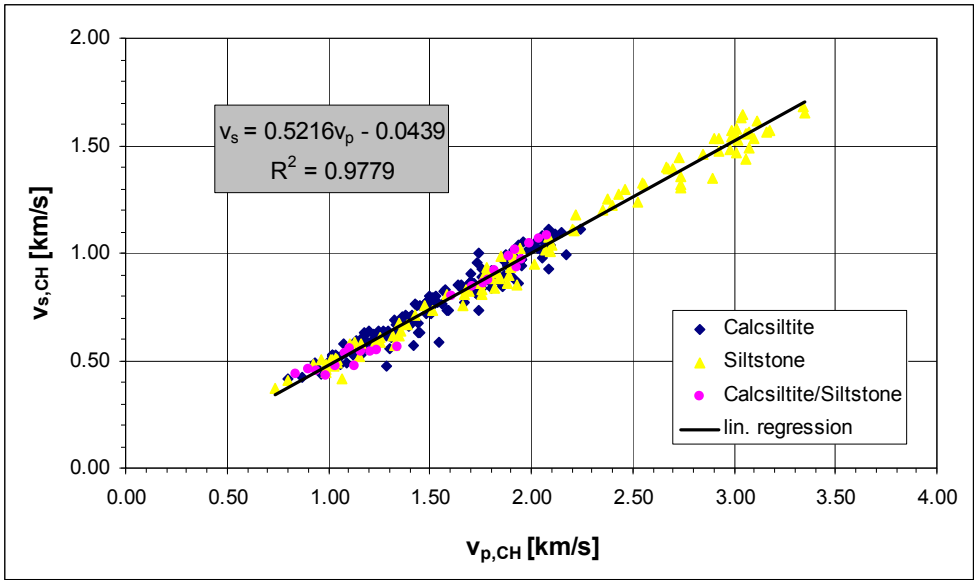

Fig.34: Velocity crossplot for crosshole seismic measurements in a siltstone-calcsiltite succession and a very good fitting linear regression to the data, suitable for appropriate shear wave estimations from v_p.

Fig.35 shows the results of PSSL measurements in a metasediment succession (metaconglomerate, mud- and –siltstone) and a microgabbro encountered by nearshore investigation boreholes in the UK area. The velocities in the metasediments cover a relative wide range and are affected by scattering. The derived linear equation shows poor fit to the data (R^2=0.64). The microgabbros show compressional wave velocities larger than 5000 m/s. A relative low number of available data points and relative massive data scatter lead to a linear regression with no significant fit to the data.

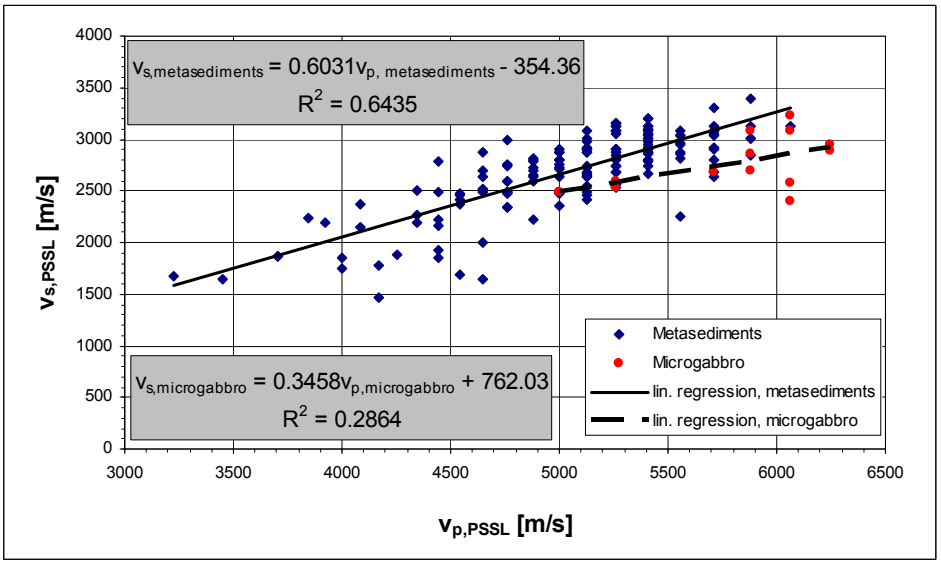

Fig.35: Velocity crossplot for PSSL-measurements in metasediments and gabbros resulting in moderate to poor fitting linear regressions for v_s.

5.1.2 v_p-v_s relations in soils and/or unconsolidated materials

The same analysis as in the chapter before has been performed for a lower number of velocity datasets from unconsolidated sediments.

Fig.36 shows a crosshole velocity crossplot for sands in Dubai, which are affected by variable, but significant cementation. The derived linear empirical relation already shows surprisingly good fit (R^2=0.80) to the data. The use of an exponential model could increase the correlation with the data to a R^2 value of 0.90. A reason for this partly non linear relation might lie in the varying grade of cementation and perhaps in different grades o f saturation.

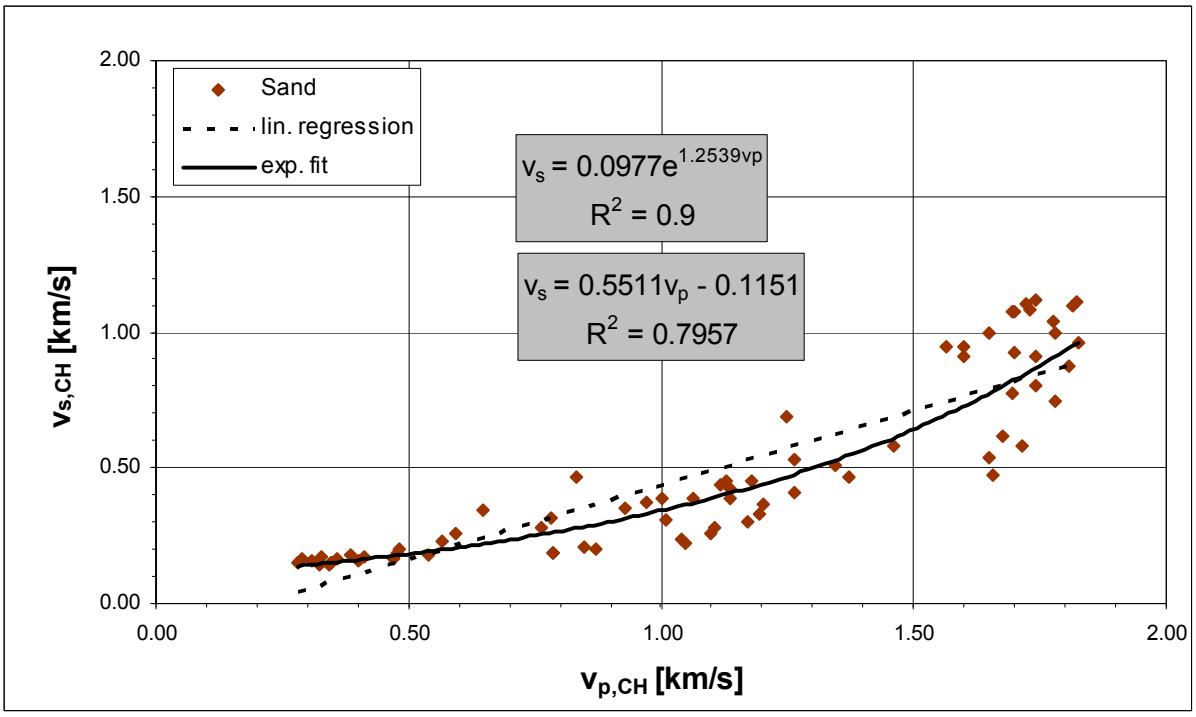

Fig.36: Velocity crossplot for partly cemented sands. The exponential fit shows better correlation with the data than the linear fit (it has to be taken into account that R^2 has to be interpreted with caution for non linear correlations). Perhaps this could be interpreted as a cementation influence.

Fig.37 presents data from strongly volcanic influenced soils in Hong Kong containing sand, silts and clay. All sediment components are affected by volcanic influence in form of dispersed and layered tuffs. The different soil components show no differentiation according to their velocities, so only one linear regression was calculated. The regression shows no fit to the data (R^2=0.09).

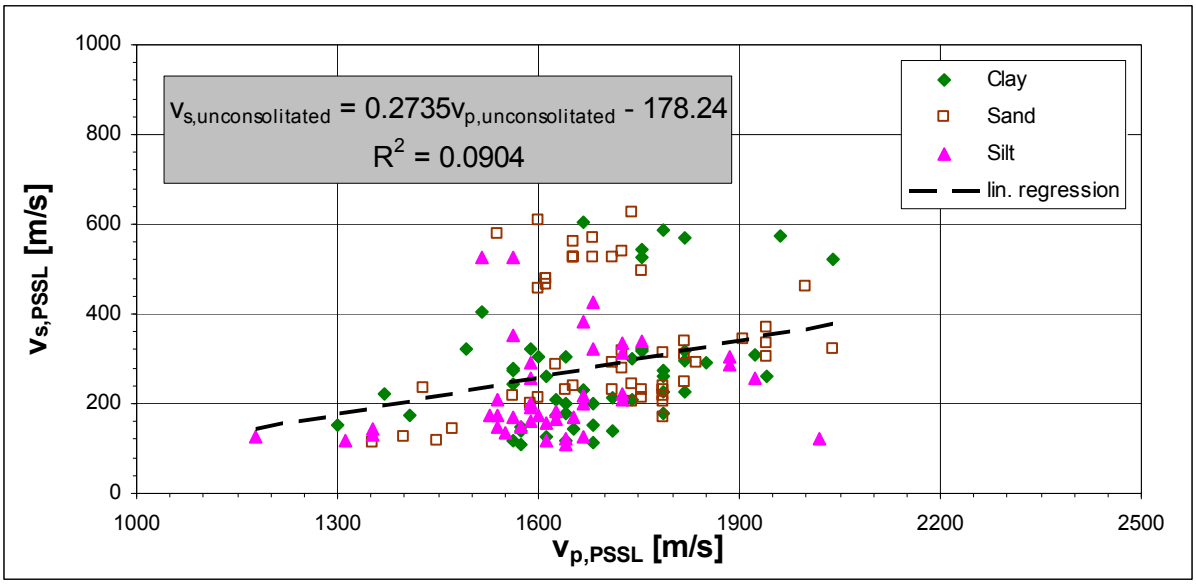

Fig.37: v_p-v_s crossplot for soils influenced by dispersed and layered tuffs. The data shows no significant fit to a linear regression.

Fig.38 shows a velocity crossplot for unconsolidated materials (residual soil, artificial fill, silt and clay and weathered limestone) measured with PSSL in a sediment succession in the US. The derived linear regression (only one because of lacking differentiation of different lithologies) offers moderate fit to the data (R^2=0.72).

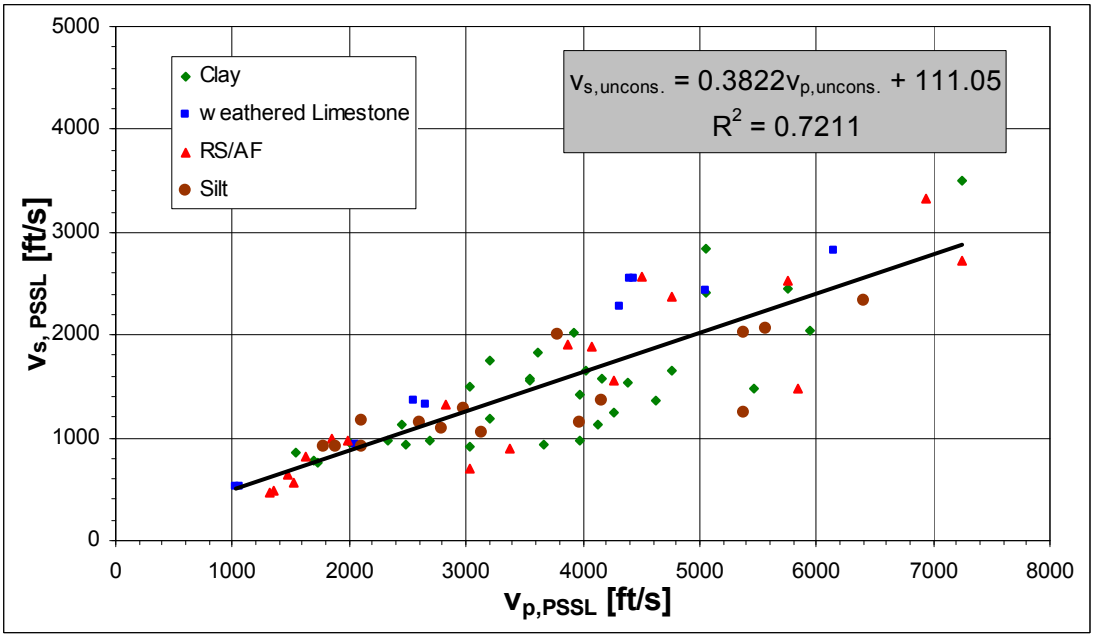

Fig.38: Velocity crossplot for different unconsolidated materials measured with PSSL. The linear regression shows moderate fit to the data.

5.1.3 Conclusions

The use of empirical relations to derive v_s from measured v_p for rocks as well as for unconsolidated materials is limited by rather moderate fit of the scattering data to a linear regression. Only rough estimations of v_s are possible. At this point it may be noted that from a physics point of view there is no strong correlation between the two parameters, because the elastic behaviour is controlled by the independent properties for compression and shear. Empirical regressions therefore can reflect only a tendency originated by similar influence of mineral composition, fracturing etc. on the two velocities.

It seems that crosshole seismic measurements offer the highest data quality for derivation of empirical relations (in rocks and soils). All empirical relations derived from crosshole measurements offered good to excellent fit (R^2>0.80) to the data.

On the other end of the scale downhole measurements and PSSL measurements in unconsolidated materials seem to offer velocity data that cannot be used for the derivation of empirical relations. In the presented datasets another problem occurs. The differentiation of similar lithologies by several geologists is not always distinct and this causes problems for rock specific empirical equations.

Another problem in deriving rock specific empirical relations might be the non uniqueness of lithology classification. The same material might be classified in a different way by different geologists. For example the distinction between shale and mud- or siltstones or the distinction between different granitic rocks might not always be that clear.

6 Correlations between static and dynamic moduli

In this chapter the available data sets are analyzed for correlations between the calculated dynamic elastic moduli and measured or calculated static moduli. Although a large amount of data was available for different methods only a few intersections were found, where direct correlations (same borehole same depth and data of a dynamic and a static measurement) were possible. It was tried to find linear relationships for the correlation between static modulus and dynamic modulus according to the ones found in literature and mentioned in chapter 2.3.2:

$$E_{stat} = aE_{dyn} + b \tag{21}$$

where a and b are empirically.

On the other hand it was tried to derive power law relations from the crossplots of static modulus versus the dynamic/static ratio to improve correlations with the same number of free parameters:

$$E_{stat} = (\frac{E_{dyn}}{c})^{d} \tag{22}$$

where c and d are empirically.

The first example presented in Fig.39 - 41 shows the comparison and correlation of dynamic modulus from crosshole seismic testing and static modulus from unconfined compression strength tests for a succession of siltstones and calcarenites in Dubai. The calculated relations with

$$E_{stat} = 0.005E_{dyn} + 422 \tag{23}$$

$$\frac{E_{dyn}}{E_{stat}} = 1234E_{stat}^{-0.84} \tag{24}$$

or solved for static modulus

$$E_{stat} = (\frac{E_{dyn}}{1234})^{6.3}) \tag{25}$$

show no fit to the data (Fig.39 and Fig.40). The direct comparison of the static and dynamic moduli shows that the dynamic moduli are much higher than the static ones. The calculated regression offers no fit to the data (R^2=0) and shows a very low gradient (nearly approaching

constant static modulus). Using the relation between the dynamic/static-ratio and the static modulus raises R^2 to 0.31, which is much better than the former approach, but still no significant fit to the data is given.

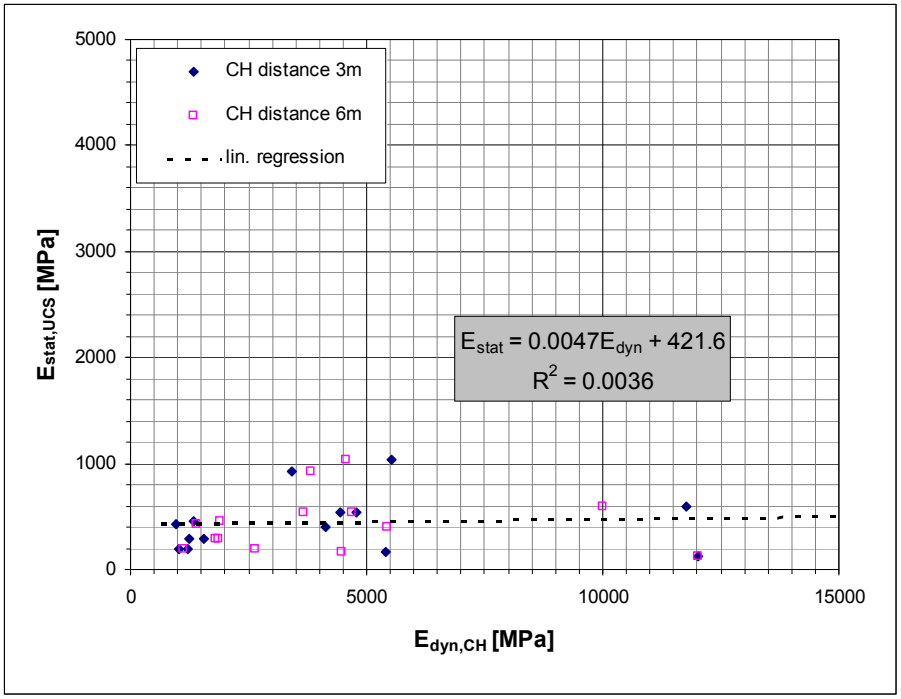

Fig.39: direct comparison between E_{dyn} and E_{stat} from crosshole seismics and UCS-tests. The dynamic moduli are much higher than the static ones. The resulting linear regression shows a very low gradient and no significant fit to the data.

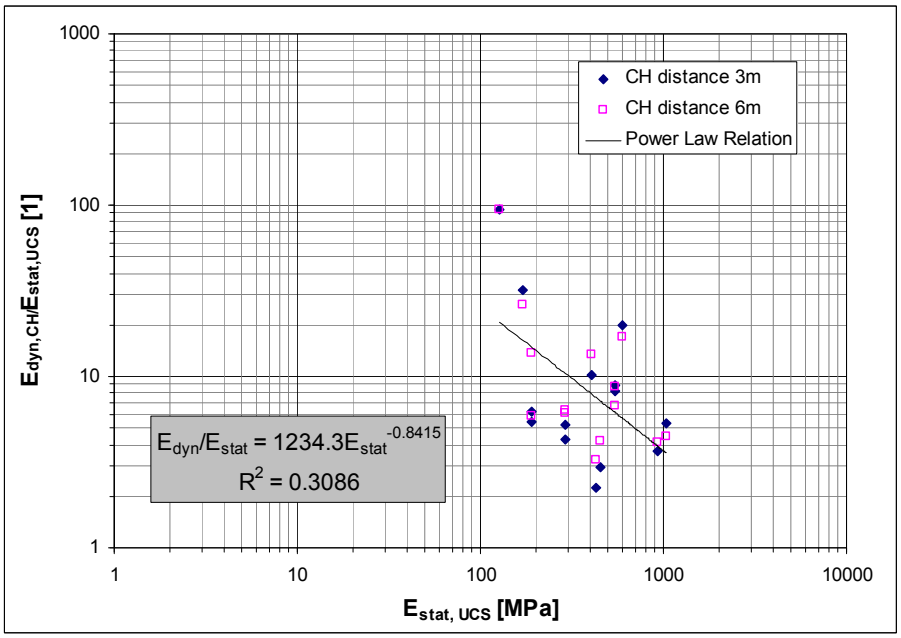

Fig.40: dynamic/static ratio as a function of E_{stat}. The ratio goes up to values of about 100. A calculated power law relation shows higher fit than the linear one but with R^2=0.31 it still shows no significant fit to the data.

The only result that can be assumed by an empirical relation seems to be the maximum dyn./stat.-ratio (Fig.41) on the linear plot of the ratio as a function of static modulus.

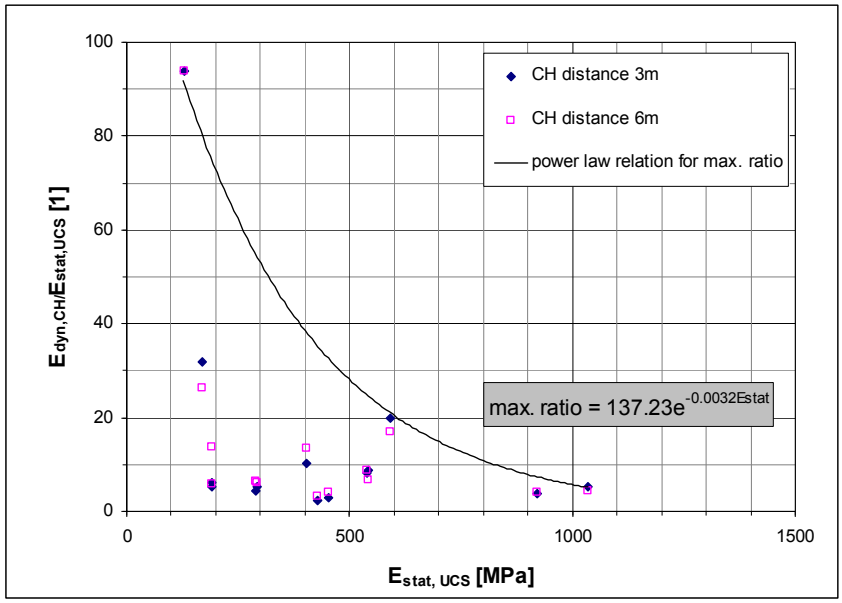

Fig.41: Linear plot for dynamic/static ratio as a function of E_{stat}. The high scatter of the data is responsible for the low fitting empirical relations. A sufficient estimation of static moduli out of the dynamic ones cannot be made. The curve in the figure is a 3 point approximation and marks the line of maximum ratio. Values on the right side of the curve are not realized on this site.

In Fig.42-43 dynamic Shear Modulus from full waveform sonic and density logging is compared and correlated with static Shear Modulus from dilatometer tests (maximum modulus out of 3 test cycles) in a mainly granitic formation of an Austrian site.

The derived linear equations for the load case

$$G_{stat,load} = 0.40 G_{dyn} - 5335 \quad (26)$$

and the unload case

$$G_{stat,unload} = 0.026 G_{dyn} - 2411 \quad (27)$$

show no significant (R^2=0.24 and 0.34) fit to the data.

The power law equations derived for the dyn./static ratio for the load case

$$\frac{G_{dyn}}{G_{stat}} = 6408 G_{stat}^{-0.85} \quad (28)$$

and for the unload case

$$\frac{G_{dyn}}{G_{stat}} = 4880 G_{stat}^{-0.83} \quad (29)$$

result in R^2=0.95 and R^2= 0.88, indicating an excellent fit to the data for the load case and good fit for the unload case.

Solving for G_{stat} gives

$$G_{stat,load} = \left(\frac{G_{dyn}}{6408}\right)^{6.67} \text{ and } G_{stat,unload} = \left(\frac{G_{dyn}}{4880}\right)^{6.67} \quad (30), (31)$$

The data distribution in the linear G_{stat} versus G_{dyn} crossplot (Fig.42) suggests a line of maximum static modulus for the analysed granitic rocks. In the same manner a line for the maximum dyn./stat.-ratio can be defined in the crossplot of G_{stat} versus dyn./stat. ratio (Fig.43).

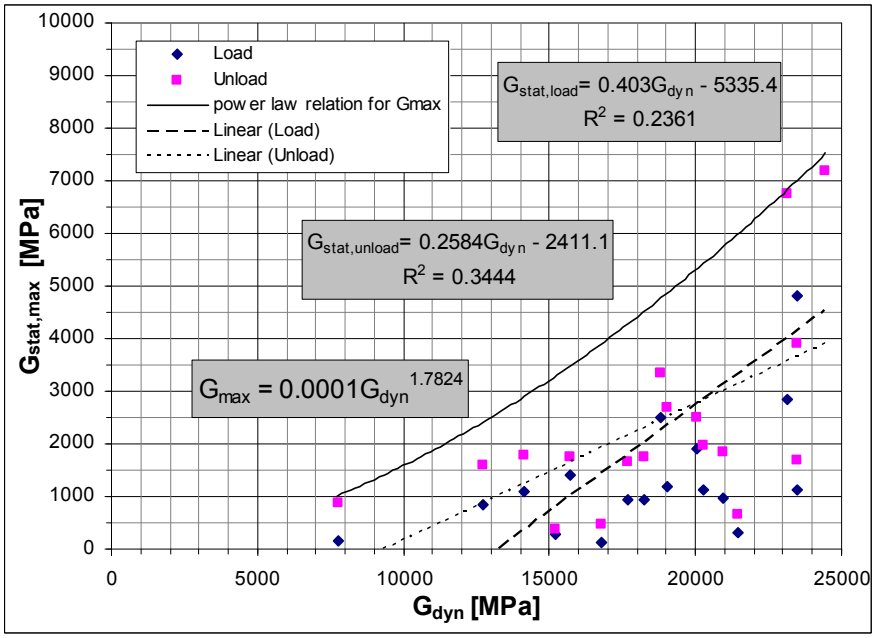

Fig.42: Direct comparison of dynamic and static Shear Modulus (maximum modulus out of three cycles) from dilatometer tests and FWS in a granitic rock formation. The data shows massive scattering. The derived linear relations show poor fit to the data. The equation for G_{max} is an assumption for the maximum occurring Shear modulus in the analysed rocks.

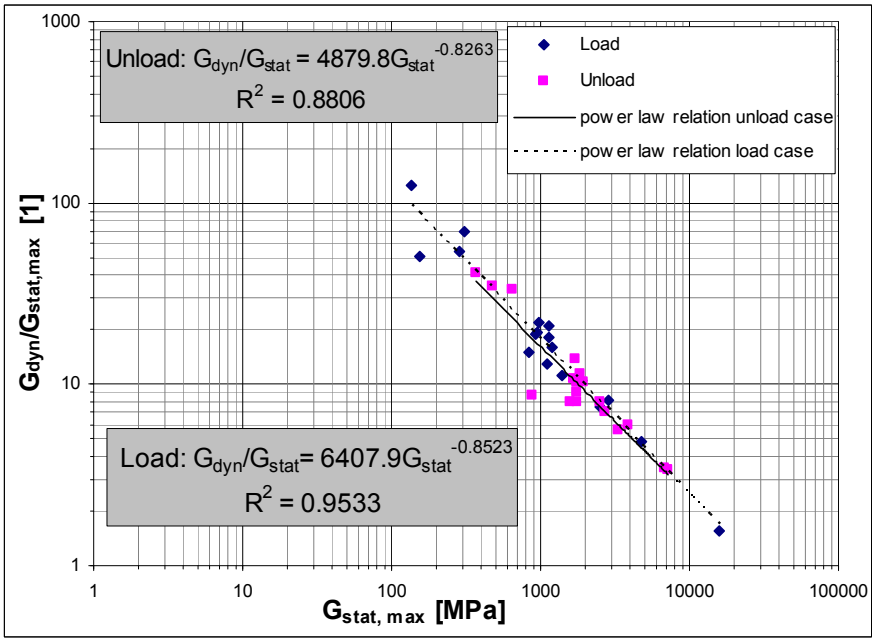

Fig.43: Logarithmic plot for dyn./stat.-ratio as a function of static Shear Modulus. The data shows good correlation to the derived power law equations for the load (R^2=095) and unload (R^2=0.88) case. The ratio varies in a range from 1 to about 100.

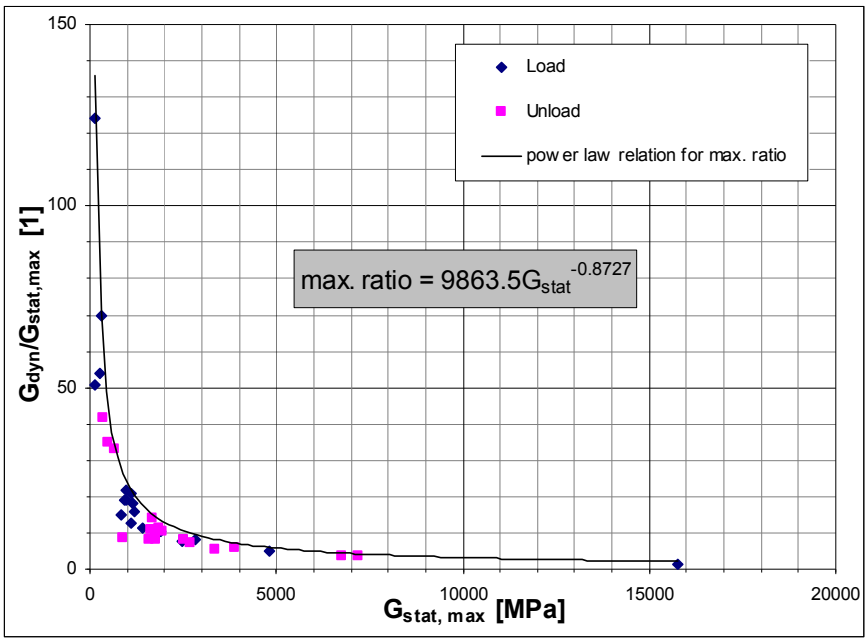

Fig.44: Linear plot for the dyn./stat.-ratio as a function of G_{stat}. The data distribution suggests a line of maximum Shear modulus occurring in the analysed rocks, which is approximated with a power law relation.

In Fig.45-47 Young's Modulus from the same measurements as before is analysed. It has to be taken into account that a Poisson's Ratio of 0.33 has been assumed by the interpreter of the dilatometer data to calculate Young's Modulus from the dilatometer measurements. Again the maximum value out of three dilatometer test cycles has been taken to compare and correlate with the values achieved with FWS and GGD measurements. The linear regressions

$$E_{stat,load} = 0.16E_{dyn} - 5428 \text{ and } E_{stat,unload} = 0.31E_{dyn} - 9189$$

(32), (33)

show a poor fit to the data (R^2<0.3). Using the dyn./stat.-ratio as a function of E_{stat} to calculate power law equations results in

$$\frac{E_{dyn}}{E_{stat}} = 17217E_{stat}^{-0.87} \text{ for the load case and} \quad (34)$$

$$\frac{E_{dyn}}{E_{stat}} = 11574E_{stat}^{-0.83} \text{ for the unload case.} \quad (35)$$

Both equations show good fit to the data (R^2>0.9).

Solving for E_{stat} gives

$$E_{stat,load} = \left(\frac{E_{dyn}}{17217}\right)^{7.69} \text{ and } E_{stat,unload} = \left(\frac{E_{dyn}}{11574}\right)^{5.88}. \quad (36), (37)$$

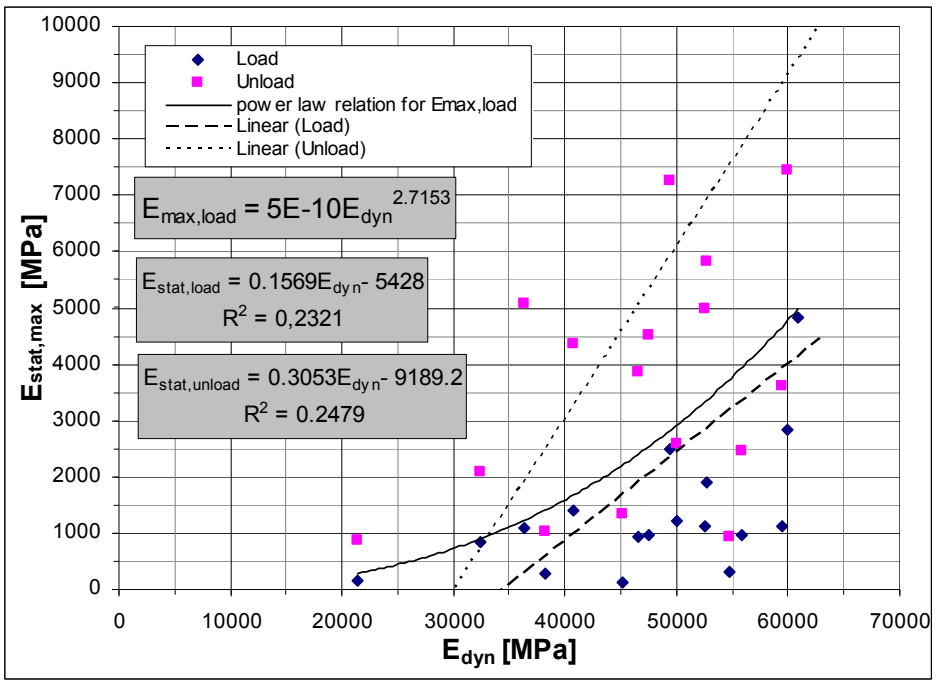

Fig.45: Static Young's Modulus from dilatometer tests in direct comparison to dynamic modulus from FWS and GGD. Data is affected by massive scattering, leading to poor fit of linear regressions to the data. For the load case an estimation for the maximum occurring E_{stat} was assumed.

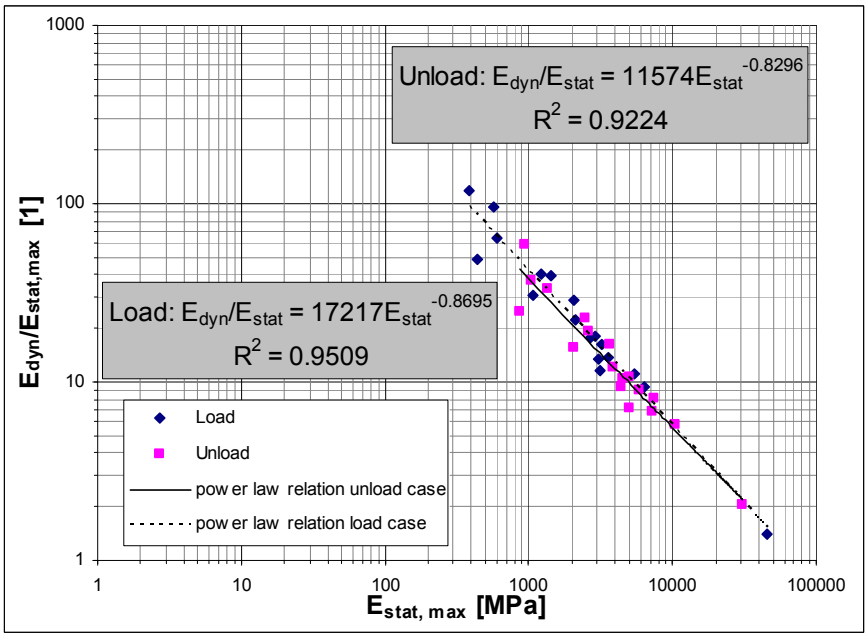

Fig.46: Dyn./stat.-ratio as a function of E_{stat}. The data shows moderate scattering. The derived power law equations for load and unload case show good fit to the data (R^2>0.90).

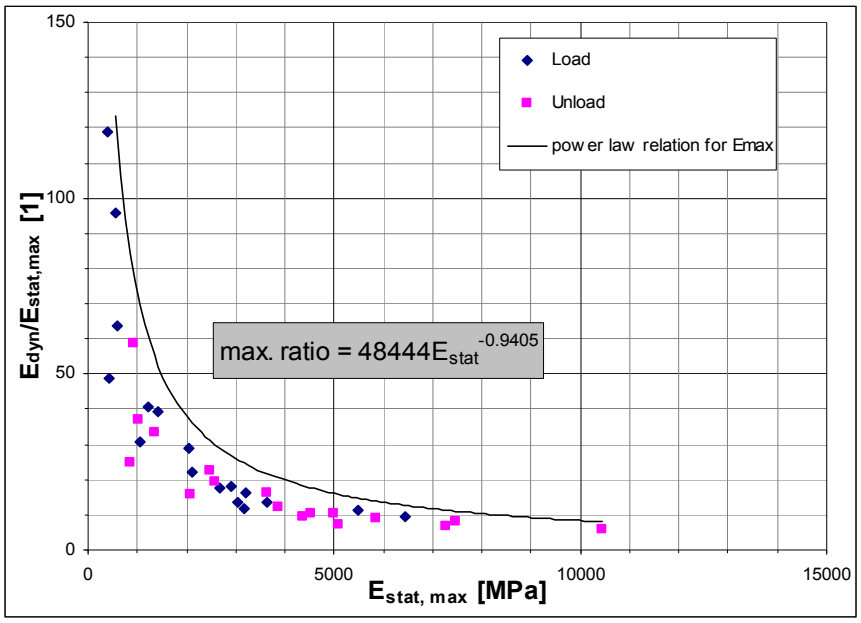

Fig.47: Rough assumption of the maximum occurring dyn./stat.-ratio in the granitic rocks.

For both moduli (E and G) the dyn./stat.-ratio in the mainly granitic lithologies shows large variations with values over 100. As shown in Fig.48 the very high ratios (>30) seem to be limited to a very shallow weathered zone. Beyond a boundary depth of about 12 m the ratio shows generally values <20.

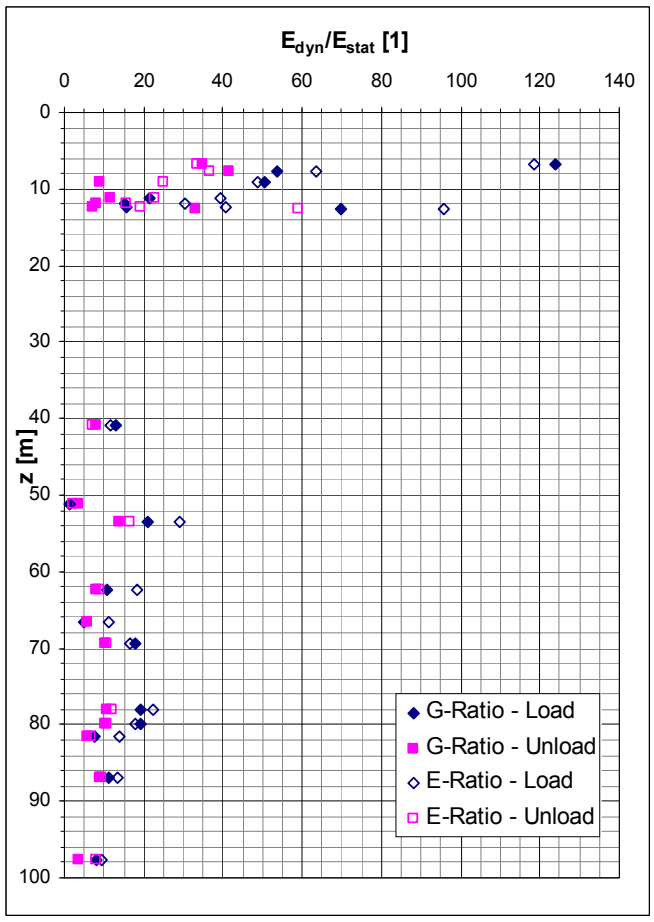

Fig.48: Dyn./stat.-ratio versus depth. The plot shows that the highest values for the ratio occur in a shallow weathered zone around 10 m.

In the same granitic lithology, but in another location FWS and GGD measurements were performed beside UCS-tests and 3-axial tests (Fig.49-51). Calculated linear regressions to derive static modulus lead to the equations

$$E_{stat,3-ax} = 0.31E_{dyn} - 6301 \text{ and } E_{stat,UCS} = 0.24E_{dyn} - 871 \quad (38), (39)$$

The regression for the 3-axial-tes data offers moderate fit (R^2=0.61), whereas the regression to the UCS-test data shows no significant fit to the data. Calculating power law equations for the dyn./stat.-ratio lead to significantly improved fit to the data. The equation

$$\frac{E_{dyn}}{E_{stat,UCS}} = 3945E_{stat,UCS}^{-0.72} \quad (40), (41)$$

offers moderate fit to the data (R^2=0.72) and using

$$\frac{E_{dyn}}{E_{stat,3-ax}} = 4780E_{stat,3-ax}^{-0.73} \quad (42)$$

leads to a good fit with R^2=0.96. Resolving for E_{stat} results in

$$E_{stat,UCS} = \left(\frac{E_{dyn}}{3945}\right)^{3.57} \text{ for UCS-tests and } E_{stat,3-ax} = \left(\frac{E_{dyn}}{4780}\right)^{3.70} \text{ for the 3-axial tests.} \quad (43), (44)$$

In this data set again an assumption for the maximum occurring E_{stat} (Fig.49) and for the maximum occurring dyn./stat.-ratio were derived (Fig.51).

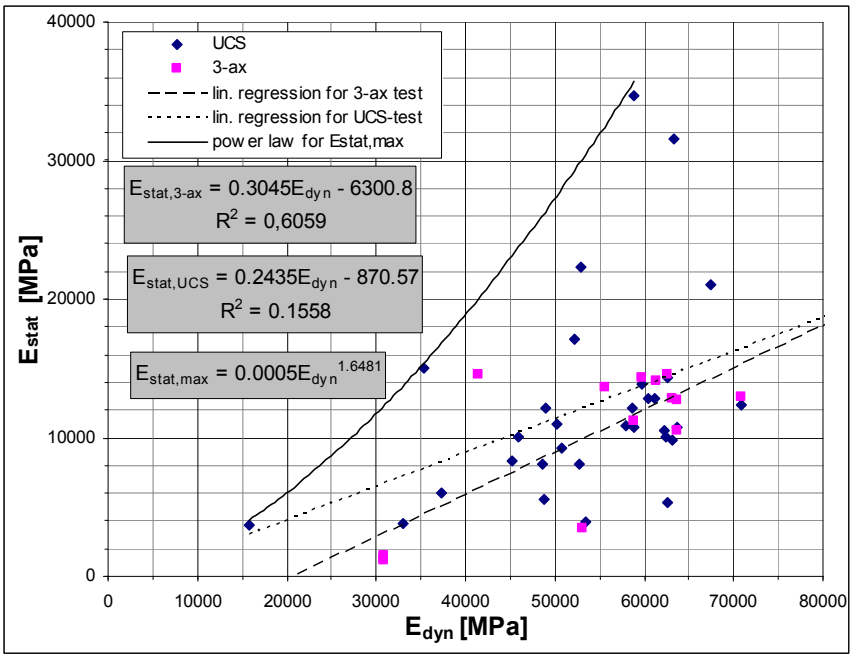

Fig.49: Direct comparison of dynamic Young's Modulus from FWS and GGD measurements and static modulus from UCS- and 3-axial testing in granitic formations. The linear regressions result in a poor fitting relation for the UCS-test data (R^2=0.16) and a moderate fitting 3-axial-test data (R^2=0.61).

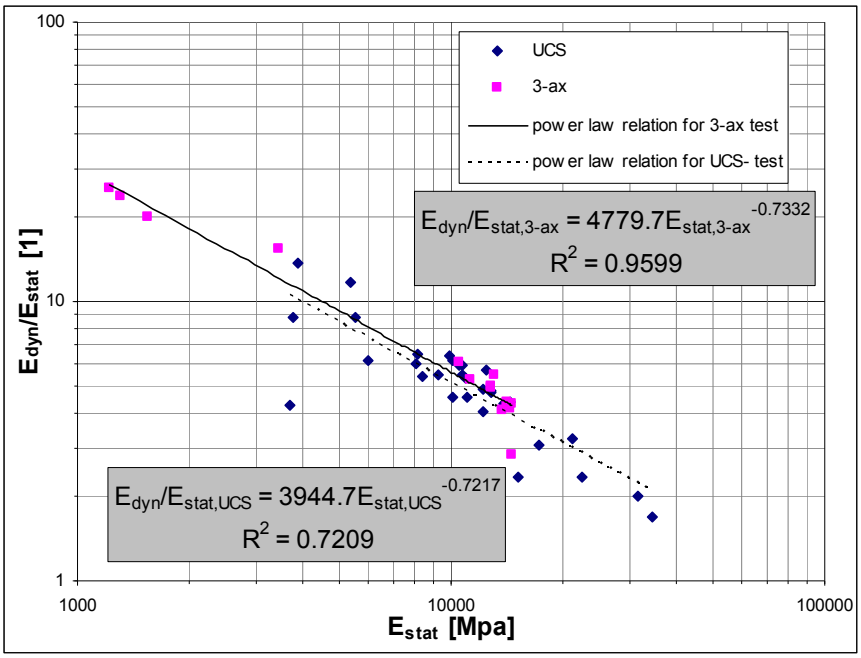

Fig.50: Logarithmic plot for dyn./stat.-ratio as a function of E_{stat} for UCS-test and 3axial tests in granites. The power law equations derived for dyn./stat. ratio show moderate fit in the case of UCS-test data and good fit for the 3-axial-test data. In both cases the fit is much better than for the linear regressions calculated in Fig.49.

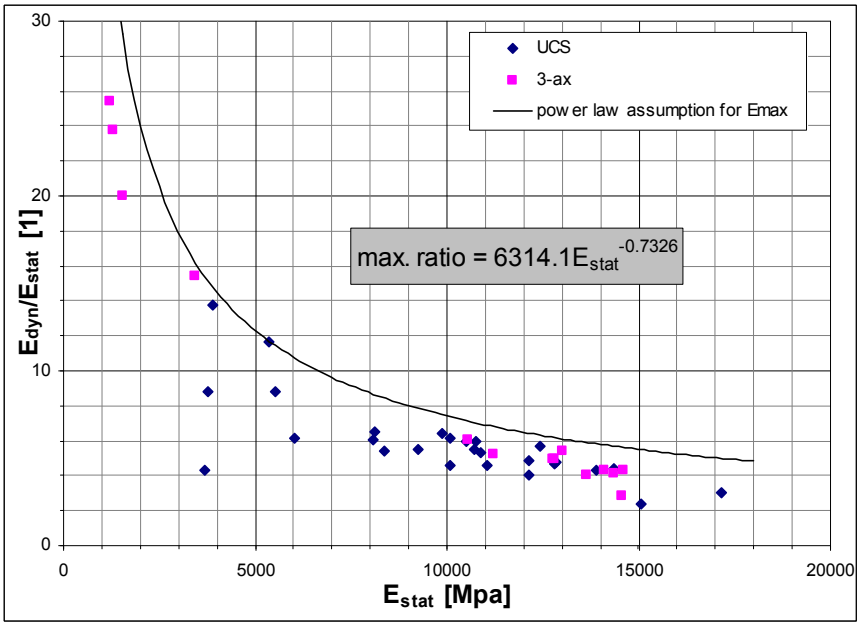

Fig.51: Dyn./stat.-ratio as a function of E_{stat} in a linear crossplot. The curve proposes a line for maximum occurring E_{stat} in the analysed granites.

An example for moduli derived from PSSL and 3-axial measurements in a metasediment succession (with microgabbro layers) is presented in Fig.52-54. The linear equation (Fig.52)

$$E_{stat} = 0.52E_{dyn} + 12142 \quad (45)$$

delivers poor fit to the data. Main reason for this bad fit seems to be a population of data values with deviating high static moduli around 80000 MPa. These values cannot be related to a specific rock property (for example high grade of cementing, quartz veins,…). Excluding this values form the regression results in moderate improvement of the fit (R^2=0.53). The

power law approach (Fig.52) gives $\frac{E_{dyn}}{E_{stat}} = 3757 E_{stat}^{-0.75}$

(46)

or resolved for the static modulus

$$E_{stat} = (\frac{E_{dyn}}{3757})^4 . \quad (47)$$

In Fig.54 an assumption for the maximum occurring E is presented.

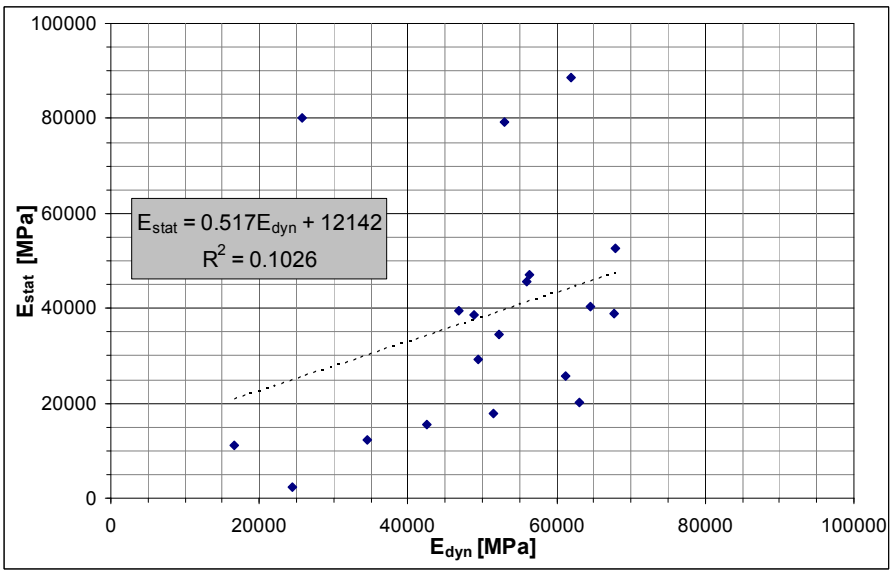

Fig.52: Linear regression for E_{stat} in a linear crossplot of dynamic Young's Modulus from PSSL and static Young's Modulus from 3-axial testing in a metasediment succession with layers of microgabbro. The linear regression shows no significant fit to the data, mainly due to a (non-rockspecific) population of very high static moduli (around 80000 MPa).

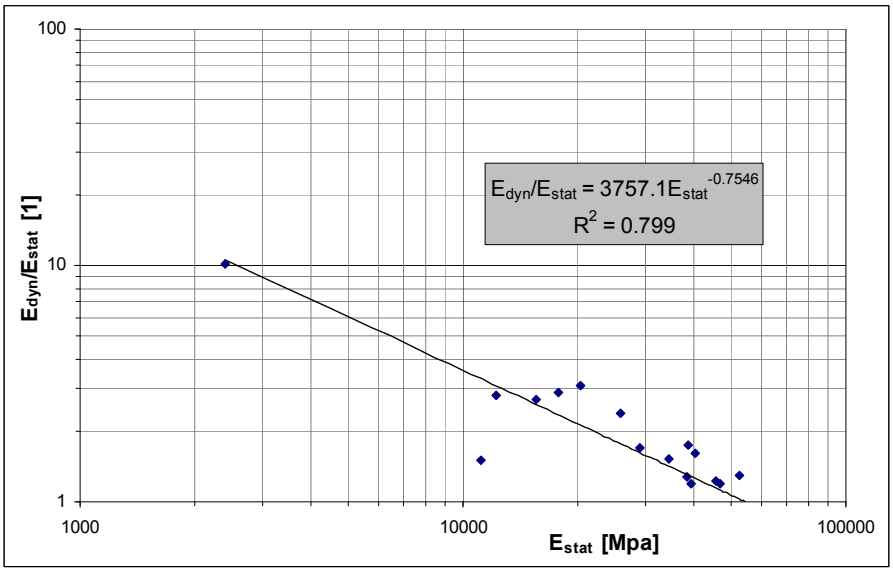

Fig.53: Power law equation for the dyn./stat.-ratio on a logarithmic plot of dyn./stat.-ratio as a function of Estat. The equation offers moderate fit to the data.

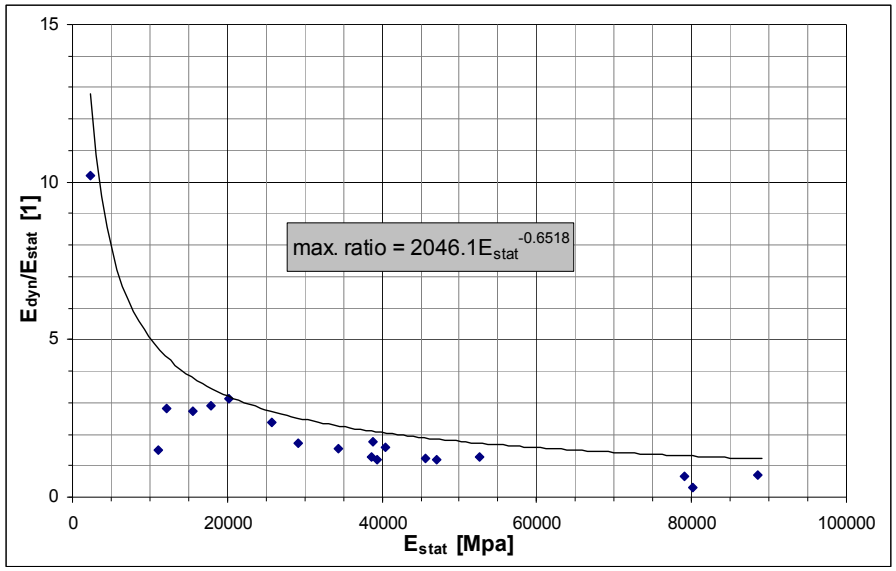

Fig.54: Assumption of the maximum occurring dyn./stat.-ratio in the analysed metasediments.

6.1.1 Conclusions

The direct comparison of dynamic and static moduli in (usually) shallow geotechnical investigation areas is problematic due to massive occurring scatter in the data. Derived empirical equations (using a linear regression in the crossplot of static modulus as a function of dynamic modulus) offer moderate or more often poor fit to the data distributions. For this reason another approach was tried. Power law equations were derived from the crossplot of the dynamic/static-ratio as a function of the static modulus. This approach improved the fit of the empirical equation to the data significantly. With one exception all the derived power law equations could be used to estimate static moduli from dynamic ones. Table 6 gives a summary on all derived empirical equations.

In all presented data examples an assumption for derivation of a maximum occurring dyn./stat.-ratio, and in some cases a direct assumption of maximum static modulus occurring in the given lithology could be derived.

Litho	Methods	Lin. Regression	R^2	Power Law Equation	R^2	Solved for E_{stat}
Siltstone Calcarenite	CH UCS	$E_{stat} = 0.005E_{dyn} + 422$	0.00	$\frac{E_{dyn}}{E_{stat}} = 1234E_{stat}^{-0.84}$	0.31	$E_{stat} = (\frac{E_{dyn}}{1234})^{6.3}$
Granitic Rrocks	Dilatom. FWS	$G_{stat,load} = 0.40G_{dyn} - 5335$ $G_{stat,unload} = 0.026G_{dyn} - 2411$	0.24 0.34	Load: $\frac{G_{dyn}}{G_{stat}} = 6408G_{stat}^{-0.85}$ Unload: $\frac{G_{dyn}}{G_{stat}} = 4880G_{stat}^{-0.83}$	0.95 0.88	$G_{stat,load} = (\frac{G_{dyn}}{6408})^{6.67}$ $G_{stat,unload} = (\frac{G_{dyn}}{4880})^{6.67}$
Granitic Rocks	Dilatom. FWS	$E_{stat,load} = 0.16E_{dyn} - 5428$ $E_{stat,unload} = 0.31E_{dyn} - 9189$	0.23 0.25	Load: $\frac{E_{dyn}}{E_{stat}} = 17217E_{stat}^{-0.87}$ Unload: $\frac{E_{dyn}}{E_{stat}} = 11574E_{stat}^{-0.83}$	0.95 0.92	$E_{stat,load} = (\frac{E_{dyn}}{17217})^{7.69}$ $E_{stat,unload} = (\frac{E_{dyn}}{11574})^{5.88}$
Granitic Rocks	FWS 3-ax-test UCS-test	$E_{stat,3-ax} = 0{,}31E_{dyn} - 6301$ $E_{stat,UCS} = 0{,}24E_{dyn} - 871$	0.61 0.16	$\frac{E_{dyn}}{E_{stat,UCS}} = 3945E_{stat,UCS}^{-0.72}$ $\frac{E_{dyn}}{E_{stat,3-ax}} = 4780E_{stat,3-ax}^{-0.73}$	0.96 0.72	$E_{stat,UCS} = (\frac{E_{dyn}}{3945})^{3.57}$ $E_{stat,3-ax} = (\frac{E_{dyn}}{4780})^{3.70}$
Metaseds. Gabbro	PSSL 3-axial test	$E_{stat} = 0{,}52E_{dyn} + 12142$	0.10	$\frac{E_{dyn}}{E_{stat}} = 3757E_{stat}^{-0.75}$	0.80	$E_{stat} = (\frac{E_{dyn}}{3757})^{4}$

Table 6: Summary of the derived empirical relations for static moduli.

7 Relations between unconfined compression strength and seismic velocities

The unconfined compression strength (UCS) is an important and often used parameter in geotechnics. In combination with the internal angle of friction it is used to construct failure criteria (CHANG et al., 2006).

Correlation between strength properties and seismic velocities within a rock type is based on some dominant influences changing both properties in a comparable direction (SCHÖN, 2011). Increasing fracturing or porosity decreases both properties and increasing cementation increases both properties (SCHÖN, 2011).

A correlation can be expected for a specific rock type, but not as a "general formula". As an example for a good correlation (see SCHÖN, 2011) the uniaxial compression strength (142 samples) and the compressional wave slowness (measured with a sonic logging tool) of fine to medium-grained sandstone from the German Creek formation (Queensland, Australia) is used (Fig.55). Two regressions are calculated:

linear regression $\sigma_c = 0.050 \cdot v_p - 114.5$ with R^2= 0.88 (48)

power law $\sigma_c = 3 \cdot 10^{-11} \cdot v_p^{3.45}$ with R^2= 0.86 (49)

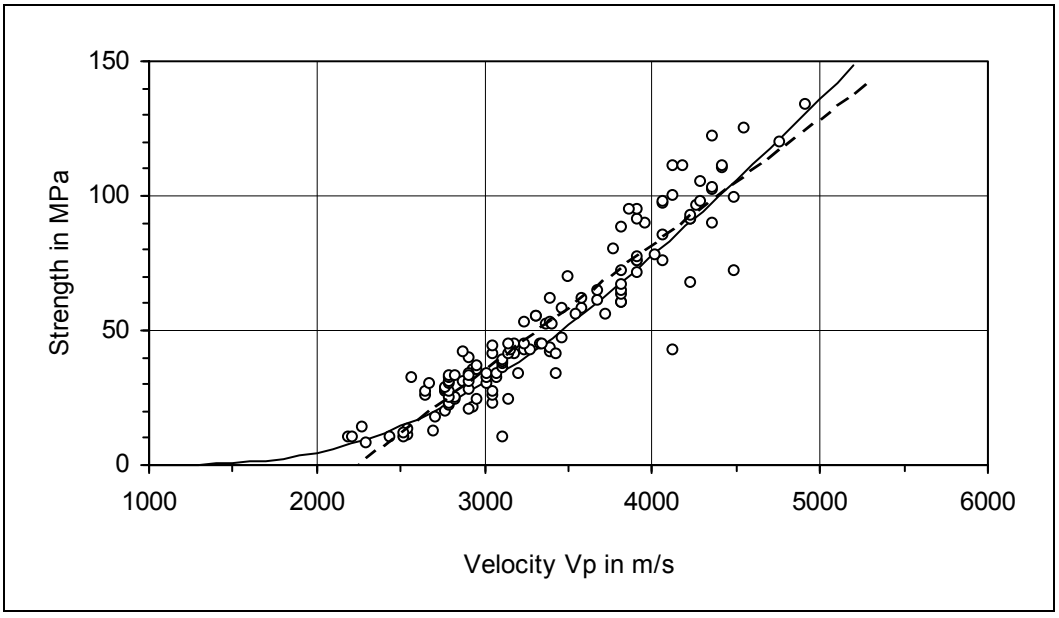

Fig.55: UCS as a function of compressional wave velocity from the German Creek Formation in Australia. The curves follow equations (48) and (49) (SCHÖN, 2011 after McN ALLY, 198[*])

[*]*: MCNALLY, G.H., 1987. Estimation of coal measures rock strength using sonic and neutron logs. Geoexploration 24, 381-395).*

According to this example the relation between seismic velocities and UCS in the given datasets are examined in this chapter. Target is to evaluate correlations between strength and velocity and to derive empirical relations to estimate UCS as accurate as possible from seismic velocities.

The first example (Fig.56 and 57) involves shaly limestones and siliciclastic rocks. Seismic velocities have been measured with PS Suspension Logger (PSSL). For siliciclastics only a low number of UCS values could have been correlated with seismic velocities. Still it seems that siliciclastic rocks offer lower UCS than the limestones. The estimation of UCS via empirical relations is not possible sufficiently in this data set. Calculated linear regressions show very low fit to the data. The use of power law relations improves the fit insignificantly to a moderate level.

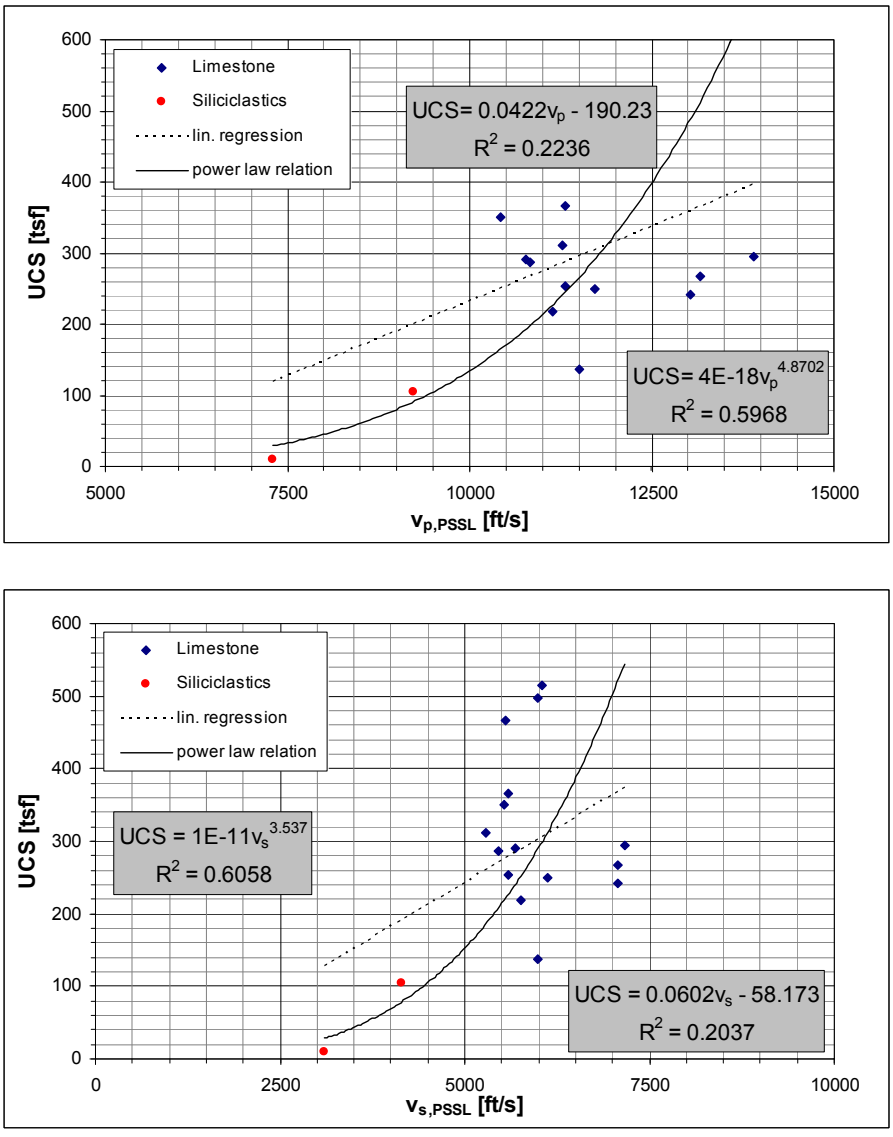

Fig.56: UCS as a function of compressional wave velocity v_p (top) and shear wave velocity $v_s$measured with PSSL in a succession of shaly limestones and siliciclastics. For the silicilastics only 2 data values could be correlated with velocities. Still it seems that the siliciclastics show much lower UCS than the limestones. The calculated linear regressions show poor fit to the data. Using power law relations improves the relations to a moderate fit. There is no significant difference between the correlation of UCS with v_p to the correlation with v_s.

The fact that the siliciclastics offer lower UCS than the limestones is mainly caused by differences in porosity. Fig.57 shows the relation between UCS and porosity for the two encountered lithologies. The siliciclastic rocks of this dataset show relative high porosities in the range between 15 and 35% compared to the limestones, which show porosities lower than 18% and therefore lower UCS.

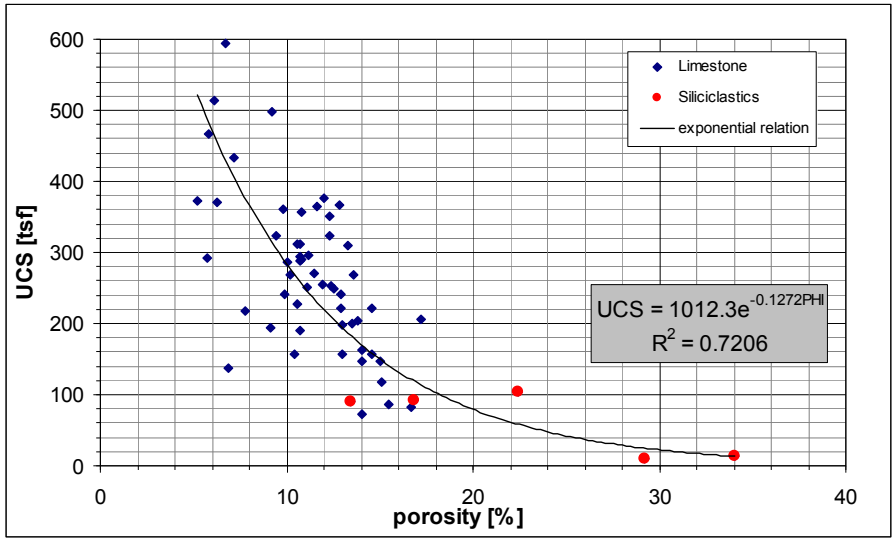

Fig.57: UCS as a function of porosity in the same shaly limestones and siliciclastic as in Fig.56. UCS is shows exponential decrease with increasing porosity. The low values for UCS of siliciclastic rocks found in Fig.56 are mainly caused by their higher (and different) porosity. UCS as function of porosity can be roughly estimated with an exponential equation.

In Fig.58 an example of data from granitic rocks is presented. UCS and seismic velocities measured with full wave form sonic log (FWS) show rather low correlation due to massive scattering data. The linear regressions and the power law relations show no significant fit to the data, which would allow sufficient estimation of UCS. Neither the use of compressional wave velocity nor the use of shear wave velocity leads to a sufficient result.

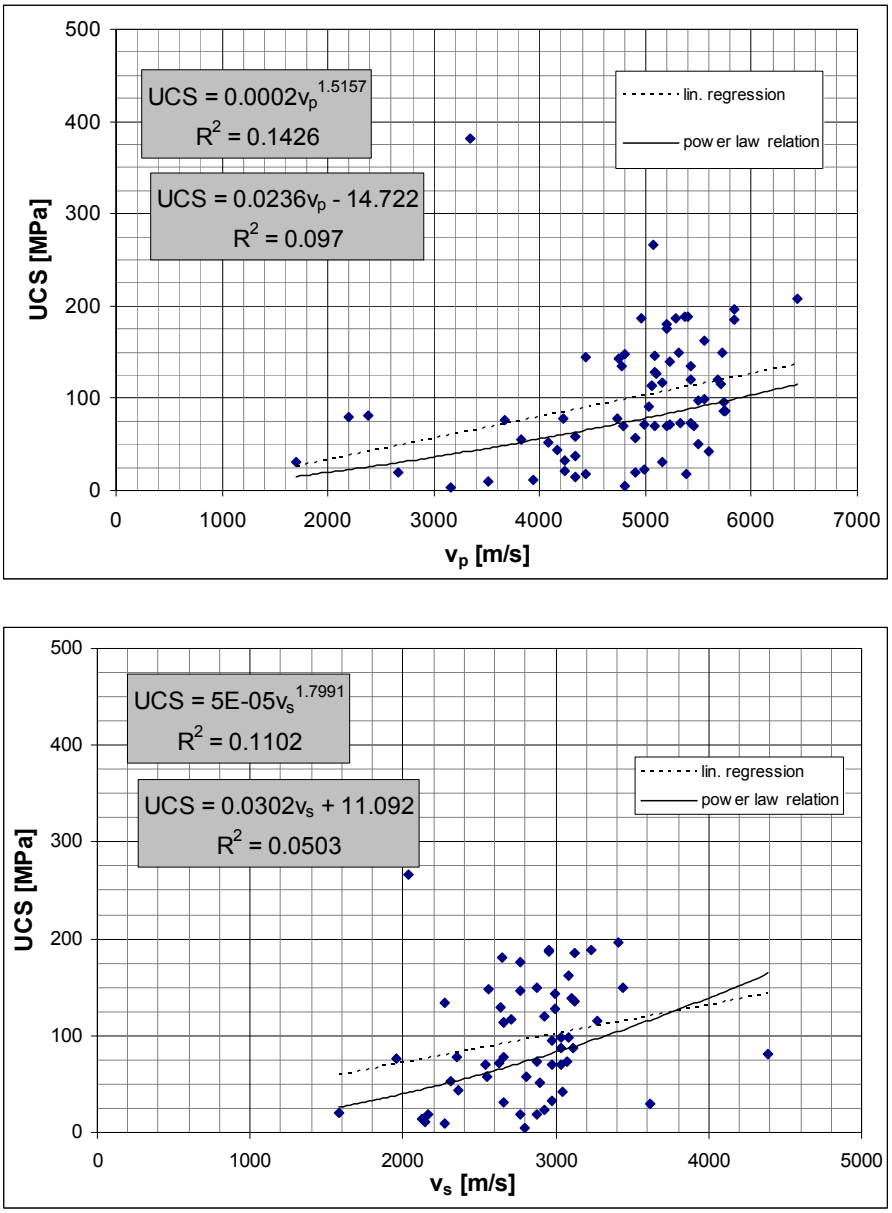

Fig.58: UCS as a function of v_p (top) and v_s (bottom) measured with FWS in granite dominated rocks. UCS is affected by massive scattering and the velocity range especially for the shear wave is rather tight (mainly 2000-3500 m/s), resulting in the fact that no sufficient empirical relation can be derived, which would allow estimation of UCS from seismic velocities.

In the dataset presented in Fig.59 seismic velocities have been measured with PSSL in a siltstone formation. The correlation with the seismic velocities is low. Increasing velocity increases UCS, but no sufficient equation for UCS estimation from seismic velocities could be derived. In the plot an attempt of estimating the maximum UCS of the encountered lithologies is presented.

For the UCS tests information about applied stress rate was also available and integrated in the plots. The stress rate describes the increment of load increase on the sample per time (here in MPa/min) during the UCS test until failure occurs. Three stress rate classes (0-5, 5-10 and 10-20 MPa/min) have been defined and colour coded in the plot. It seems that increasing the stress rate increases the measured UCS for the given siltstones.

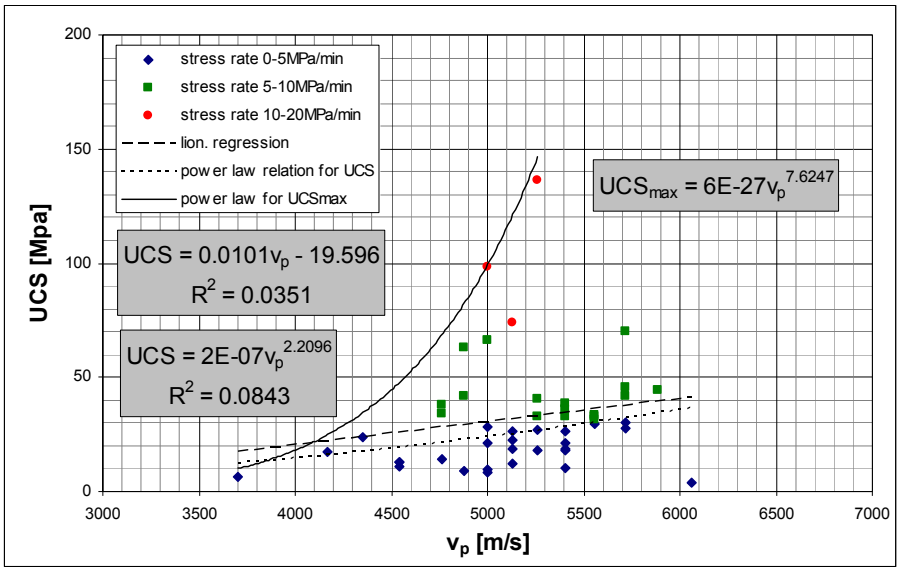

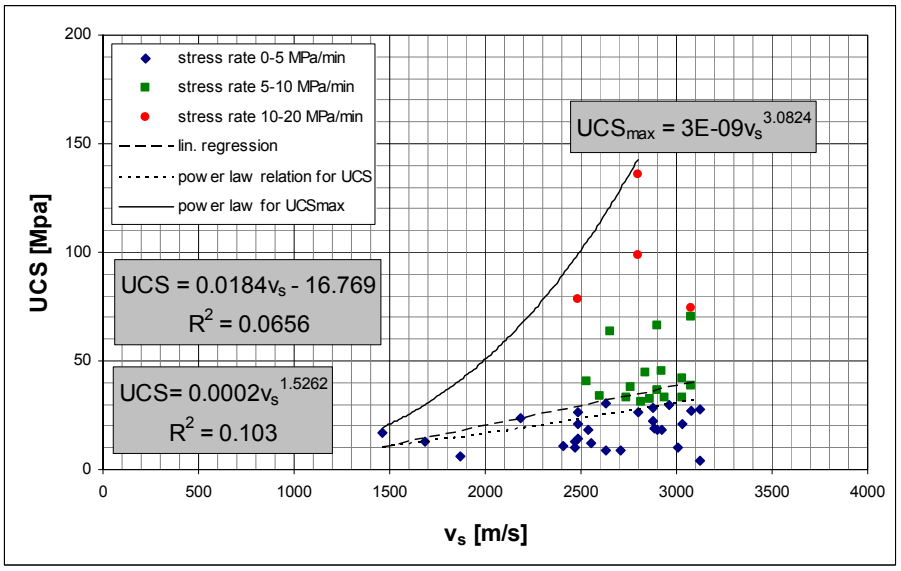

Fig.59: UCS as a function of v_p (top) and v_s (bottom) measured with PSSL in a siltstone succession. Again the data is affected by massive scattering, which inhibits estimation of UCS from seismic velocities. UCS is dependant on the applied stress rate. Increasing stress rate increases UCS in the siltstones (color coded in the plot).

In Fig.60 the dependence of UCS from the applied stress rate and from porosity is separately shown in. As already suggested in Fig.59 a linear dependence can be observed between UCS and stress rate. The decrease of UCS with porosity is affected by stronger scatter but seems to follow an exponential function.

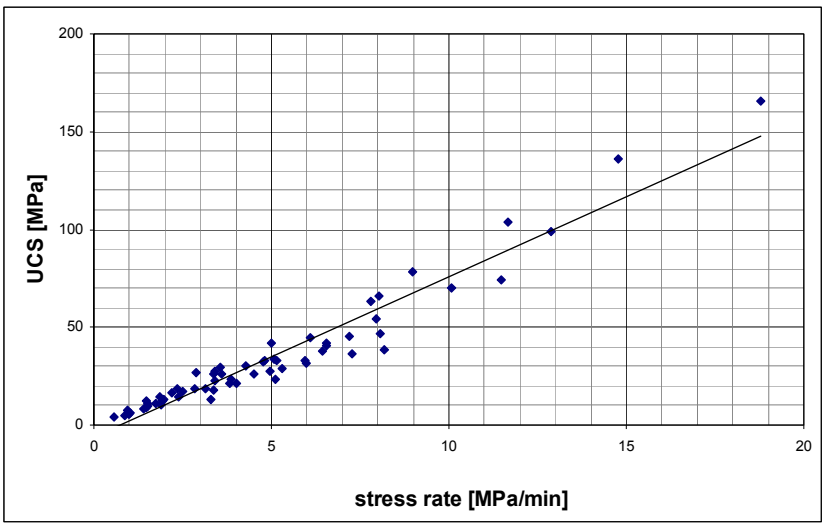

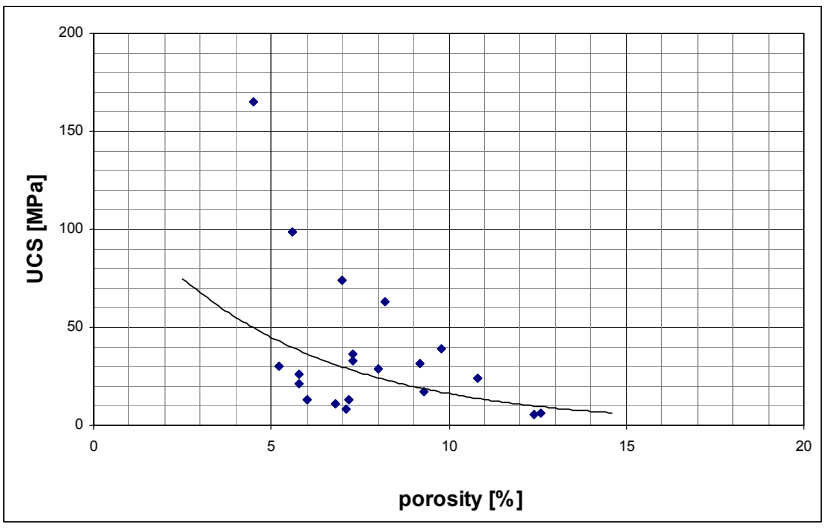

Fig.60: Dependance of UCS from the applied stress rate and from porosity on a test series on siltstone samples. UCS shows (linear) increase with increasing stress rate and a decrease with with porosity.

Summing up the influences of wave velocity, porosity and applied stress rate (SR) on the UCS of the given rocks gives:

$$UCS \propto v_{p/s}, \frac{1}{\phi}, SR \tag{59}$$

To derive an equation for UCS as a function of velocity, porosity and stress rate, the parameters were combined according to relation (59) to one new defined factor

$$F = \frac{v_p \cdot SR}{\phi} \tag{60}$$

In Fig.61 UCS as a function of F is plotted. The data distribution shows surprisingly good fit (R^2=0.89) to linear equation for UCS(F):

$UCS = 0.82\frac{v_v \cdot SR}{\phi} + 1.82$ (61) with F=f(v_p [m/s], 1/Φ and SR [MPa*m/s*min]).

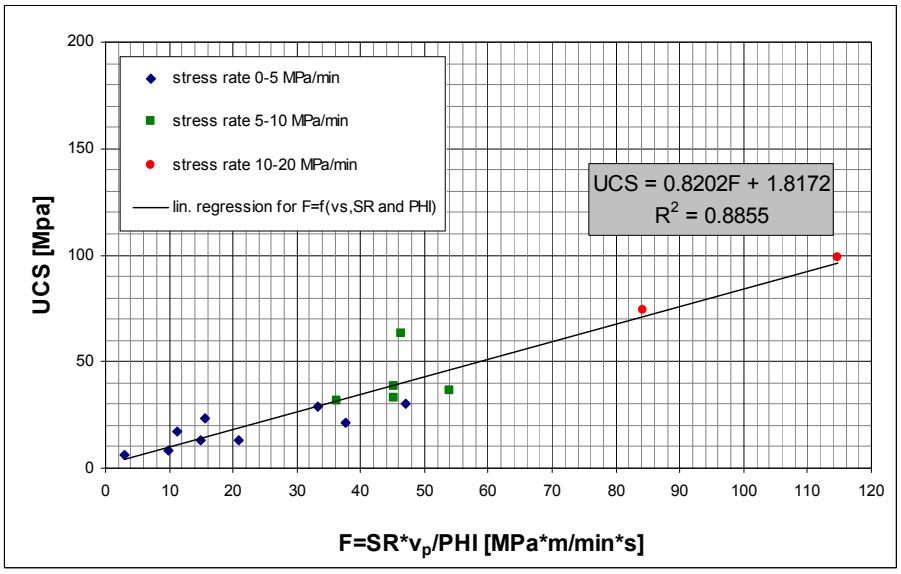

Fig.61: Derivation of an empirical "model" for UCS in dependence of porosity, v_p and applied stress rate. The resulting linear function for UCS as a function of factor F shows surprisingly good fit to the data.

Using shear wave velocity instead of compressional wave velocity neither increases nor decreases the fit to the data significantly (Fig.62).

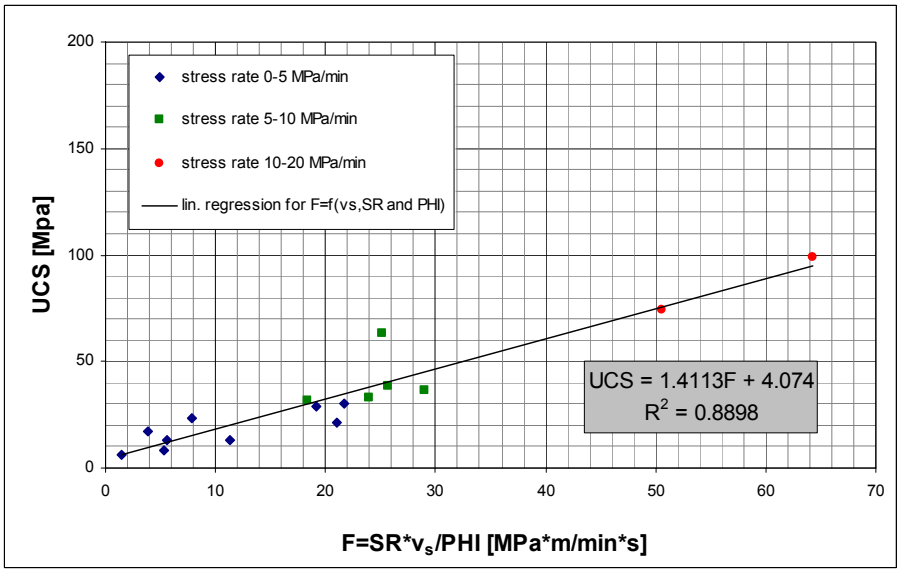

Fig.62: Use of shear wave velocity for F does not change the quality of the derived equation significantly.

The last example (Fig.62) shows an example of a very well fitting empirical relation for UCS in dependence of v_p measured with PSSL in calcarenites and limestones from Dubai. The fit to the derived exponential function is excellent and the derived equation seems to be appropriate enough to estimate UCS directly from PSSL velocities.

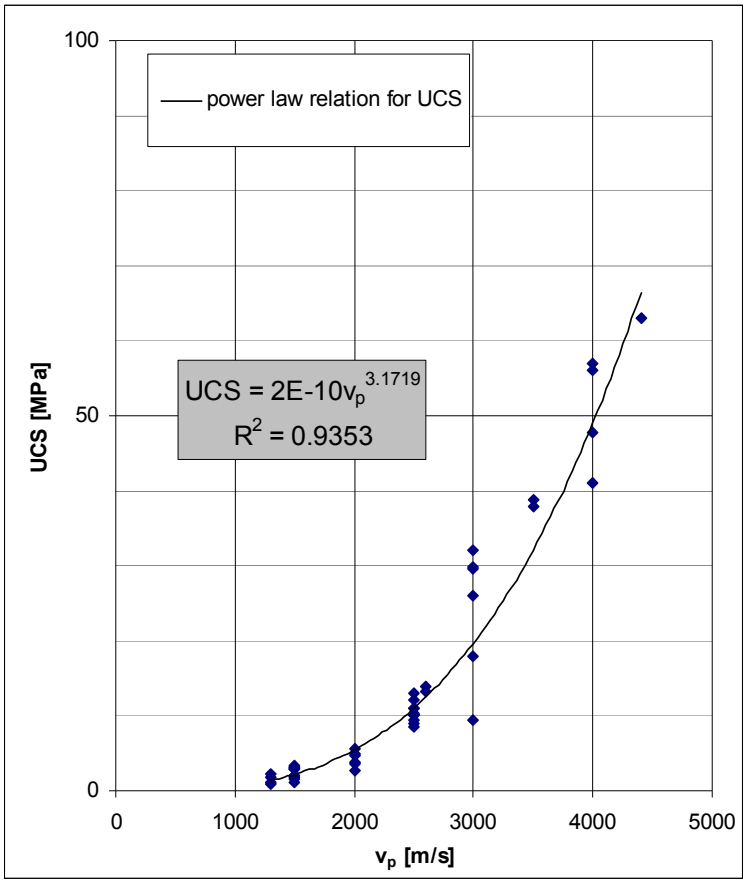

Fig.63: Very well fitting empirical equation for UCS as a function of v_p measured with PSSL in calcarenites and limestones.

7.1.1 Conclusions

In the presented data examples only one case shows well correlating UCS with seismic velocities. In all other cases no sufficient correlation for a derivation of an empirical equation for estimation of UCS from seismic velocities could be found.

One important influencing factor for UCS is the porosity of the analysed rocks. UCS is highly sensitive to porosity. Increasing porosity leads to exponential decrease of UCS.

Also an important role for measured UCS plays the applied stress rate during the tests. Between UCS and stress rat a clear linear dependence was found in one of the data examples. It was possible to derive an equation for UCS as a function of porosity, velocity and stress rate.

8 Conclusions and discussion

Deformation moduli of soil and rock are important parameters for geotechnical site investigations and design. Static methods are well established in geotechnics and are seen to offer reliable modulus values over a broad range of stress and strain, whereas dynamic moduli are restricted to very small strains. Static methods are often costly and time consuming compared to dynamic methods that can provide investigation of larger volumes at a reasonable amount of time and money. To overcome the disadvantages and to combine the advantages of both approaches, it was tried to find correlations between static and dynamic moduli with the intention to find reliable empirical relations to extend the static point information to larger volumes.

In a first step it was intended to perform a direct comparison of different static and different dynamic measurement techniques to get an idea of how congruent (or incongruent) different static and different dynamic results are. A direct comparison of static methods was unfortunately not possible due to lack of “data intersection”. Different static methods have not been applied in the same location/borehole in the given data sets.

The comparison of wave velocities measured with different dynamic methods shows that generally small differences between velocities from different methods occur. These differences are mainly caused by different measurement frequencies and different resolutions and occur especially between non invasive surface methods like the spectral analysis of surface waves and borehole methods like full wave form sonic logging or PS Suspension Logging. An exception from this trend seems to be the downhole seismic method. Velocity values obtained with downhole seismics show good correlation with other methods in some sections, but also low or no correlation in other sections. This is seen to be mainly caused by the fact that source receiver offset is increasing during measurements leading to an increase of wave energy attenuation especially of high frequencies with increasing investigation depth resulting in difficulties in accurate and distinct first arrival determination. Therefore PS Suspension Logging for soils and unconsolidated materials and full waveform sonic logging in rocks, providing constant source receiver offset should be preferred if the borehole conditions (fluid filled, open hole and acceptable hole inclination) allow this measurements.

Beside the availability of density values, the determination of shear wave velocity is often the limiting factor for the dynamic methods, especially for full waveform sonic and PS Suspension Logging. For this reason it was tried to estimate shear wave velocities from v_p/v_s crossplots. This site and lithology specific approach offered moderate to poor success. Only crosshole measurements seem to provide sufficient data quality for accurate shear wave velocity estimations in rocks as well as in unconsolidated materials. For other methods the fit

of derived equations to the given data distributions was generally moderate to poor. An appropriate estimation of v_s is therefore not recommended.

The correlation between static and dynamic moduli showed that in shallow geotechnical investigations the ratio of dynamic over static modulus can range over two or three decades. The dynamic modulus can reach values that are 100 times the static one. Static methods cover a broad stress and strain range and are (or can be) performed until material failure. Therefore also non elastic deformation processes can be analysed. The dynamic methods offer measurements in a very small strain area and cover only elastic deformations resulting in higher dynamic moduli. Beside these fundamental differences, weathering seems to be an important factor for massive increases of the dynamic/static ratio.

The direct correlation between static and dynamic moduli to derive linear relationships for estimation of static moduli did not provide sufficient results. The derived equations offered poor or no fit to the given data distributions, which were affected by massive scattering. A result that could be obtained from the direct approach in nearly all cases is a derivation of maximum occurring static modulus of the site or the investigated lithology.

To increase the quality of empirical relations for the static parameters an indirect approach was selected. The dynamic/static ratio was plotted as a function of static modulus. This approach decreased the scattering in the data distributions for all presented examples. The derived equations for the ratio as a function of static modulus were solved for the static modulus. In all examples the fit of derived equations was increased successfully with this approach (compared to the linear approach). Except two examples R^2 was raised to values above or equal to 0.80 indicating good to excellent fit to the data.

Because of abundant data for the unconfined compression strength, correlations between this strength property and acoustic velocities were included in this report. Relating UCS only to the wave velocities did generally not provide sufficient relations, because of massive scattering in the data distributions. Only one case was found, where PSSL velocities can be used to estimate UCS accurate enough. Similar to the linear modulus correlation, only a function for maximum occurring UCS in the investigated lithologies could be derived.

In one example additional information about porosity and applied stress rate were included in the analysis. Seismic velocity, porosity and stress rate were combined to a new factor F and plotted against the UCS, resulting in a good linear correlation between F and UCS. Involving porosity and stress rate would allow relative accurate estimation of UCS.

9 Indices

9.1 References

BARTON, N., 2007. Rock quality, seismic velocity, attenuation and anisotropy. Taylor & Francis Group, London, UK, 2007, 729 p.

BATZLE, M. and WANG, Z., 1992. Seismic properties of pore fluids. Geophysics 57 (11), p. 1396-1408.

BOYER, S., MARI, J.-L., 1997, Oil and Gas Exploration Techniques: Seismic Surveying and Well Logging. Editions Technip, Paris, 1997, 192 p.

CASTAGNA, J.P., BATZLE, M.L., EASTWOOD, R.L., 1985. Relationships between compressional-wave and shear wave velocities in clastic silicate rocks. Geophysics 50, p. 571-581.

CASTAGNA, J.P., BATZLE, M.L., KAN, T.K., 1993. Rock Physics – The link between rock properties and AVO response. In: CASTAGNA, J.P., BACKUS, M.L.(eds.),Offset-Dependant Reflectivity – Theory and Practice of AVO analysis. Investigations in Geophysics, 8, 348 p.

CHANG, C., ZOBACK, M.D., KHAKSAR, A., 2006. Empirical relations between rock strength and physical properties in sedimentary rocks. Journal of Petroleum Science and Engineering, Vol. 51, Elsevier 2006, p. 223-237.

DE VALLEJO, G. and FERRER, M., 2011. Geological engineering. CRC Press, Balkema, Boca Raton, 2011, 678 p.

ELLIS E.V., SINGER J.M., 2007, Well Logging for Earth Scientists. 2nd Edition, Springer Verlag, Dortrecht, 2007, p.247-322.

FJAER E., HOLT R.M., HORSRUD P., RAAEN A.M. AND RISNES R., 1992, Petroleum related rock mechanics. Developments in Petroleum Science, Vol. 33, Elsevier, 1992, 338p.

HALDORSEN J. B. U., JOHNSON D. L., PLONA T., SINHA B., VALERO H.-P., WINKLER K., Borehole Acoustic Waves, Oilfield Review, 2006, p. 34-43.

HAN, D., NUR, A. and MORGAN, D., 1986. Effects of porosity and clay content on wave velocities in sandstones. Geophysics, 51 (11), p. 2093-2107.

HELBIG, K., 1992. Coordinate-free representation of the elastic tensor. EAGE 54th Meeting and Technical Exhibition, Paris, 1-5 June, paper A049.

HORSRUD, P., 2001. Estimating mechanical properties of shale from empirical correlations. SPE drill. Complet. 16, 68-73.

KING, M.S., SHAKEEL, A. AND CHAUDRY N.A., 1997, Acoustic wave propagation and permeability in sandstones with systems of aligned cracks. IN: LOVELL, M.A. AND HARVEY, P.K. (eds), 1997, Developments in Petrophysics, Geological Society Special Publication No. 122, p. 69-85.

LAMA, R.D. AND VUTUKURI, V.S., 1978, Handbook on Mechanical Properties of rocks – Testing Techniques and results, Volume II. In: Series on rock and soil mechanics, Vol.3, No.1, 1978, Trans Tech S.A., Switzerland, 1978, 481p.

LOOK, B., 2007.Handbook of Geotechnical Investigation and Design Tables.Taylor&Francis Group, London (and others), 2007, 331p.

LUNNE T., ROBERTSON P.K., POWELL J.J.M., 1997, Cone Penetration testing in Geotechnical Practice. Blackie Acad. & Professional, London, 1997, p.179-181.

MAVKO,G., MUKERJI and DVORKIN, J., 1998. The rock physics handbook. Tools for seismic analysis in porous media. Cambridge University Press, first published 1998, 329p.

MOGI, K., 2007, Experimental Rock Mechanics. In: Kwasniewski, A.M. (editor in chief), 2007, Geomechanics Research Series Vol. 3. Taylor&Francis Group, London, UK, 2007, p. 3-193.

SCHÖN, J., 1983, Petrophysik. Physikalische Eigenschaften von Gesteinen und Mineralen. Ferdinand Enke Verlag Stuttgart, 1983, p.349ff.

SCHÖN J.H., 1996, Physical properties of rocks: fundamentals and principles of petrophysics. Handbook of geophysical exploration, Seismic Exploration, Vol. 18, K. Helbig and S. Treitel (eds.), Pergamon Press London , 1996, 1st edition, p.133-273.

SCHÖN J.H., 2011, Physical properties of rocks: A workbook. Handbook of petroleum exploration and production, Vol. 8, CUBITT, J. (series editor), Elsevier, 2011, p149-272.

TELFORD, W.M., GELDART, L.P., SHERIFF, R.E., Applied geophysics, Second Edition, reprint 2004. Cambridge University Press, first published 1990, p.149ff.

THOMSEN, L., 1986. Weak elastic anisotropy. Geophysics 51 (10), p.1954-1967.

WHITE J.E., 1983, Underground Sound, application of seismic waves. Methods in Geochemistry and Geophysics, 18, Elsevier Science Publishers B.V., 1983, 253p.

WIDARSONO, B., MARSDEN, J.R. AND KING, M.S., 1998, In situ stress prediction using differential strain analysis and ultrasonic shear wave splitting. In: HARVEY, P.K. AND LOVELL, M.A. (eds) Core-Log Integration, Geological Society, London, Special Publications, 136, p. 185-195.

ZHANG, L., 2005. Engineering properties of rocks. Elsevier geo-engineering book series, Vol. 4, Elsevier, Amsterdam, 2005, 290 p.

9.2 Tables

9.3 Figures

Appendix

Description of involved methods

Seismic Surface Waves - Spectral Analysis of Surface Waves (SASW)

Method description

SASW uses Surface Wave (especially Rayleigh Wave) dispersion to evaluate shear wave velocity and shear modulus profiles. About 2/3 of the energy produced by seismic sources are imparted into Rayleigh waves (also “ground roll”), which show very high dependence on shear wave velocity of the ground. Dispersion means that different frequency components of the surface wave travel at different velocities (phase velocity) in a layered medium. According to that the use of a wide frequency range allows sampling of different portions of the ground. High frequencies (wavelengths shorter than the top layer thickness) propagate only through surface layers, whereas lower frequencies also propagate through deeper soils. SASW uses a pair of receivers (velocity transducers or accelerometer), which is configured according to the frequency range that should be detected. Vibrations of known frequency travel from source to receiver along the surface, are recorded, digitized and transformed into frequency domain via Fast Fourier Transformation.

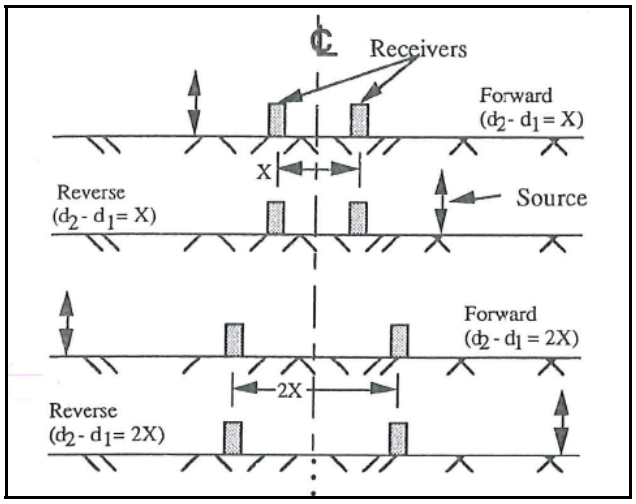

Fig.64: Scheme of a common mid point (CMP) geometry spread used for SASW measurements. Source receiver distances and receiver spacings ar increased in steps (from STOKOE et al., 1994).

The source is normally used in a forward and reverse position. The result of the measurements is a dispersion curve, plotting phase velocity versus frequency or wavelength. To obtain shear wave velocity profiles an iterative inversion is applied, including estimations of Poisson’s Ratio, layer thickness and density.

System data	Spacing	typically 0.5 m, 1 m, 2 m, 4 m, 8 m, 16 m, 32 m and 64 m
	Vertical resolution	low to medium, controlled by local properties (velocity contrasts, layer thickness,…). Rule of thumb: Layer thickness should be at least 1/5 of its depth to be resolved.
	frequency	low (several to several tens of Hz)
	investigated volume	high
	Seismic Sources	for spacings up to 8 m: (sledge) hammers, dropped weights up to 70 kg. For spacings above 8 m: dropped weights up to 900 kg, bulldozers or large dynamic compaction weights
Formation	Preferred soils. Receiver coupling and source energy transmission must be possible.	
Depth limit	PARK et al, 2007: generally 10 to 30 m with possibility of site specific variations	
Parameters	measured	travel time of surface waves with a known frequency
	calculated	velocities of s-waves
Measuring progress	medium to high	

Comment Problems for SASW:

- Near field effects of surface waves that travel only short distances from the source (non planar wave geometry)
- The use of only a pair of receivers may lead to difficulties in distinguishing between noise and signal
- Far field effects caused by attenuation of higher frequencies and noise contamination at higher offsets
- Stiff over soft layers
- Stiff Sides overlaid by water
- Gravity effect leading to increased surface wave velocities in very soft undergrounds and at very large wavelengths. STOKOE et al., 1994 calculate the critical wavelength, where gravity starts to play a role with: $$\lambda_{critical} = \frac{2\pi v_s^2}{\sqrt{1-(\frac{v_s^2}{v_p^2})^2}}$$
- Inversion of dispersion curves requires preliminary knowledge of underground conditions.

Seismic Surface Waves - Active Multichannel Analysis of Surface Waves (MASW)

Method description

Active MASW is a refinement of SASW using faster multichannel acquisition (12 or more channels) with linear receiver spreads, allowing better frequency identification and easier selection of data processing parameters than SASW. Active means that the method uses an artificial seismic source (hammers,…). MASW can also be applied in shallow water offshore environments using airguns as source and hydrophone streamers as receivers. The surface wave occurring at the water-seabed interface is called Scholte wave.

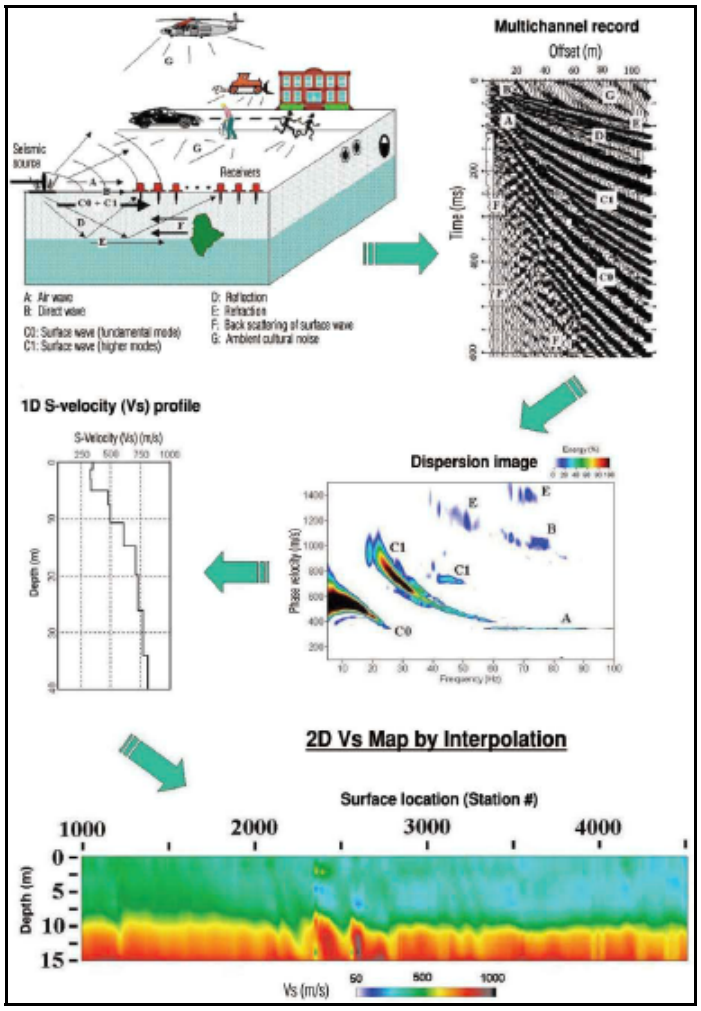

Fig.65: scheme of the different MASW acquisition steps (PARK et al., 2007). Surface waves created by different types of sources are recorded by a multichannel recording system. Inversion of constructed dispersion curves leads to shear wave velocity versus depth profiles. Interpolation between different profiles allows construction of extended 2D-profiles.

System data

Spacing	usually 0.5 m, 1 m, 2 m, 4 m, 8 m, 16 m, 32 m and 64 m.
Vertical resolution	low to medium, controlled by local properties (velocity contrasts, layer thickness,…). Rule of thumb: Layer thickness should be at least 1/5 of its depth to be resolved

	frequency	Low (several to several tens of Hz)
	investigated volume	medium to high
	Seismic Sources	for spacings up to 8 m: (sledge) hammers, dropped weights up to 70 kg. For spacings above 8 m: dropped weights up to 900 kg, bulldozers or large dynamic compaction weights, VIBROSEIS and airguns for offshore applications.
Formations	Preferred soils. Receiver coupling and source energy transmission must be possible.	
Depth limit	PARK et al, 2007: generally 10 to 30 m with possibility of site specific variations.	
Parameters	measured	travel time of surface waves with a known frequency
	calculated	velocities of s-waves
Measuring progress	medium to high	

Comment

The use of only a pair of receivers may lead to difficulties in distinguishing between noise and signal

Problematic cases for MASW:

- Near field effects for surface waves that travel only short distances (low offset) from the source (non planar wave geometry)
- Far field effects caused by attenuation of higher frequencies and noise contamination at higher offsets
- Stiff over soft layers
- Stiff Sites overlaid by water
- Gravity effect leading to increased surface wave velocities in very soft undergrounds and at very large wavelengths. STOKOE et al., 1994 calculate the critical wavelength, where gravity starts to play a role with : $$\lambda_{critical} = \frac{2\pi v_s^2}{\sqrt{1-(\frac{v_s^2}{v_p^2})^2}}$$
- Tide and currents in the offshore environment have to be respected while planning MASW offshore profiles.

Seismic Surface Waves - Refraction Micro Tremor (ReMi), Passive and Interferometric Multichannel Analysis of Surface Waves (MASW)

Method description

Refraction Microtremor or Microtremor Survey Method and passive MASW are generally working like the SASW and MASW method. Passive means that surface waves are not generated by artificial seismic sources but by cultural (traffic,…) or natural activities (tidal motion,…). PARK et al., 2007 distinguish two different methods of passive MASW; the passive remote MASW and the passive Roadside MASW: A recent development on the field of surface wave methods is the Interferometric MASW, which uses slowness-frequency slant-stack analysis combined with interferometric time-domain dispersion analysis to improve resolution and maximum investigation depth of MASW.

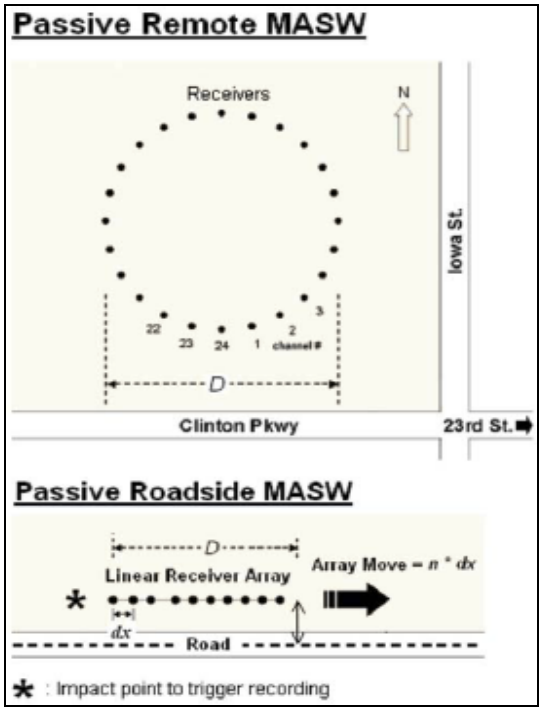

Fig.66: Passive MASW-methods and their measurement geometries. Passive remote MASW can use any symmetric receiver array (PARK et al., 2007).

The passive remote MASW can use any symmetric receiver array for data acquisition, whereas the roadside method uses linear arrays. The combination of active and passive methods can enlarge the analyzable frequency.

Comment

Combination of active and passive surface wave methods can improve quality of results.

For further information on interferometric MASW Daniel R. H. O'Connell and James P. Turner (Fugro Will Lettis & Associates, Inc) should be contacted.

References

STOKOE K.H., WRIGHT, S.G., BAY, J.A., ROESSET, J.M., 1994. Characterization of geotechnical sites by SASW method. IN: Geophysical Characterization of Sites, Volume prepared by ISSMFE Technical Committee #10 for XIII ICSMFE, 1994, New Delhi, India. Edited by Richard D. WOODS, International Science Publisher, New York, 1994, p.15-25.

PARK B.C., Miller R.D., Jianghai X., 1999, Multichannel analysis of surface waves, Geophysics, Vol.64, No. 3, May-June 1999, p.800-808.

PARK., B.C., MILLER, R.D., XIA, J. and IVANOV, J., 2007. Multichannel analysis of surface waves (MASW) – active and passive methods. The leading edge, January 2007, p. 60-64.

ANDERSON N., CHEN G., KOCIU S., LUNA R., THITIMAKORN T., MALOVICHO A., MALOVICHKO D., SHYLAKOV D., 2003, Final report RDT 03-006, Vertical Shear-Wave Velocity Profiles Generated From Spectral Analysis Of Surface Waves: Field Examples. Prepared for Missouri Departement of Transportation, Research, Development and Technology, Jefferson City, Missouri, April 2003.

O'CONNELL, D.R.H. and TURNER, J.P., 2011. Interferometric Multichannel Analysis of Surface Waves (IMASW). Bulletin of the seismological society of America, 10/2011, Vol. 101, p.2122-2141.

Borehole Extension Testing

Method description

This kind of tests uses devices in prebored holes in soils and rock. Many tools use drilled pockets of a smaller diameter than the main hole. Lengths of this pockets vary usually between 1.5 m and 3.0 m. The devices are lowered down to the wished depth and apply pressure on the borehole wall. The resulting deformation is measured. "Seitendrucksonden" use hydraulic cylinders for load application and electrical distance measurement, the Menard Probe or Pressuremeter uses tube packers and volumetric borehole extension measurement and Dilatometers use tube packers combined with electrical distance measurement. The tests can comprise between 2 to 14 circles of loading and unloading at one depth. The maximum applied pressure depends on the building planned or is reached when the rock formation fails or the loading limit of the tool is reached. From the recorded stress strain diagram the mechanical properties can be derived.

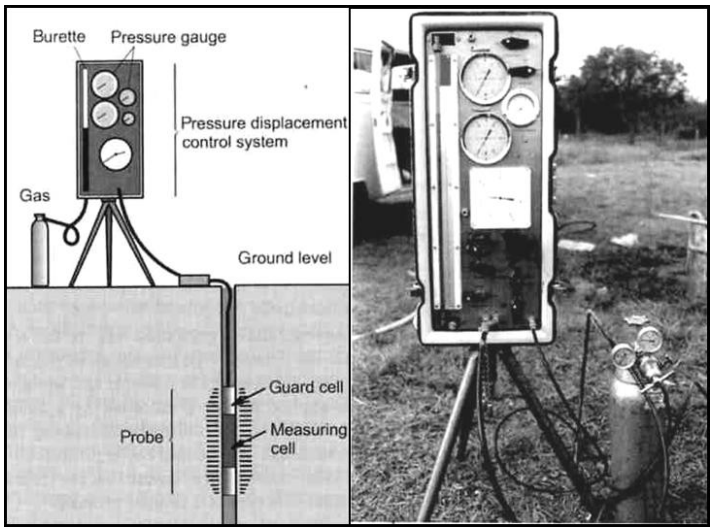

Fig.67: Example for a Menard Probe and its use in a borehole (SCHNAID, 2009).

For the analysis cycles after onset of plasticity (if reached) are preferred. To derive the shear modulus 3 parts of the pressure-deformation curve are interesting:

- The initial slope of the elastic loading phase (initial shear modulus)
- The slope of the chord bisecting small rebound cycles
- The slope f the first part of the contraction curve

For the reason that strain-stiffness relationships are not strictly linear more comprehensive interpretation methods have been developed, looking at smaller steps of the curve and not the extreme ends of the cycles.

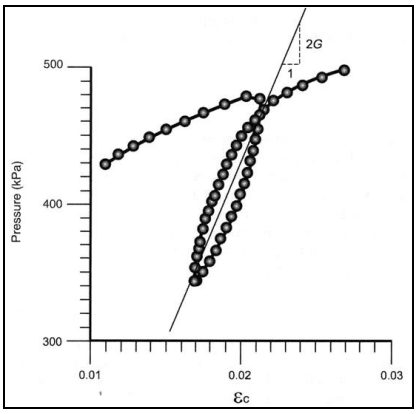

Fig.68: Load-Unload Loop and estimation of deformation modulus from the loop (SCHNAID, 2009).

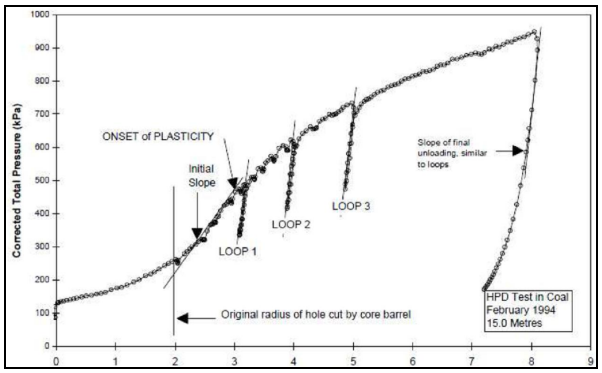

Fig.69: Load-Unload Loops and interpretation of pressuremeter tests in coal (FUGRO internal material).

	System data	frequency	very low, “quasi-static”
		investigated volume	low
Borehole requirements:	no. of BH’s	1	
	BH-medium	dry or fluid filled	
	BH-completion	open hole	
	BH diameter	equipment dependant	
	BH inclination	vertical or slightly inclined wells	
Formation	Soils and rocks		
Depth limit	limited by tool construction		
Parameters	measured	pressure-displacement curves	
	calculated	deformation moduli (initial tangent modulus, secant modulus, onload-reload modulus)	
Measuring progress	low		

Comment

Aspects that should be taken into account for the use extension tests:

- Experiments should start in the first 24 hours after finishing the borehole in water flushed holes. In rammed or dry holes longer times can be accepted-
- The use of load plates for pressure application involves the danger of “line loading”, because the plates do not respect borehole wall relief.
- Tube packers allow radialsymmetric loading of the borehole wall in soils. In rocks low diameter changes might not be measured accurate enough with this systems.
- Strain curves derived from expansion curves are often not reliable, because of disturbances, errors in the reference state, partial drainage and because of a high strain rate variation with radial distance from the cavity.
- Testing in hard rocks is often limited by the pressure range of the tool. This can lead to pure elastic deformation only. In this case only shear modulus estimation is possible. In an isotropic medium conversion to Young’s Modulus is possible, if Poisson Ratio is known or estimated (E=2G(1+v).
- Extension tests perform tests usually on horizontally expanding cavities. The derived moduli are restricted to this plane.
- Testing should not be performed in heaviliy fractured areas, because analysis is based on the assumption of +/- intact material. To avoid such areas cores should be observed carefully (if

available), optical or acoustic borehole imagers can be run or sonic logging (FWS or PSSL) can help. Also caliper logs can help to avoid testing in zones where the borehole diameter is highly different from the nominal diameter.

- Exact placement of the tool is a critical point in pressuremeter testing. Core descriptions/photos and/or image logs and/or caliper logs can improve tool positioning.
- Unconsolidated materials are highly disturbed through drilling processes:

References

FECKER E., 1997, Geotechnische Meßgeräte und Feldversuche im Fels. Hrsg.: Edwin Fecker, 1997, Ferdinand Enke Verlag, Stuttgart, p.133-171.

LUNNE T., ROBERTSON P.K., POWELL J.J.M., 1997, Cone Penetration testing in Geotechnical Practice. Reprinted by E&FN Spon, London, 1997, p.179-181.

SCHNAID, F., 2009. In-situ testing in geomechanics, the main tests. Taylor&Francis, London, 2009, 329 p.

HUNT, R.E., 2005. Geotechnical engineering investigation handbook. Tayor&Francis, CRC, Boca Raton, 2005, 1066 pages.

Full Waveform Sonic Log (FWS)

Method description

The Sonic Log transmits a sonic signal and generates a p-wave in the borehole fluid. The p-wave radiates away from the transmitter in all directions and strikes the borehole wall. Some of the energy will propagate still as p-wave, some of it is converted into an s-wave. These waves generate elementary waves in each position radiating back at the critical angle of refraction and hit the receivers (receiver arrays with at least 2 receivers) located on the tool at defined distances. From the differences in travel time at the receivers and the tool geometry p- and s-wave velocities are calculated.

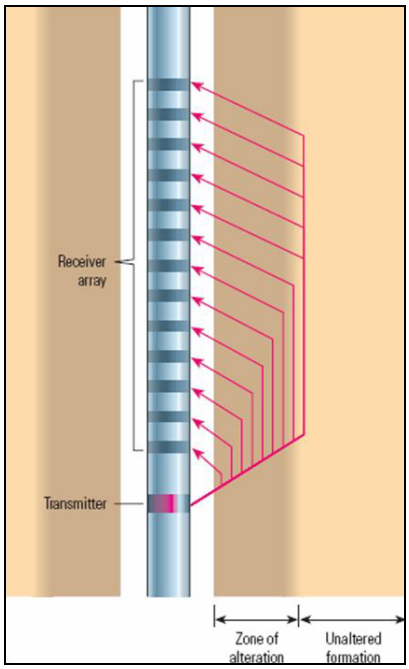

Fig.70: Principle of a FWS-tool. The energy emitted by a source is recorded by a series of receivers. In geotechnical applications typically 2-4 receivers are used (Picture from HALDORSEN et al., 2006).

The wave velocities can be obtained by direct manual picking of wave arrivals in the receiver data and by calculating the velocities from traveltime differences between the receivers (spacing is well defined). Another possibility is extracting the wave velocities via cross correlation using semblance algorithms.

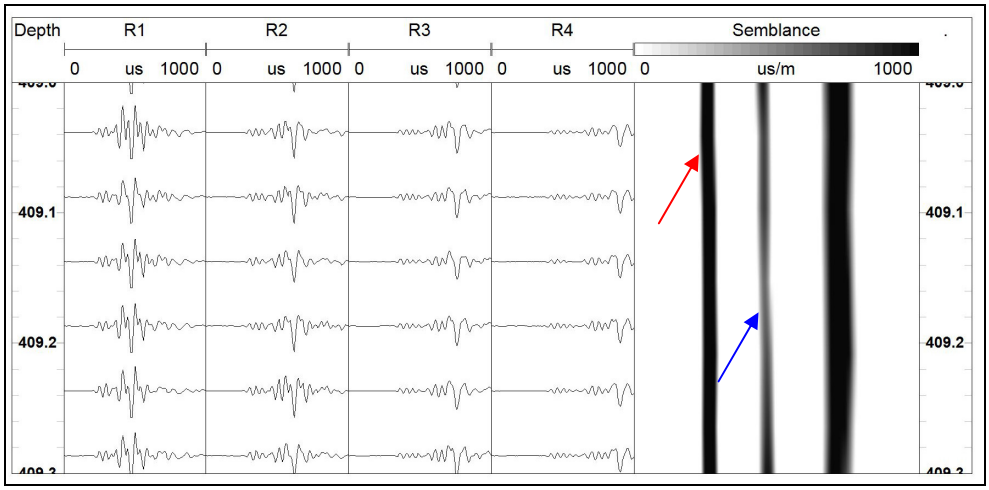

Fig.71: Example for a FWS record and a calculated Semblance cross correlation. The record consists of 4 receivers (R1-R4) that record the whole wavetrain. Spacings for this system are 0.6 m, 0.8 m 1.0 m and 1.2 m. The semblance gives correlation maximums for the p-wave (red arrow) and for the s-wave (blue arrow). The broad maximum at the right end includes a correlation maximum for the Stoneley wave (Fugro internal material).

System data	spacing	constant (typically 0.5m – 1.5m)
	verticalresolution	high and constant (≈spacing)
	sampling interval	high and constant (typically 5cm – 10cm)
	frequency	high (typically 5kHz - 20kHz)
	investigated volume	small and constant
Borehole requirements	no. of BH	1
	BH medium	water or drilling mud
	BH completion	open borehole
	BH inclination	90° - 30° from horizontal
Formation	limited to formations with v_p >1500m/s (usually consolidated materials and rocks)	
Depth limit	limited by logging cable or pressure rating of downhole tool	
Parameters	measured	travel time of acoustic waves
	calculated	velocities of p- and s-waves
Measuring progress	high (typical vertical logging speed is 4 m/min)	
Comment	Aspects that should be taken into account for the use of FWS: - FWS needs fluid filled and open boreholes. - FWS is highly dependant on the borehole conditions. Massively fractured zones, wall breakouts, soft layers, fault gauges, etc. can be the cause for data gaps in compressional and shear wave velocity data. - FWS does not work properly in unconsolidated materials or soils.	

References

HALDORSEN J. B. U., JOHNSON D. L., PLONA T., SINHA B., VALERO H.-P., WINKLER K., Borehole Acoustic Waves, Oilfield Review, 2006, p34-43.

ELLIS E.V., SINGER J.M., 2007, Well Logging for Earth Scientists. 2nd Edition, Springer Verlag, Dortrecht, 2007, p.247-322.

PS-Suspension Log (PSSL)

Method description

PSSL is using a single downhole probe, suspended by a cable containing a combined reversibly horizontal solenoid source and two biaxial geophones, separated by a flexible isolation tube. It is intended to provide relative low frequency measurements of traveltimes of p- and horizontal polarised, vertical propagating shear waves.

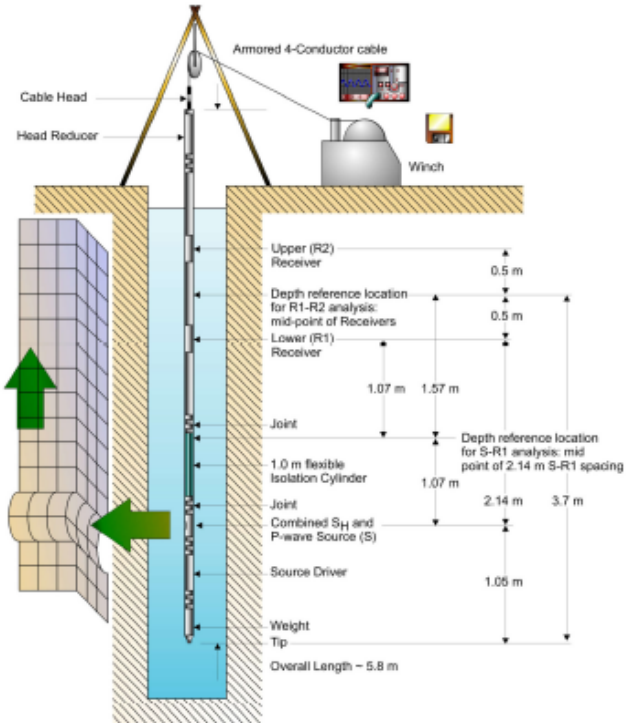

Fig.72: Functional units and measurement geometry of the PSSL tool (FUGRO internal material).

The source is activated in two opposite directions for generation of p- and horizontal polarised s-waves (in reality it is a flexural wave similar to a shear wave, but not quite the same). Each geophone is ideally recording signals with different pulses as nearly inverted images of each other. Stacking of up to 8 records can increase s/r-ratio.

PSSL measurements can be used in boreholes on- and offshore for measurements in low velocity soils as well as in hard rock. The possibility to analyse velocities between source and first receiver gives a possibility to check back the receiver to receiver velocities.

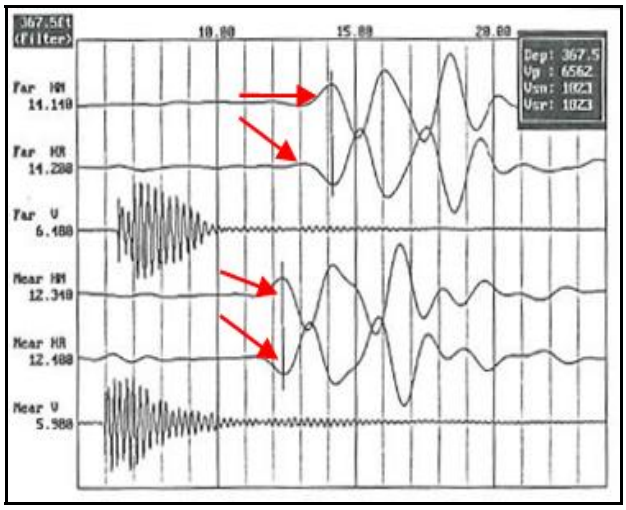

Fig.73: Ideal signal of one PSSL measurement at a certain depth. High frequency p-wave wave trains and lower frequency s-wave trains are recorded separately. Ideally the wave trains recorded at a certain receiver spacing are inverted images of each other, allowing easier identification of the wave onset (RED ARROWS): Receiver spacing is 1 m so that travel time difference between the receivers can easily be inverted to velocity (NIGBOR & IMAI, 1994).

System data	Spacing	1 m for receiver to receiver analysis About 3 m for source to first receiver analysis
	Vertical resolution	high and constant (no change in resolution with depth)
	sampling interval	user defined, usually 0.5 m
	frequency	medium (0.5 – 5 kHz)
	investigated volume	low and constant (1m for receiver to receiver to receiver measurements, 3 m for source to receiver measurements)
	Seismic Source:	horizontal, solenoid source hammer
Borehole requirements	no. of BH's	1
	BH-medium	water or drilling mud, well circulated before measurements
	BH-completion	open borehole for best results PVC cased boreholes with good coupling to formation (grouting)
	BH inclination	only in vertical, downward heading boreholes
Formation	Rocks and unconsolidated, "slow" formations wit v_p<1500 m/s	
Depth limit	limited by tool construction	
Parameters	measured	travel time of compressional and shear wave
	calculated	velocities of p- and s-waves

Measuring progress low to medium due to stationary measurements every 0.5 m (or other user defined sampling interval).

Comment Aspects that should be taken into account for the use of PSSL:

- Source to first receiver measurements are affected by an internal source delay that can be easily verified, but which can change within a logging section due to deterioration or damaging of source springs.
- Measurements in PVC casings are possible, but casing should be carefully grouted at least 48 hours before measurements, to provide good coupling to the formation. Voids in the grouting cause problems with de data.
- Measurements in steel casing do not provide sufficient results.
- Highly fractured rocks cause problems due to attenuation, complex refraction and reflection of wave energy. First arrival picking might be impossible or lead to unreliable results.
- Highly alteration of the borehole wall (f.ex due to repeated rod movement) causes problems.
- Mispicking of non corresponding phases can cause errors in the range of about 5 – 50 ms especially in unconsolidated sediments.

References on PSSL

ELLIS E.V., SINGER J.M., 2007, Well Logging for Earth Scientists. 2nd Edition, Springer Verlag, Dortrecht, 2007, p.247-322.

NIGBOR, R.L. and IMAI, T., 1994. The Supension P-S Velocity Logging Method. IN: Geophysical Characterization of Sites, Volume prepared by ISSMFE Technical Committee #10 for XIII ICSMFE, 1994, New Delhi, India. Edited by Richard D. WOODS, International Science Publisher, New York, 1994, p.57-61.

DIEHL., J.G., MARTIN, A.J. and STELLER, R.A., 2006. Twenty year retrospective on the OYO P-S-suspension logger. Proceedings of the 8th U.S.National Conference on Earthquake Engineering, April 18-22, 2006, San Francisco, California, USA, Paper No. 319.

INAZAKI, T. Relationship between s-wave velocities and geotechnical properties of alluvial sediments, 2006. Public Works Research Institute, Tsukuba, Japan, 2006.

Gamma Gamma Density Log

Method description

Gamma-Gamma-Density Logging (GGD) uses artificial sources of radiation (usually ^{137}Cs or ^{60}Co) to measure interaction between emitted radiation and rock formations in boreholes. The dominant interaction process is the Compton effect. Proper calibration of the tool allows measurement of electron density using a GGD-tool comprising a Gamma radiation source, 1 or more detectors (preferred 2 to overcome artefacts caused by wall roughness, mud cakes or break outs) and a positioning system to press the tool against the wall (usually a mechanical arm that is capable of measuring the borehole caliper). A lead isolation prevents direct radiation from source to receiver. The bulk density is calculated from the electron density.

GGD measurements are mainly used for porosity estimations (petroleum industry), for density measurements as input parameter for mechanical property derivation (combined with velocity measurements) and as a support in lithological classification.

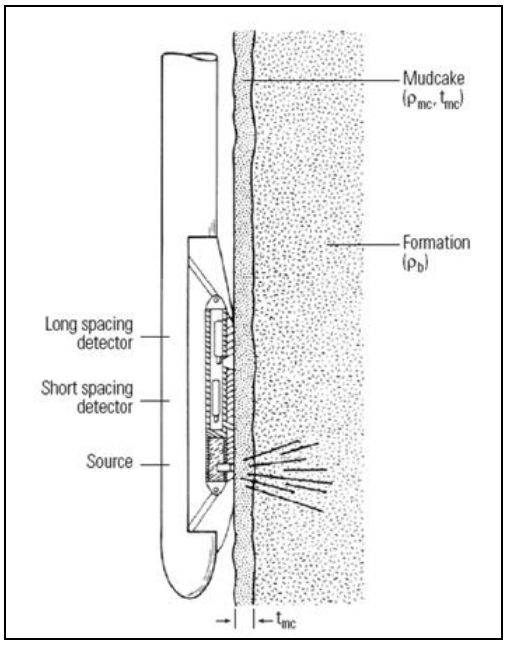

Fig.74: GGD tool and its use in a borehole (ELLIS, 2007).

System data

Vertical resolution	high and constant
sampling interval	user defined (usually around 0.1 m)
investigated volume	low and +/- constant (radiation penetration depth might vary for different materials)
Radiation Source:	^{137}Cs or ^{60}Co

Borehole requirements	no. of BH's	at least 1
	BH-medium	fluid filled (no extremely heavy weight muds) In dry holes absolute density values are unreliable, but relative changes can still be interpreted (lithological changes, fractured zones)
	BH-completion	open borehole for best results In cased water wells GGD can be run to check material in the annular space.
	BH diameter	dependant on the tool (especially the positioning system), usually in the range between 70 – 220 mm
	BH inclination	best results in vertical holes. In high quality boreholes (f.ex. in granites) inclinations up to 25° can be measured without significant data quality loss. Theoretically if wall contact can be provided higher inclinations are possible, but risk of tool loss or tool damage is increasing with higher inclinations.
Formation	Rocks and soils	
Depth limit	limited by tool construction	
Parameters	measured	Formation electron density and borehole caliper
	calculated	Formation Bulk density
Measuring progress	medium to high	
Comment	Aspects that should be taken into account for the use of GGD: - Handling radioactive materials needs special training and surveillance (dosimeter). - Radioactive tools need more time for international transport and its organisation (special papers for customs, …).	

References on GGD

ELLIS E.V., SINGER J.M., 2007, Well Logging for Earth Scientists. 2nd Edition, Springer Verlag, Dortrecht, 2007, p.247-322.

Downhole Seismic

Method description

Downhole seismic measurements (Vertical Seimic Profiles-VSP, well velocity surveys) record seismic signals created by surficial sources with geophones or hydrophones at different depths in a well. BOYER&MARY, 1997 describe the VSP as an acoustic log at seismic frequencies.

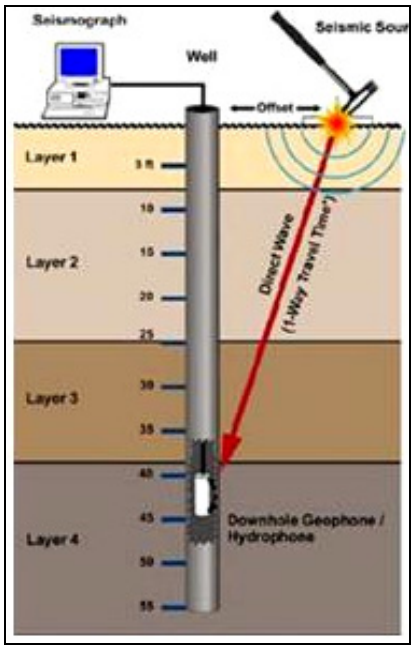

Fig.75: Principle of downhole seismic measurements in a layered medium. (http://seismo.geology.upatras.gr). Seismic signals produced by a surficial source are recorded by receivers (geo- or hydrophones) in a well.

For the measurements the receivers (1 geophone or an array) are lowered in the borehole to a certain depth and clamped to the borehole wall to increase signal to noise ratio and to avoid receiver movement. After source activation and signal recording receivers are unclamped and moved to the next depth. The use of a reference geophone on the surface provides measurements significance.

To obtain velocity data first arrivals are picked. For the fact that normally source and receiver are not on the same vertical, corrections are necessary. ANDERSON et al., 2003 recommend the use of two opposite polarized shear wave records for shear wave travel time measurements. Traveltime plots versus depth allow the differentiation of layers with approximately constant velocities.

The downhole wavefield is composed by downgoing body waves (direct arrivals from the source or reflected waves from markers above the receiver), upgoing body waves (primary or multiple reflected p- and s-waves) and Stoneley waves (guided interface modes linked to well and fluid).

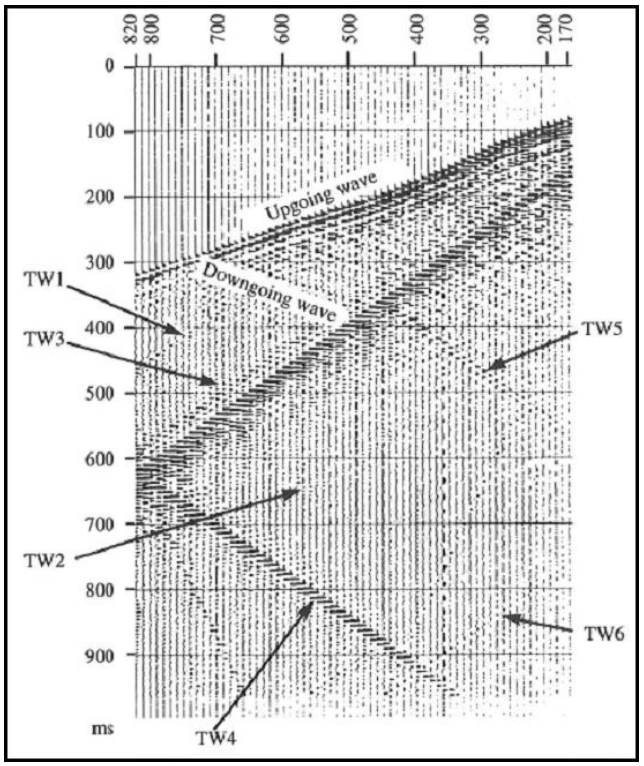

Fig.76: Downhole data example (BOYER&MARY, 1997). The wave field is composed of downgoing and upgoing bodywaves and tube waves (TW1, 3 and 6 are downgoing; TW 2, 4 and 5 are upgoing).

System data	Spacing	user defined, usually in the range between 1 and 5 m
	Vertical resolution	medium to low, dependant on the receiver spacing
	sampling interval	user defined (usually from 1 m to 10 m)
	frequency	medium to low, source dependant
	investigated volume	high, lateral investigation distance is about half the well head-source offset, but limited by the fact that the incident angle must be beneath 30-35° to markers.
	Seismic Source:	Onshore: sledge hammers, low charge explosives, dropped weights or offshore sources in mudpits Offshore: Airguns
Borehole requirements	no. of BH's	1
	BH-medium	dry or fluid filled holes
	BH-completion	preferred in cased holes (PVC), accurate coupling of the receivers to the formation must be possible (grouting)
	BH diameter	equipement dependant

	BH inclination	possible in vertical, inclined and deviated wells
Formation	Rocks and soils	
Depth limit	limited by tool construction and source range	
Parameters	measured	travel time of compressional and shear wave
	calculated	velocities of p- and s-waves as a function of depth
Measuring progress	medium to high, equipment dependant	

Comment Aspects that should be taken into account for the use of downhole seismics:

- Equipment cables in the borehole should be slackened during recording to avoid cable waves.
- Ideally measurement points lie beneath markers to avoid interference between downgoing and a reflected upgoing waves.
- Normally measurements are performed downwards. Remeasurement of some points while raising the tool provides repeatability of the measurements. Stacking of (usually up to 5) consecutive shots increases the signal to noise ratio significantly.
- The long travel paths lead to wave energy loss due to attenuation, to reflections and to mode conversions (f.ex. in shallow fractures).
- Increasing source receiver spacing increases the influence of attenuation (especially of the higher frequencies). On the one hand this is a problem for the measurements (especially for manual first arrival picking) on the other hand downhole seismics can be used for macro attenuation analysis using for example “Spectral ratio method” or “rise time method for VSP recorded with impulsive sources”.
- Derived velocity functions are estimated via linear trend lines. Deviations away from the best fit line are result of small scale variations in material velocity and errors deriving from source-receiver geometry assumptions, picking insecurities and refraction effects.
- The use of triaxial geophones allows picking of vertical p-wave components arrivals and the two horizontal shear wave components. This can be used for rough anisotropy estimations.
- Triaxial geophones should be oriented parallel to the axis of excitation at the surface to insure maximal signal amplitude in the records (f.ex. Geostuff BHG-3 system). Orientation also avoids errors in travel time caused by incorrect phase of first arrival picks.

- Tube waves can be used to identify fractured and permeable zones.

- Verticality of the hole is mostly assumed, although vertical drilled holes can show significant inclinations especially with increasing borehole depth. Additional borehole deviation measurements can provide data for more exact surface to borehole data processing. In inclined or deviated wells borehole deviation must be measured. Another possibility to remove or reduce inclination effects is the use of two receivers and the calculation of interval velocities.

References

CHEN S.T., ZIMMERMANN L.J., TUGNAIT J.K., 1990, Subsurface imaging using reversed vertical seismic profiling and crosshole tomographic methods. Geophysics, Vo.55, No.11, November 1990, p.1478-1487.

BOYER, S., MARI, J.-L., 1997, Oil and Gas Exploration Techniques: Seismic Surveying and Well Logging. Editions Technip, Paris, 1997

Crosshole Seismic

Method description

For crosshole seismic measurements sources and receivers are installed in certain depth positions in separated boreholes ("source-"and "receiver hole").

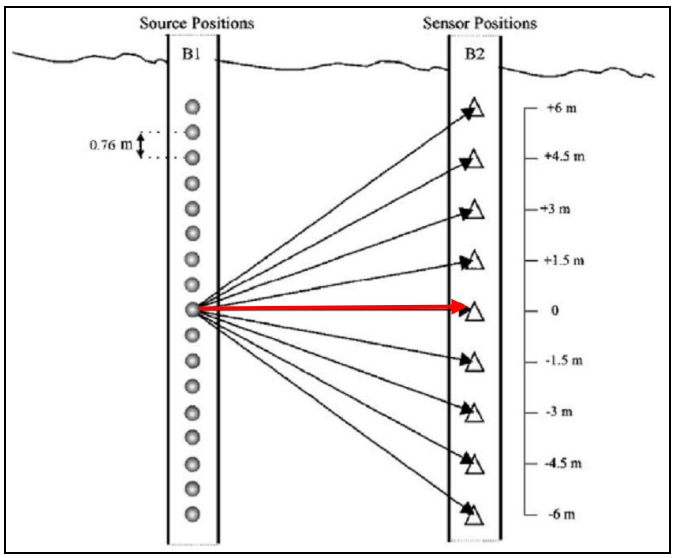

Fig.77: Principal of crosshole surveys. Source and receiver are positioned in separated holes. For "classic" crosshole seismic source and receiver are usually positioned in the same depth (red arrow)

The source is activated in several positions in the source hole and the emerged waves are recorded by a receiver or a receiver array in the

receiver hole. The crosshole wavefield is mainly composed by direct p-waves from source hole to receiver, p-waves emitted from the source and reflected from the surface, p-waves from the source travelling to the bottom/ground of the receiver hole and converted into a tube wave going downward/upward to the receivers, p-waves reflected from structures between the holes and multiple reflected modes of the former generated tube waves. Velocity can be calculated from manual picking of first arrivals or by tomographic inversion. Source receiver geometries can be varied. Simplest geometry is one source and one receiver installed at the same depth. For tomographic measurements receiver arrays are used to provide better ray path coverage

Stacking increases signal to noise ratio. Borehole deviation must be measured to determine exact distances for velocity calculations.

System data	Spacing	user defined
	Lateral resolution	medium to high
	Vertical resolution	medium to high
	sampling interval	user defined
	frequency	medium to low, source dependant
	investigated volume	high, dependant on the hole distance
	Seismic Source:	low charge explosives, hammer sources, sparker sources
Borehole requirements	no. of BH's	at least 2, preferred 3 or more
	BH-medium	fluid filled holes, dry holes
	BH-completion	cased and cemented holes (PVC or aluminium)
	BH diameter	equipment dependant
	BH inclination	possible in vertical, inclined and deviated wells
Formation	Soils and rocks	
Depth limit	limited by tool construction	
Parameters	measured	travel time of compressional and shear wave
	calculated	velocities of p- and s-waves
Measuring progress	low to medium	
Comment	Aspects that should be taken into account for the use of CH:	

- Potential sources of error for velocity estimation are recognition and subsequent correct picking of arrival times, source trigger timing, difficult borehole conditions and geometric effects.

- Low velocity layers can cause problems in shear wave velocity estimation, because the first arrival tends to be a refraction from the adjacent higher velocity layer.
- Optimal data quality is provided by performing separate tests for p- and s-wave measurements.

References

ANDERSON N., CHEN G., KOCIU S., LUNA R., THITIMAKORN T., MALOVICHO A., MALOVICHKO D., SHYLAKOV D., 2003, Final report RDT 03-006, Vertical Shear-Wave Velocity Profiles Generated From Spectral Analysis Of Surface Waves: Field Examples. Prepared for Missouri Departement of Transportation, Research, Development and Technology, Jefferson City, Missouri, April 2003.

CHEN S.T., ZIMMERMANN L.J., TUGNAIT J.K., 1990, Subsurface imaging using reversed vertical seismic profiling and crosshole tomographic methods. Geophysics, Vo.55, No.11, November 1990, p.1478-1487.

ANGIONI T., RECHTIEN R.D., CARDIMONA S.J., LUNA R., 2003, Crosshole seismic tomography and borehole logging for engineering site characterization in Sikeston, MO, USA. Tectonophysics, 368, Elsevier, 2003, p.119-137.

3-Axial and Unconfined Compression Test

Method description

Triaxial testing applies a vertical load (σ_1) and radial confining pressure (σ_2, σ_3) on a cylindrical or a cuboid sample with mechanic pistons or fluids. Compression can be realized as well as extension. Different combinations of stress relations allow testing under different conditions. The conventional triaxial test shows two equal stresses ($\sigma_1>\sigma_2=\sigma_3$ or $\sigma_1=\sigma_2>\sigma_3$). The true triaxial test is performed in a more general stress state ($\sigma_1\geq\sigma_2\geq\sigma_3$). Unconfined compression tests are performed applying only axial stress without confining pressures.

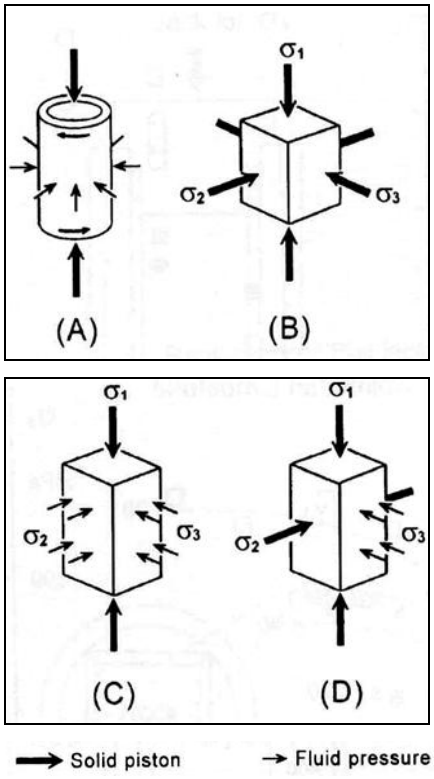

Fig.78: Different stress conditions realized in triaxial experiments. A: only fluid pressure. B: piston pressure C,D: Combination of pistons and fluid pressures (MOGI, 2009)

Usually the specimen is jacketed with rubber and connected with a hydraulic pressure machine. Pressure measurements are realized via Bourdon Gauge and a load cell over electrical resistance strain gauge. According to the geometry an internal and an external method can be differentiated.

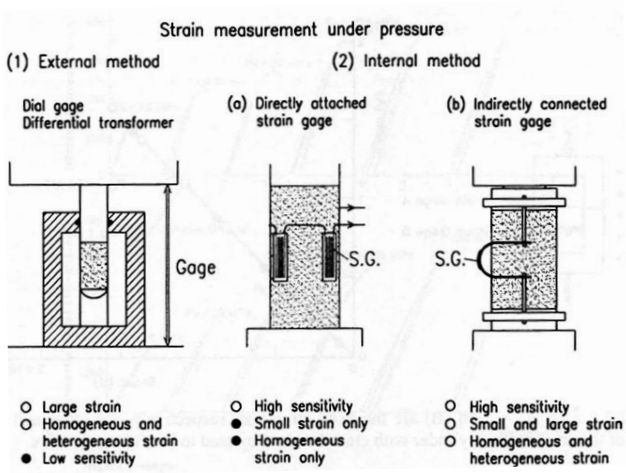

Fig.79: Internal and External methods (MOGI, 2009)

The triaxial test can be performed under drained and under undrained conditions. Fluid conditions are controlled by a valve system.

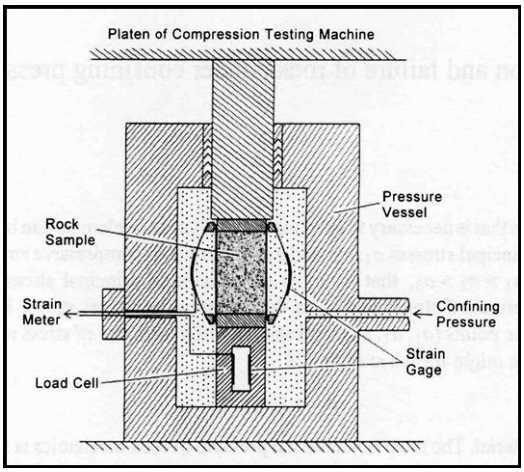

Fig.80: Triaxial Cell and its main compinents.

Accordint to the different conditions of testing the following triaxial test methods can be sifferentiated:

- Consolidated and drained (CD- or S-) compression or extension test
- Consolidated and undrained (CU- or R-) compression or extension test
- Unconsolidated and undrained (UU- or Q-) compression or extension test

The Unconfined compression test is the simplest form of a triaxial testing. The sample is loaded axial without confining pressure until failure. The pressure at failure is the Unconfined Compression strength, which is a widely used parameter in geo-engineering (UCS).

System data aspect Ratio usually 2:1

investigated volume low to medium

Borehole requirements no. of BH's at least 1 hole with coring for sample material

Formation Rocks and soils

Depth limit limited by depth of the sampling borehole

Parameters measured fracture/failure stress, yield stress, ductility
fracture angle between shear fault plane and σ_1-axis

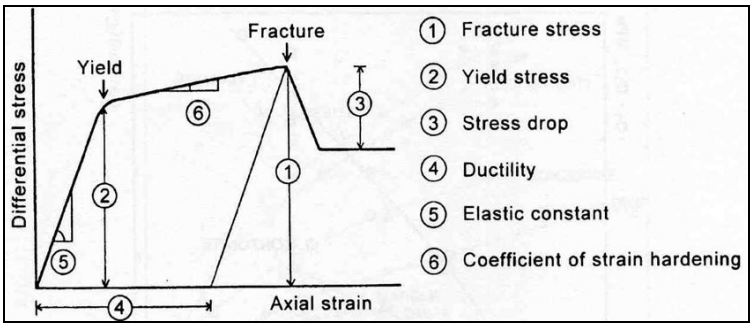

Fig.81: Stress.strain curve measured in triaxial experiments and derived parameters. (MOGI, 2009).

calculated moduli, cohesion, internal angle of friction, shear trength

Measuring progress low (coring-transportation to lab-sample preparation-test)

Comment Aspects that should be taken into account for the use of triaxial tests

- A pressure effect at the end of the specimens leads to a decreasing strength with increasing confining pressure. Conventional tests with small cylindrical samples are accompanied by stress concentration and a clamping effect at the end part of the specimen.
- In drained measurements the loading rate plays an essential role. If loading rate is too high the pore pressure increases and the elastic constants measured are approaching the ones measured under undrained conditions. According to this the undrained test allow application of higher stress rates.
- Friction between sample and pistons lead to a barrel form of the sample during testing. This effect can be minored by aspect ratios of at least 2.
- Friction occurring at moving pistons can produce hysteresis effect during unloading.

References

CHARLEZ, A.P., 1991, Rock Mechanics, Volume 1, Theoretical Fundamentals. Editions Technip, Paris, 1991, p. 159-174.

HUNT, R.E., 2005. Geotechnical engineering investigation handbook. Tayor&Francis, CRC, Boca Raton, 2005, 1066 pages.

MOGI, K., 2007, Experimental Rock Mechanics. In: Kwasniewski, A.M. (editor in chief), 2007, geomechanics Research Series Vol. 3. Taylor&Francis Group, London, UK, 2007, p. 3-193.

ZHANG, L., 2005. Engineering properties of rocks. Elsevier geo-engineering book series, Vol. 4, Elsevier, Amsterdam, 2005, 290 p.

Piezo-Element testing (transmission and Bender elements)

Method description

A cylindrical sample is fixed between two ultrasonic, usually piezo-transducers. Piezoceramic elements can be mechanically stressed by an applied voltage or can produce an electrical charge when stressed by an applied force. For traveltime measurements the sample of known length (travel path) is positioned between a transmitting and a receiving element. For the fact that “normal” piezoceramic elements are not adequate to measure shear wave velocity in soil samples (weak s-wave directivity, poor coupling, high operating frequencies) bender elements have been developed. Bender elements are thin, two layered plates consisting of two conductive outer electrodes, two piezoceramic sheets and a conductive metal shim at the centre. Series and parallel elements have to be distinguished. Parallel elements show twice the displacement of the series element for the same applied voltage and are used as sources, whereas series elements are used as receivers.

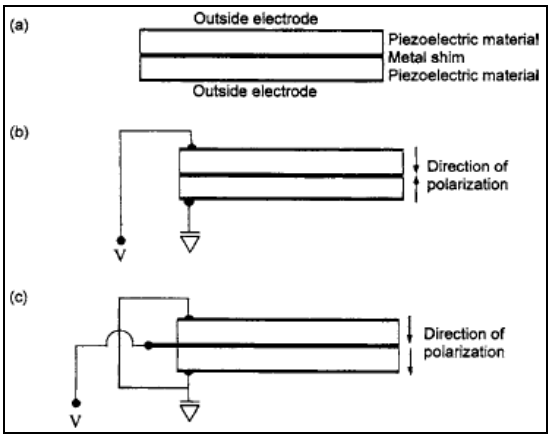

Fig.82: (a) schematic representation of a bender element, (b) series type element and (c) parallel element (LEE&SANTAMARINA, 2005).

Traveltime determination can be done in different ways:

- First arrival picking
- Determination between characteristic points
- Cross correlation of input and output signal
- Determination of group traveltimes for a range of frequencies
- Use of second (or third) arrivals (reflections)

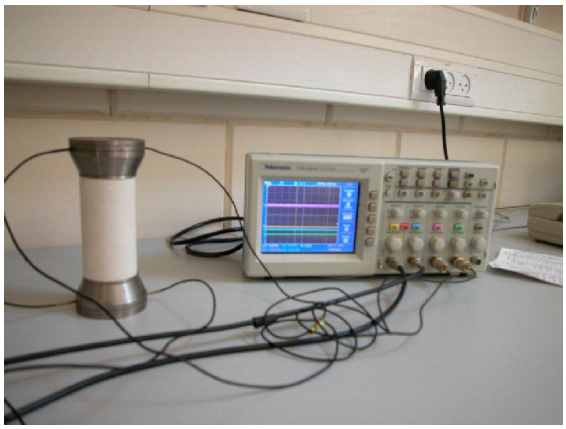

Fig.83: Principle setup for laboratory velocity measurements using piezo-elements. (http://www.bgu.ac.il/geol/rockmech/lab/ultrasonic.html)

System data	aspect Ratio:	different geometries possible
	frequency	high, > 6 kHz
	investigated volume	low
Borehole requirements:	no. of BH's	at least 1 hole with coring for sample material
Formation	Rocks and soils (bender elements)	
Depth limit	limited by borehole depth	
Parameters	measured	p- and s-wave travel time
	calculated	wave velocity
Measuring progress	low (coring-transportation to lab-sample preparation-test)	

Comment Aspects that should be taken into account for the use of Piezoceramic element tests.

- Bender elements involve some sources of travel time errors like interference of p- and s-wave arrivals, near field effects, reflections at sample boundaries resulting in non directive wave travel paths through the sample, rotational compliance of the bender to cap connection, disturbances at the sample-bender-interface, imperfect alignment of the benders and the fact that for given geometries the source cannot be seen as a point source. This error sources are still subject to research.
- ARULNATHAN et al., 1998 mention a high dependence of travel time errors on bender length to wavelength ratio, on the method of

traveltime determination and on the relative stiffness of sample and bender element.

- Electromagnetic coupling can lead to “crosstalk”, an early signal component that is quasi-simultaneous with the input signal.

References

ARULNATHAN, R., BOULANGER, R.W. and RIEMER, M., 1998. Analysis of Bender Element Tests. Geotechnical Testing Journal, GTJODJ, Vol. 21, No. 2, 1998, p. 120-131.

LEE, J.-S. and SANTAMARINA, C., 2005. Bender Elements: Performance and Signal Interpretation. Journal of Geotechnical and geoenvironmental Engineering, ASCE, September 2005, p. 1063-1070.